



Joint RTK and Attitude Determination

Andreas Sperl

A Thesis submitted for the Degree of
Master of science

Institute for Communications and Navigation

Prof. Dr. Christoph Günther

Supervised by Dr.-Ing. Patrick Henkel

München, September 2015

Abstract

The precise knowledge of the position and attitude is of essential importance in geodesy and the automotive, maritime, aerospace and robotics industry.

The sensor fusion of GNSS and INS measurements and a virtual reference station is needed to achieve the necessary accuracy and reliability. The GNSS carrier phase measurements can be tracked with millimeter-level accuracy and enable a millimeter-level positioning accuracy if the ambiguities and cycle slips are correctly estimated. The inertial measurements are needed for cycle slip correction, for fast ambiguity-refixing after losses of lock (e.g. due to passing of bridges) and for an increased update rate. A tight coupling of all sensors fully exploits the complementary advantages of the sensors and the correlation of the measurements.

In this thesis, the following extensions were made to the tightly coupled sensor fusion of *ANavS* – *Advanced Navigation Solutions*¹:

- Replacement of double difference measurements by single difference measurements to maintain the *absolute* position information
- Estimation of noise statistics directly from the measurements instead of using an elevation-dependent model
- Cycle slip correction for attitude and RTK baselines using INS-predicted attitude and position (the precise prediction of the absolute position as the is more challenging than the prediction of the attitude as the double integration of the acceleration results in a larger drift and as orientation errors of the gravity vector add to the acceleration biases)
- Integration of uncorrected phase and code measurements of virtual reference station of known position in sensor fusion
- Improved ambiguity fixing of the attitude- and RTK-baseline, that takes the length residuals (only for attitude-baseline), the measurement residuals and the baseline stability into account
- Introduction of a cascaded position and attitude determination with *fault-back* solutions (fixed - float - code-only)

The developed algorithms were tested with measurements from a research car of Volkswagen, which was also equipped with a geodetic GPS/ INS reference (Applanix from Trimble). We obtained an absolute positioning accuracy in the order of a few centimeters in case of correct fixing.

¹Homepage: www.anavs.de

Zusammenfassung

Eine hochgenaue Positions- und Lagebestimmung ist für Anwendungen in der Geodäsie als auch in der Automobil-, Schifffahrt-, Luftfahrt- und Robotikindustrie von besonderer Wichtigkeit. Die Sensordatenfusion von GNSS- und INS-Messdaten, als auch von unkorrigierten Trägerphasen- und Code-Messungen einer virtuellen Referenzstation (VRS) werden für die geforderte Genauigkeit und Zuverlässigkeit benötigt. Trägerphasen-Messungen eines GNSS können mit Millimeter-Genauigkeit getrackt werden, was eine Positionsgenauigkeit in diesem Bereich bereitstellt, falls die Phasen-Mehrdeutigkeiten und mögliche Cycle-Slips korrekt gelöst wurden. Die inertialen Messdaten werden entsprechend für die Cycle-Slips benötigt, aber auch für ein schnelles Re-Fixing der Mehrdeutigkeiten nach kurzzeitigen Signalausfällen (bspw. nach Tunnelpassagen, Brücken, etc.) als auch für eine Erhöhung der Update-Rate. Ein Tight-Coupling all dieser Sensoren nutzt die komplementären Vorteile der benutzten Sensorik, als auch die Korrelation der Messungen aus.

In dieser Arbeit wurde an folgenden Erweiterungen der bestehenden Tight-Coupled Sensordatenfusion von *ANavS – Advanced Navigation Solutions* gearbeitet:

- Integration von Single-Differenz Messungen anstatt Doppel-Differenz Messungen, um eine absolute Positionsangabe bereitstellen zu können.
- Schätzung der Rausch-Statistik direkt anhand der Messungen anstatt eines elevationsabhängigen Modells.
- Cycle-Slip Korrektur sowohl für die Attitude- als auch für RTK-Baseline mithilfe einer INS-prädizierten Lage und Position. Eine präzise Prädiktion der absoluten Position stellt hierbei die größte Herausforderung aufgrund der zweifachen Integration der Beschleunigungsmessdaten dar. Dies führt zu einem erhöhten Drift (Verglichen zur Integration von Drehraten hinsichtlich der Prädiktion der Lage), da auch der Orientierungsfehler des Gravitationsvektors dem Beschleunigungsbias zugeteilt wird.
- Implementierung der unkorrigierten Trägerphasen- und Pseudorange-Messungen einer virtuellen Referenzstation mit bekannter Position in die Sensordatenfusion.
- Verbesserte Bestimmung der ganzzahligen Phasen-Mehrdeutigkeiten (Attitude- und RTK-Baseline), welches sowohl die Längen-Residuen (nur Attitude-Baseline), Mess-Residuen als auch die Baseline-Stabilität betrachtet.
- Einführung einer kaskadierten Positions- und Lagebestimmung mit Rücksprung-Lösungen (fixed-float-code-only)

Die entwickelten Algorithmen wurden mithilfe von Messdaten anhand eines Forschungsfahrzeugs von Volkswagen getestet, welches zusätzlich noch mit einem geodätischen GPS/INS Referenzsystem ausgestattet war (Applanix von Trimble). Wir erreichten eine Genauigkeit der absoluten Position im Bereich von wenigen Zentimetern im Falle eines korrekten Fixings.

Contents

1	Introduction	3
1.1	Motivation	3
1.2	Methodology	4
2	Fundamentals	6
2.1	Pseudorange, carrier phase and Doppler measurement-models	6
2.2	Single-difference (SD) measurement	8
2.3	Double-difference (DD) measurement	10
2.4	Triple-difference (TD) measurement	11
2.5	Measurement model of the IMU	11
2.6	Network-RTK with a virtual reference-station (VRS)	13
2.6.1	Motivation for implementing a Network-RTK	13
2.6.2	The general concept of a Network-RTK	14
2.6.3	The different concepts in detail	14
2.6.4	Limits and future of network-RTK	16
3	State of the Art	17
3.1	Consideration of a low-cost GPS/INS-system	17
3.1.1	Piksi by the company Swift-Navigation	17
3.1.2	$i\mu$ VRU-01 by the company iMAR	18
3.1.3	Validation	19
3.2	Consideration of the autonomous driving	19
3.2.1	Validation	21
4	Modeling and concept of a joint RTK and Attitude determination	22
4.1	Modeling with an extended Kalman filter (EKF)	24
4.1.1	State-space-model	24
4.1.2	The observation-model	26
4.2	Algorithm of an extended Kalman filter	28
4.2.1	The prediction	28
4.2.2	The state-update	29
4.3	Concept of the joint RTK and Attitude determination	29
5	Joint fixing of attitude- and RTK-baseline	33
5.1	The float Kalman filter of the attitude-baseline	33
5.1.1	The synchronization-correction	33
5.1.2	The parametrization of the Kalman filter	34
5.2	Ambiguity-fixing of the attitude-baseline	39
5.2.1	The mathematical model	39
5.2.2	The practical implementation	40
5.3	The float Kalman filter of the RTK-baseline	46
5.3.1	The parametrization of the float Kalman filter	48

5.4	Ambiguity-fixing of the RTK-baseline	52
6	Joint RTK and attitude determination in a tight-coupled system	55
6.1	The measurement-model of the tight-coupled EKF	55
6.2	The parametrization of the fixed tight-coupled EKF	59
6.3	The update-step of the fixed tightly coupled EKF	62
6.4	Detection and correction of cycle slips	66
6.4.1	Cycle-slip on the attitude-baseline	66
6.4.2	Cycle-slip on the RTK-baseline	68
6.5	The integrity-check based on the dynamic float-solution	69
6.5.1	The parametrization of the RTK float Kalman filter	69
6.5.2	The integrity-check of the RTK-baseline	71
6.5.3	The integrity-check of velocity	72
6.5.4	The integrity-check of heading	72
7	Measurement results	74
7.1	The test-drive in an urban environment	74
7.2	The test-drive on a highway	79
8	Conclusion	84
A	The baseline vector and its linearization	86
B	Covariance-matrix with an elevation-dependent model	88
C	Derivations for the decomposition in view of ambiguity fixing	90
	Acronyms	91

Chapter 1

Introduction

1.1 Motivation

The "autonomous" car is right now on everybody's lips and a central topic for all well-known automobile manufacturers. In addition to the traditional manufacturers, companies like Google or organizations like NASA are also very active in research. The manufacturers introduce media-effective the newest research and development results to the customers by presenting them high-end equipment and test-drives.

To get a precise position and attitude for the highly automated driving, you have to use a global navigation satellite system (GNSS) with correction data and with support of an inertial navigation system (INS). At the current stage of development, a relatively expensive equipment is necessary to get a precise position and attitude information. This concerns first of all the INS, which should provide a highly accurate integration of the acceleration and rotation rate in all three axes without much drift. Another big cost driver are the geodetic GNSS-receivers (dual-frequency receivers), which are used to get the required precision and reliability for the absolute position and attitude.

A solution for this cost-benefit-problem is described in the present thesis. It can be solved just with a low-cost GNSS/INS-system and the help of correction-data of a virtual reference-station. The company *Advanced Navigation Solutions - ANavS GmbH* is therefore a leading company in the development of ultra-precise positioning and attitude solutions with the help of a low-cost GNSS/INS-system. Therefore the sensor-fusion is combined in such a sense, that the disadvantages of both low-cost components are compensated with the advantages of that (see table 1.1). For this, a tight coupling of the measurement-data is implemented, which combines the GNSS pseudo-range, phase- and Doppler-measurement with the data of the INS, byword acceleration and rotation-rate in all three axes, to get always one navigation solution per epoch for all desired states.

To improve the existing position and attitude determination of the tight coupled and low-cost GNSS/INS-system of the *Advanced Navigation Solutions - ANAVS GmbH*, the software will be expanded with an additional virtual reference-station (VRS) in this thesis. The used network-RTK provides here corrected pseudo-range and phase-measurements with respect to the interpolated VRS. Corrected means, the measurements don't contain multipath and also the ambiguities are fixed for the reference station. This additional datasets should increase the accuracy of the position and attitude determination. Furthermore the reliability of the determined states should also be affected through the corrected measurements of the VRS. Besides this adoptions, other improvements for the existing algorithm are implemented, which is also

¹Microelectromechanical systems (MEMS): is the technology of very small devices

Table 1.1: Combined benefits of coupled GPS/INS

Low-cost GPS chips and patch-antennas	Low-cost inertial measurement unit (MEMS ¹)
+ unbiased positioning	– biases in acceleration and angular rate measurement result in a Drift
– sensitive to signal reception	+ robust, i.e. functional independent of environment

explained step-by-step in this thesis.

1.2 Methodology

The first chapter is focused generally on the concept and tasks and the second chapter explains the theoretical background. At first, the fundamental measurement models of GPS are described. After that, the functionality and implementation of an (extended) Kalman filter is shown. Finally, the different types of network-RTK and the corresponding benefits are analyzed, especially the implementation with a virtual reference-station (VRS).

The state-of-the-art consideration follows in the third chapter. Besides the analysis of further tight-coupled systems in the low-cost segment on the market, the development of the autonomous driving with all his predicted milestones and notations is shown.

In the fourth chapter, the implemented concept of the joint RTK and attitude determination with the help of low-cost (μ -blox) GNSS-Receiver, low-cost inertial sensor and a virtual reference-station is explained. For this purpose, the single processing steps of the tight-coupling are pointed out.

A precision in centimeter range through tight-coupling with GPS/INS and a virtual reference-station is only possible with fixed double-difference ambiguities of the phase-measurement. How this initialization-phase is made for the attitude-baseline as well as for the RTK-baseline is described in the fifth chapter. The definition includes the mathematical derivation and the implementation. The parameterization of the necessary Kalman filter is also described in this step.

After the double-difference ambiguities of the attitude- and RTK-baseline are solved, a dynamic process (coasting-phase) is possible. In this chapter, the tight-coupling of GPS/INS with a VRS is introduced. This includes in general the measurement-models, the parameterization of the extended tight-coupled Kalman filter and the integrity-check of all important states in the update-step.

In chapter seven, the reached results of the implemented tight-coupling of a low-cost GNSS/INS-system with a virtual reference-station is introduced and discussed. Hereby, the most important determined states (position, velocity, attitude) are analyzed and compared to the available applanix-reference solution. Besides this, the reliability of the system is also checked.

The last chapter summarizes the results, improvements and the remained difficulties.

Chapter 2

Fundamentals

To describe the concept of a joint RTK and attitude determination with tight-coupling of GPS/INS and correction data with a virtual reference-station, this chapter explains first of all the different measurement models for GPS and INS. The used models and concepts for the IMU, consisting of three orthogonally arranged accelerometer-sensors and gyroscope-sensors, are also explained in brief. However, the thesis will mainly focus on the GPS-part. To ensure the understanding of the tightly-coupled GPS/INS system, aspects in terms of the IMU are declared at all necessary points in the thesis.

Besides the measurement-models of GPS and INS, the basics of an (extended) Kalman filter (EKF) for the sensor-fusion are also described in this chapter. The explanation is taking especially the principle models, concepts and advantages of a Kalman filter (KF) for the tight-coupling into account.

The correction data include uncorrected pseudorange and carrier phase measurements and are obtained from a virtual reference-station (VRS). This chapter explains the motivation for the implementation of a VRS and also other concepts for the realization of a network-RTK.

2.1 Pseudorange, carrier phase and Doppler measurement-models

The absolute position is determined with the help of a Global Navigation Satellite-System (GNSS) through the signal propagation delay from the satellites to the receivers. Every satellite transmits for that continuously his own spreading-code and the ephemeris-data with the navigation-message. Through adjustment by the help of time- and frequency-shifting, the receiver is able to determine precisely the signal propagation delay. The multiplication of this measured time-shift with the signal velocity (nearly speed of light) gives the so-called pseudorange from the satellite to the receiver. This value corresponds to the true satellite-receiver-range plus additional error-terms. The pseudorange measurement from satellite k to receiver r is modeled as follows [1]:

$$\begin{aligned} \rho_r^k(t_n + \delta t_r(t_n)) = & \vec{e}_r^k(t_n + \delta t_r(t_n))(\vec{x}_r(t_n + \delta t_r(t_n)) + \Delta\vec{x}_{ET_r}(t_n) - \vec{x}^k(t_n + \delta t_r(t_n)) - \Delta\vec{x}^k(t_n)) \\ & + c(\delta t_r(t_n) - \delta t^k(t_n)) + T_r^k(t_n) + I_r^k(t_n) + b_r(t_n) + b^k(t_n) + \Delta\rho_{MP,r}^k(t_n) \\ & + \eta_r^k(t_n) \end{aligned} \tag{2.1}$$

with the following notations:

t_n	signal reception time of the receiver [s]
δt_r	clock-error of receiver r [s]
\vec{e}_r^k	normalized line-of-sight (LOS) vector from satellite k to receiver r
\vec{x}_r	position of receiver r [m]
$\Delta \vec{x}_{ET_r}$	position-offset of receiver r due to tidal forces [m]
\vec{x}^k	position of satellite k [m]
$\Delta \vec{x}^k$	position-error of satellite k [m]
c	speed of light in vacuum [m/s]
δt^k	clock-error of satellite k [s]
T_r^k	tropospheric propagation-delay of satellite k and receiver r [m]
I_r^k	ionospheric propagation-delay of satellite k and receiver r [m]
b_r	bias of receiver r [m]
b^k	bias of satellite k [m]
$\Delta \rho_{MP,r}^k$	multipath of satellite k and receiver r [m]
η_r^k	noise of pseudorange measurement [m]

In this work, another index for the distinction of multi-frequency receivers is not necessary. In case of using only low-cost GNSS-receivers, which are in principle single-frequency receivers, this index plays no role. The used terms and models in this thesis refer to the ECEF (Earth-Centered, Earth-Fixed)-frame as it is not explicitly stated otherwise. For the introduced measurement-models, the receiver- and satellite-position is defined for time $t_n + \delta t_r$. Other parameters are changing less dynamical, so the time change δt_r can be neglected.

In addition to the pseudorange measurement, a GNSS-receiver tracks also the sinusoidal phase of the signal. With the help of this measurement, the precision of GPS is strongly increased. A challenge of this measurement results in the periodicity of the signal. It leads to ambiguities, which can not be solved by the receivers alone. To exploit the advantages of the carrier phase measurement, thus the low phase-noise and the small phase multipath, we have to solve this ambiguities first of all. For this, there are several possibilities explained in [2], [3], [4], [5] and [6] for multi-receiver constellations. In this thesis, a successful method in theory and also in practice with the help of the baseline-constraint is later clarified.

The phase-measurement from the satellite k to the receiver r is modeled as follows [1]:

$$\begin{aligned}
\lambda \varphi_r^k(t_n + \delta t_r(t_n)) = & \vec{e}_r^k(t_n + \delta t_r(t_n))(\vec{x}_r(t_n + \delta t_r(t_n)) + \Delta \vec{x}_{ET_r}(t_n) - \vec{x}^k(t_n + \delta t_r(t_n)) - \Delta \vec{x}^k(t_n)) \\
& + c(\delta t_r(t_n) - \delta t^k(t_n)) + T_r^k(t_n) - I_r^k(t_n) + \lambda N_r^k + \lambda/2 \Delta N_r^k(t_n) + \lambda \beta_r(t_n) \\
& + \lambda \beta^k(t_n) + \lambda \Delta \varphi_{PW,r}^k(t_n) + \lambda \Delta \varphi_{PCO,r}^k(t_n) + \lambda \Delta \varphi_{MP,r}^k(t_n) + \varepsilon_r^k(t_n)
\end{aligned} \tag{2.2}$$

with the additional parameters:

λ	wavelength of the L1-carrier-frequency (1575,42 MHz) [0.19 m]
N_r^k	integer ambiguities of phase measurement [Cycles]
ΔN_r^k	cycle-slips [Cycles]
$\lambda \beta_r$	bias of receiver r [Cycles]
$\lambda \beta^k$	bias of satellite k [Cycles]
$\Delta \varphi_{PW,r}^k$	wind-up error-term [Cycles]
$\Delta \varphi_{PCO,r}^k$	phase-offset from the center of the receiver-antenna [Cycles]
$\Delta \varphi_{MP,r}^k$	multipath of satellite k and receiver r [Cycles]
ε_r^k	noise of phase-measurement [m]

It should be noted, that the error-term of the ionospheric propagation-delay is subtracted and not added as it is done in the pseudorange measurement.

Furthermore the GNSS-receiver tracks also the Doppler-frequency of all received satellite-signals. With the help of this measurements, the velocity of the receiver can be determined. The measurement-model is defined as follows [1]:

$$f_D(t_n) = -\frac{f_T}{c} \left(\vec{e}_r^k(t_n)(\vec{v}_r(t_n) - \vec{v}^k(t_n)) \right) + f_T \left(\delta\dot{\tau}_r(t_n) - \delta\dot{\tau}^k(t_n) \right) + \eta_{D_r^k}(t_n) \quad (2.3)$$

with the parameters:

f_T	L1-carrier-frequency [1575,42 MHz]
\vec{v}_r	velocity of receiver r [m/s]
\vec{v}^k	velocity of satellite k [m/s]
$\delta\dot{\tau}^k$	drift of satellite-clock [s/s]
$\delta\dot{\tau}_r$	drift of receiver-clock [s/s]
ε_r^k	noise of Doppler-measurement [Hz]

With eqn. (2.1) to eqn. (2.3) the basic measurement models are briefly presented. For elimination of error-terms and also for precise and reliable determination of the states of a tight-coupled GPS/INS-system, combinations of the introduced models can help.

2.2 Single-difference (SD) measurement

Linear combinations of pseudorange, carrier phase- and Doppler-measurements are used to improve the relative and absolute accuracy of positioning. The combinations results in an elimination or decreasing of potential and hardly modelable error-terms. The determination of the integer ambiguities is also much easier and more reliable with a linear-combination of measurements.

In this sub-chapter, the measurement-model for the single-difference (SD) measurement between a satellite k and a reference-satellite l is explained. The selection of the reference-satellite is based on the elevation-angle, i.e. the satellite nearest to the zenith. Such a selection is based on the assumption, that the reference-satellite has the best noise-properties in terms of his measurements and the highest SNR (Signal-Noise-Ratio) with the lowest multipath.

The single-difference (SD) pseudorange measurement-model is obtained from eqn 2.1 as

$$\begin{aligned} \rho_r^{kl}(t_n + \delta t_r(t_n)) &= \rho_r^k(t_n + \delta t_r(t_n)) - \rho_r^l(t_n + \delta t_r(t_n)) \\ &= \vec{e}_r^k(t_n + \delta t_r(t_n))(\vec{x}_r(t_n + \delta t_r(t_n)) + \Delta\vec{x}_{ET_r}(t_n) - \vec{x}^k(t_n + \delta t_r(t_n)) - \Delta\vec{x}^k(t_n)) \\ &\quad - \vec{e}_r^l(t_n + \delta t_r(t_n))(\vec{x}_r(t_n + \delta t_r(t_n)) + \Delta\vec{x}_{ET_r}(t_n) - \vec{x}^l(t_n + \delta t_r(t_n)) - \Delta\vec{x}^l(t_n)) \\ &\quad + c\delta t^{kl}(t_n) + T_r^{kl}(t_n) + I_r^{kl}(t_n) + b^{kl}(t_n) + \Delta\rho_{MP,r}^{kl}(t_n) + \eta_r^{kl}(t_n) \end{aligned} \quad (2.4)$$

With such a combination of measurements, all receiver-based error-terms are eliminated, assuming that the measurements are in the same epoch. This affects the clock-error δt_r and the bias

b_r of receiver r . A disadvantage of this approach is the increased noise by a factor around $\sqrt{2}$. The same factor also affects the single-difference of the phase and Doppler-measurements.

The transmitted navigation-message of the satellite and a precise model about Earth tides lead to other known states. Now, all known terms can be transferred to the left-hand side of eqn. (2.4):

$$\begin{aligned}
\tilde{\rho}_r^{kl}(t_n + \delta t_r(t_n)) &:= \rho_r^{kl}(t_n + \delta t_r(t_n)) \\
&\quad - \vec{e}_r^k(t_n + \delta t_r(t_n))(\Delta \vec{x}_{ET_r}(t_n) - \vec{x}^k(t_n + \delta t_r(t_n)) - \Delta \vec{x}^k(t_n)) \\
&\quad - \vec{e}_r^l(t_n + \delta t_r(t_n))(\Delta \vec{x}_{ET_r}(t_n) - \vec{x}^l(t_n + \delta t_r(t_n)) - \Delta \vec{x}^l(t_n)) \\
&\quad - c\delta t^{kl}(t_n) - T_r^{kl}(t_n) \\
&= \vec{e}_r^{kl}(t_n + \delta t_r(t_n))\vec{x}_r(t_n + \delta t_r(t_n)) + I_r^{kl}(t_n) + \Delta T_r^{kl}(t_n) + b^{kl}(t_n) \\
&\quad + \Delta \rho_{MP,r}^{kl}(t_n) + \eta_r^{kl}(t_n)
\end{aligned} \tag{2.5}$$

The linear combination of the phase measurement in eqn. (2.6) causes also an elimination of error-terms [7]:

$$\begin{aligned}
\lambda \varphi_r^{kl}(t_n + \delta t_r(t_n)) &= \lambda \varphi_r^k(t_n + \delta t_r(t_n)) - \lambda \varphi_r^l(t_n + \delta t_r(t_n)) \\
&= \vec{e}_r^k(t_n + \delta t_r(t_n))(\vec{x}_r(t_n + \delta t_r(t_n)) + \Delta \vec{x}_{ET_r}(t_n) - \vec{x}^k(t_n + \delta t_r(t_n)) - \Delta \vec{x}^k(t_n)) \\
&\quad - \vec{e}_r^l(t_n + \delta t_r(t_n))(\vec{x}_r(t_n + \delta t_r(t_n)) + \Delta \vec{x}_{ET_r}(t_n) - \vec{x}^l(t_n + \delta t_r(t_n)) - \Delta \vec{x}^l(t_n)) \\
&\quad + c\delta t^{kl}(t_n) + T_r^{kl}(t_n) - I_r^{kl}(t_n) + \lambda N_r^{kl} + \frac{\lambda}{2}\Delta N_r^{kl}(t_n) + \lambda \beta^{kl}(t_n) \\
&\quad + \lambda \Delta \varphi_{PW,r}^{kl}(t_n) + \lambda \Delta \varphi_{PCO,r}^{kl}(t_n) + \lambda \Delta \varphi_{MP,r}^{kl}(t_n) + \varepsilon_r^{kl}(t_n)
\end{aligned} \tag{2.6}$$

Known terms are also brought on the left-hand side again:

$$\begin{aligned}
\lambda \tilde{\varphi}_r^{kl}(t_n + \delta t_r(t_n)) &:= \lambda \varphi_r^{kl}(t_n + \delta t_r(t_n)) \\
&\quad - \vec{e}_r^k(t_n + \delta t_r(t_n))(\Delta \vec{x}_{ET_r}(t_n) - \vec{x}^k(t_n + \delta t_r(t_n)) - \Delta \vec{x}^k(t_n)) \\
&\quad + \vec{e}_r^l(t_n + \delta t_r(t_n))(\Delta \vec{x}_{ET_r}(t_n) - \vec{x}^l(t_n + \delta t_r(t_n)) - \Delta \vec{x}^l(t_n)) \\
&\quad - c\delta t^{kl}(t_n) - T_r^{kl}(t_n) - \lambda \Delta \varphi_{PW,r}^{kl}(t_n) - \lambda \Delta \varphi_{PCO,r}^{kl}(t_n) \\
&= \vec{e}_r^{kl}(t_n + \delta t_r(t_n))\vec{x}_r(t_n + \delta t_r(t_n)) - I_r^{kl}(t_n) \\
&\quad + \lambda N_r^{kl} + \frac{\lambda}{2}\Delta N_r^{kl}(t_n) + \lambda \beta^{kl}(t_n) + \lambda \Delta \varphi_{MP,r}^{kl}(t_n) + \varepsilon_r^{kl}(t_n)
\end{aligned} \tag{2.7}$$

A Doppler-frequency can also be tracked. The single-difference (SD) Doppler measurement is modeled as [7]

$$\begin{aligned}
f_D^{kl}(t_n) &= f_D^k(t_n) - f_D^l(t_n) \\
&= -\frac{f_T}{c} \left(\vec{e}_r^k(t_n)(\vec{v}_r(t_n) - \vec{v}^k(t_n)) - \vec{e}_r^l(t_n)(\vec{v}_r(t_n) - \vec{v}^l(t_n)) \right) + f_T \delta \dot{\tau}^{kl}(t_n) + \eta_{D_r}^{kl}(t_n)
\end{aligned} \tag{2.8}$$

The known terms come to the left-hand side of the equation (2.8):

$$\begin{aligned}
\tilde{f}_D^{kl}(t_n) &= f_D^{kl}(t_n) - \frac{f_T}{c} \left(\vec{e}_r^k(t_n)\vec{v}^k(t_n) - \vec{e}_r^l(t_n)\vec{v}^l(t_n) \right) - f_T \delta \dot{\tau}^{kl}(t_n) \\
&= -\frac{f_T}{c} \vec{e}_r^{kl}(t_n)\vec{v}_r(t_n) + \eta_{D_r}^{kl}(t_n)
\end{aligned} \tag{2.9}$$

The single-difference (SD) of pseudorange, carrier phase- and Doppler-measurement is also possible between two receivers and only one satellite. With this model, all error-terms, which depend on a satellite k , are eliminated. It should be noted that this special single-difference (SD) model is not closer discussed here, because it is not used in the thesis.

2.3 Double-difference (DD) measurement

A linear combination of satellite k , reference-satellite l and two receivers (index: 1 and 2) describes a further possibility of differentiating measurements (see figure 2.1). Through this step, all error terms depending on receivers and satellites are eliminated. A big disadvantage is the loss of the absolute position information. There remains only the relative position in terms of the baseline $\vec{b}_{12}(t_n) = \vec{x}_1 - \vec{x}_2$, thus the vector of receiver 2 to receiver 1 (see appendix A). The measurement noise is again increased by a factor of $\sqrt{2}$.

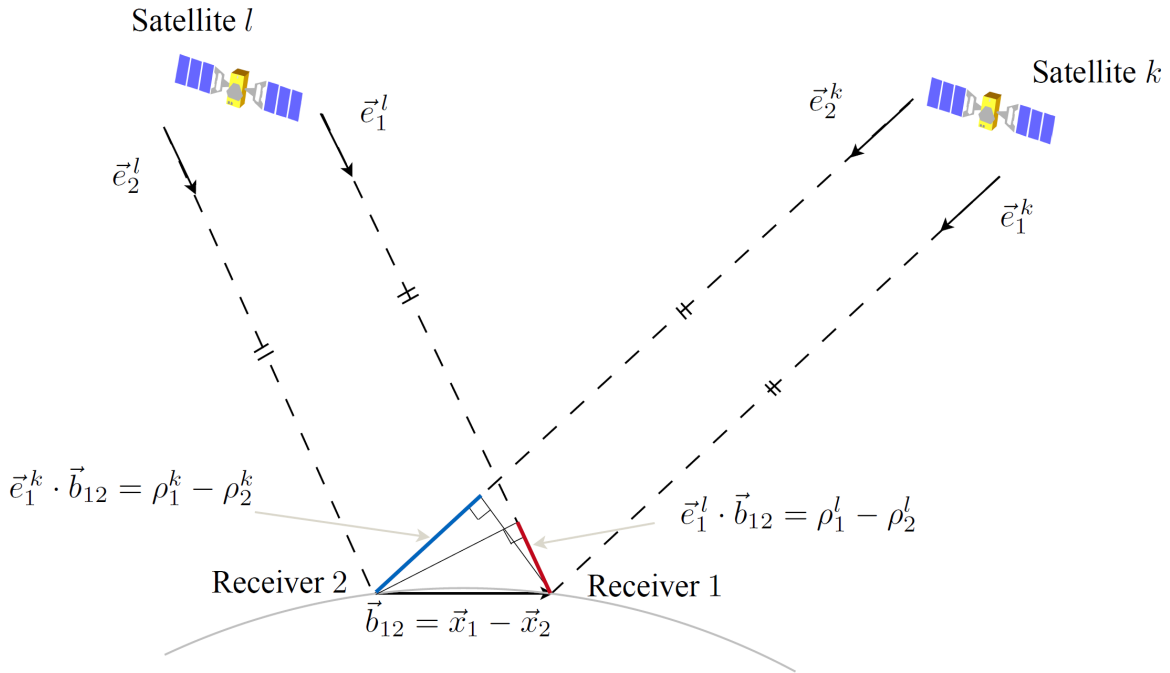


Figure 2.1: A double-difference linear combination with the baseline \vec{b}_{12} . [8]

The measurement-model for a double-difference (DD) pseudorange is described in eqn. (2.10) as follows [9]:

$$\begin{aligned}
 \tilde{\rho}_{12}^{kl}(t_n) &= \tilde{\rho}_1^{kl}(t_n) - \tilde{\rho}_2^{kl}(t_n) \\
 &= (\vec{e}_1^{kl}(t_n) - \vec{e}_2^{kl}(t_n))(\vec{x}_1(t_n) - \vec{x}_2(t_n)) + c_{12}^{kl}(t_n) + \Delta\rho_{MP,12}^{kl}(t_n) + \eta_{12}^{kl}(t_n) \quad (2.10) \\
 &= \vec{e}_{12}^{kl}(t_n)\vec{b}_{12}(t_n) + c_{12}^{kl}(t_n) + \Delta\rho_{MP,12}^{kl}(t_n) + \eta_{12}^{kl}(t_n)
 \end{aligned}$$

In the double-difference, the movement of both receivers and the satellites between the clock-offset $\delta t_1(t_n) - \delta t_2(t_n)$ must be considered. For this purpose we introduce the parameter c_{12}^{kl} as synchronization-correction. The derivation is explained in a later step in this thesis, as this correction compensates also a further error in the RTK with virtual reference-station (VRS).

The double-difference measurement for the phase is described in eqn. (2.11) [9]:

$$\begin{aligned}
\lambda\tilde{\varphi}_{12}^{kl}(t_n) &= \lambda\tilde{\varphi}_1^{kl}(t_n) - \lambda\tilde{\varphi}_2^{kl}(t_n) \\
&= (\vec{e}_1^{kl}(t_n) - \vec{e}_2^{kl}(t_n))(\vec{x}_1(t_n) - \vec{x}_2(t_n)) + c_{12}^{kl}(t_n) + \lambda N_{12}^{kl} + \frac{\lambda}{2}\Delta N_{12}^{kl}(t_n) \\
&\quad + \lambda\Delta\varphi_{MP,12}^{kl}(t_n) + \varepsilon_{12}^{kl}(t_n) \\
&= \vec{e}_{12}^{kl}(t_n)\vec{b}_{12}(t_n) + c_{12}^{kl}(t_n) + \lambda N_{12}^{kl} + \frac{\lambda}{2}\Delta N_{12}^{kl}(t_n) + \lambda\Delta\varphi_{MP,12}^{kl}(t_n) + \varepsilon_{12}^{kl}(t_n)
\end{aligned} \tag{2.11}$$

2.4 Triple-difference (TD) measurement

This thesis includes also the triple-difference measurement in a few implementations. With the differentiating over two subsequent epochs, the state of integer ambiguities is eliminated for this triple-difference measurement-model [9].

$$\begin{aligned}
\Delta\lambda\tilde{\varphi}_{12}^{kl}(t_{n+1}) &= \lambda\tilde{\varphi}_1^{kl}(t_{n+1}) - \lambda\tilde{\varphi}_2^{kl}(t_n) \\
&= \vec{e}_{12}^{kl}(t_{n+1})\Delta\vec{b}_{12} + \Delta c_{12}^{kl}(t_{n+1}) + \frac{\lambda}{2}\Delta N_{12}^{kl}(t_{n+1}) + \lambda\Delta\varphi_{MP,12}^{kl}(t_{n+1}) + \Delta\varepsilon_{12}^{kl}(t_{n+1})
\end{aligned} \tag{2.12}$$

With this step, the relative position \vec{b}_{12} of the receiver-pair is eliminated. It stays in principle only the change of baseline $\Delta\vec{b}_{12}$. The multipath $\lambda\Delta\varphi_{MP,12}^{kl}$ and the change of the synchronization-correction Δc_{12}^{kl} between the epochs are negligible. The biggest advantage of the triple-difference measurement lies in a possible detection of phase-jumps (cycle-slips), which are especially for low-cost receivers a critical point. In case of a static system, the triple-difference is in normal-case the phase multipath and phase noise. Therefore, if this measurement contains a multiple of a half wavelength, cycle-slips occurred in this epoch. As one can see, this differentiating is elementary for a possible cycle-slip-correction (CSC).

2.5 Measurement model of the IMU

Inertial sensors are able to provide the acceleration and rotation-rate in a much higher data-rate as it is possible with today's low-cost GPS receivers. A further positive aspect is the independency of the measurements from signal-strength and urbanity (buildings, trees, etc.). This aspects leads to a reliable prediction of the position, velocity and attitude within a short time-range in GPS-signal outages. Another aspect is the reliable detection and correction of cycle-slips in dynamic systems. The three-dimensional acceleration and rotation-rate is measured in a sensor-fixed (s-) frame, which is centered on the sensor-chip and aligned on the principle axes of the chip. We assume here, that the s-frame is aligned with the body-fixed (b-) frame. The b-frame provides the center-point of the vehicle and is aligned with the longitudinal- and transversal-axes of the vehicle.

Due to different frames for GNSS and INS, a frame-transformation is necessary. In this thesis, the e-frame (ECEF) is used for sensor-fusion. This frame is centered at the earth-center, by which the x-axis is in equatorial-plane along the 0-degree-meridian and the z-axis along the geographical north-pole aligned. The navigation (n-) frame is centered in the vehicle center of gravity and points along the north-, east- and down-direction. In this case, the n-frame represents the reference-frame for the attitude of the vehicle.

Accelerometer-measurements are provided in the b-frame and according to Jekeli in [10] described as

$$a^b(t_n) = R_n^b(t_n)R_e^n(t_n)a^e(t_n) + b_a^b(t_n) + g \begin{pmatrix} \sin(\theta(t_n)) \\ \cos(\theta(t_n))\sin(\varphi(t_n)) \\ \cos(\theta(t_n))\cos(\varphi(t_n)) \end{pmatrix} + \varepsilon_a^b(t_n) \quad (2.13)$$

with the rotation matrices R_n^b and R_e^n , the acceleration a^e in the e-frame, the acceleration biases b_a^b of the sensor in the b-frame, the gravitational acceleration g , the pitch angle θ , the roll angle φ and the measurement noise ε_a^b .

The rotation from the e-frame into the n-frame depends on the latitude φ_1 and longitude λ_1 of receiver 1 and is given by

$$R_n^e(t_n) = R_1(\pi/2 - \varphi_1(t_n))R_3(\pi/2 + \lambda_1(t_n)) \quad (2.14)$$

The rotation from the n-frame into the b-frame depends on the heading ψ and pitch θ of the vehicle and is given by

$$R_b^n(t_n) = R_2(-\theta(t_n))R_3(\pi/2 - \psi(t_n)) \quad (2.15)$$

The gyroscope senses the angular rates ω_{ib}^b of the body-fixed (b-) frame with respect to the inertial (i-) frame in the b-frame. The angular rate measurements can be expressed as the sum of ω_{in}^b , ω_{nb}^b , a bias $b_{\omega_{ib}}^b$ and a noise $\eta_{\omega_{ib}}^b$, i.e.

$$\omega_{ib}^b(t_n) = R_n^b(t_n)\omega_{in}^n(t_n) + \omega_{nb}^b(t_n) + b_{\omega_{ib}}^b(t_n) + \eta_{\omega_{ib}}^b(t_n) \quad (2.16)$$

The angular rates ω_{nb}^b are related to the rates of the Euler-angles according to Jekeli in [10] as

$$\begin{aligned} \omega_{nb}^b &= R_1(\varphi)R_2(\theta) \begin{pmatrix} 0 \\ 0 \\ \dot{\psi} \end{pmatrix} + R_1(\varphi) \begin{pmatrix} 0 \\ \dot{\theta} \\ 0 \end{pmatrix} + \begin{pmatrix} \dot{\varphi} \\ 0 \\ 0 \end{pmatrix} \\ &= \begin{pmatrix} 1 & 0 & -\sin(\theta) \\ 0 & \cos(\varphi) & \cos(\theta)\sin(\varphi) \\ 0 & -\sin(\varphi) & \cos(\theta)\cos(\varphi) \end{pmatrix} \begin{pmatrix} \dot{\varphi} \\ \dot{\theta} \\ \dot{\psi} \end{pmatrix} \end{aligned} \quad (2.17)$$

with $R_i(\alpha)$ being a rotation around the i -th axis by an angle α . The rotation ω_{in}^n of the navigation frame with respect to the inertial frame depends on the latitude φ_1 , the rates $\dot{\varphi}_1, \dot{\lambda}_1$ of latitude and longitude, and the Earth rotation rate ω_e , and is given by Jekeli [10] as

$$\omega_{in}^n = \begin{pmatrix} (\dot{\lambda}_1 + \omega_e)\cos(\varphi_1) \\ -\dot{\varphi}_1 \\ -(\dot{\lambda}_1 + \omega_e)\sin(\varphi_1) \end{pmatrix} \quad (2.18)$$

2.6 Network-RTK with a virtual reference-station (VRS)

Network RTK allows a wider separation of reference stations than conventional RTK as the ionosphere gradients are determined and used to extrapolate the corrections to the VRS location. A service-provider operates a net of reference-stations, which processes the measurements of all his stations in real-time and provides the calculated correction-data over one or more communication-channels (3G/4G) for potential users. With the help of this technique, an accuracy in centimeter-level for real-time positioning with only one GNSS-receiver is possible. [11]

2.6.1 Motivation for implementing a Network-RTK

In order to provide centimeter precise real-time positioning with only low-cost receivers for use-cases like the autonomous driving, we need other solutions as the normal RTK-technique with only a fixed reference-station. The Real-Time-Kinematic, which means centimeter precise real-time positioning based on the phase-measurement with fixed ambiguities, works only reliable in a narrowly limited place around the fixed reference-station. A maximum distance between reference-station and user is in the range of 5 to 20 km. The main reason for this limitation is caused by the influence of the ionospheric delay for relative observations (reference-station and vehicle). In case of higher distances, a reliable fixing of the ambiguities is not reachable, what leads to a negative achievement of the required positioning accuracy. With this knowledge of the dependency of the distance to the reference-station, a comprehensive service with only the old technique is not realizable.

If one extends the RTK-approach to a Network-RTK, which means a precise positioning is no longer based on only one reference station but in relation to a net of surrounding reference stations (see figure 2.2), the distance can be largely extended. A space of 50 km between the reference-stations meet the requirements for precise real-time positioning. This allows the provider to integrate fewer reference-stations in comparison to the traditional RTK, what leads to a possibility for a widespread implementation for the autonomous driving.

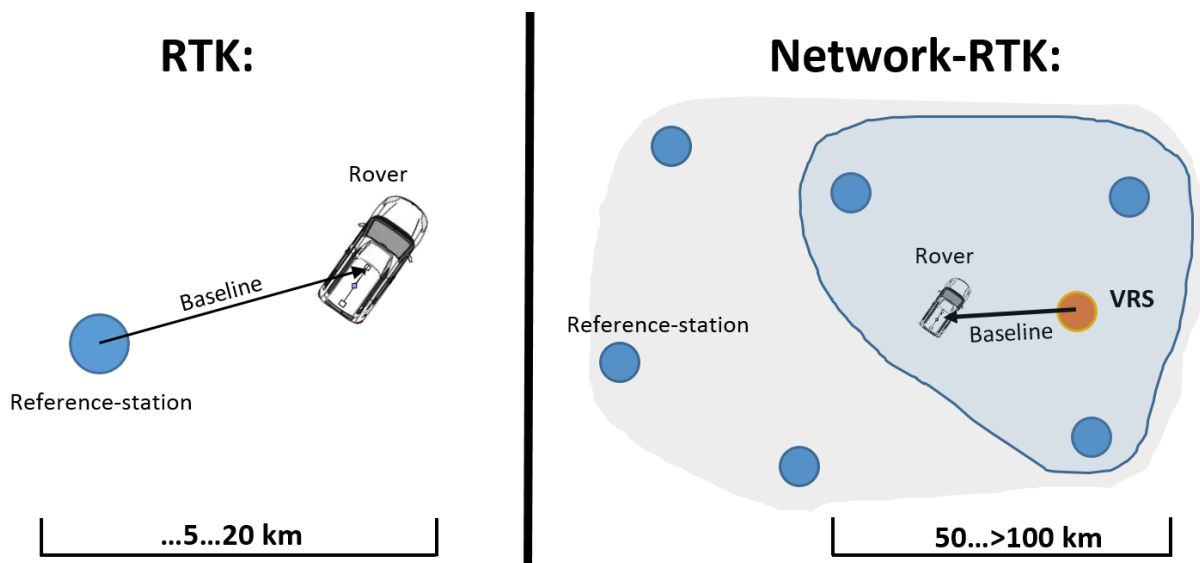


Figure 2.2: The principle of RTK and Network-RTK.

2.6.2 The general concept of a Network-RTK

The limitation of RTK to the close range around the reference-station is caused by the influence of range-depended error-terms like the ionospheric and tropospheric refraction. As it was already pointed out, the starting point is to capture now the error-terms in a correction-model to increase the possible space between the reference-stations. The correction values should have an accuracy of 1 cm. This mark is only reachable with phase-measurements, so the ambiguities have to be fixed.

The concept of the correction-model is the interpolation of the range-depended error-terms within the net of reference-stations. With the help of these values, corrections for arbitrary baseline-vectors in the area of the reference-stations are generated. A typical application is the calculation of correction-values for the baseline between the selected master-reference-station and the position-approach of the user, calculated with the help of pseudorange measurements. A minimum count of three reference-stations for modeling the error-terms is necessary. Are more stations available, a joint modeling of the parameters with all allocated reference-stations is performed. Another way is to calculate different models for subnets. [11]

The necessary data-processing, based on the measurement-data of the reference-stations and the receivers of the vehicle, leads to following steps (see also figure 2.3) :

1. transmission of the recorded data of each reference-station to the master-station
2. fixing of the double-difference ambiguities of the phase-measurement (dual-frequency receivers) in real-time and also for satellites with low elevation
3. determination of correction-parameter with interpolation
4. determination of correction with respect to the position of the vehicle
5. precise calculation of the vehicle-position with the help of the transmitted correction data

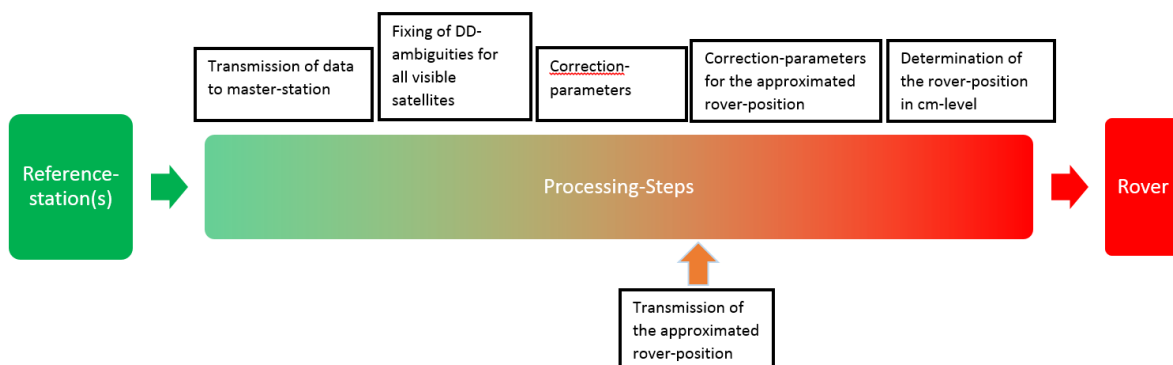


Figure 2.3: Processing-steps for the network-RTK

2.6.3 The different concepts in detail

The existing approaches of network-RTK differ especially in the division of data-processing-steps between central data-processing in a data-center of a reference-station network and de-central

in the vehicle respectively on user-side. This split of data-processing-steps has a direct impact in terms of data-content, data-size, format and communication-linking between the data-center and the user.

The following concepts describe an Observation-State-Representation (OSR). For this purpose, all reference-stations, satellites, frequencies and signals (phase-measurement and pseudorange) form in each case observation-models, for which the approximated position of the vehicle for a precise solution of the position is needed. For OSR are the following methods possible:

Master-Auxiliary-Concept (MAC): In this method, the communication takes place in form of reference-station observations, which are used in a pre-processing step to fix the ambiguities of all reference-stations. Hence the critical step is done in the data-center, where all information respectively measurements of the past epochs are. The naming of the concept derives from the method to transmit the reference-station observations: the observations of the master-station in form of complete corrections, and in contrast the observations of further reference-stations (auxiliary-stations) as correction-differences against the master-station to minimize the data-content. The vehicle respectively the user has now the choice, in which form the corrections for his special position are interpolated and what auxiliary-stations the user wants to use. This interpolation would not require considerable processing power, so the calculation can be done in the vehicle respectively on user-side. [11]

FKP Reference Station Information: The FKP(Flächenkorrekturparameter)-method is a further option of transmitting the information of the reference-station to the user. In this case, no approximated position of the vehicle is needed to get a suitable correction-data. The correction-parameters are implemented as gradients to determine a precise position of the vehicle. By using this concept, no bi-directional communication is needed. However, with this setting, the positioning-solution is not as accurate as if the approximated vehicle-position is transmitted to the service-provider. [12]

iMAX: The iMAX-method, developed by Leica Geosystems, calculates the correction-parameters with the help of the vehicle-position, comparable with MAC and VRS. In this implementation, however, no correction-data for the approximated position of the vehicle is calculated and interpolated. The data sent to the user contains here only the corrections, which are determined for the position of the reference-station and transmitted to the vehicle in compact form. [12]

Virtual Reference Station (VRS): The method with a virtual reference-station (VRS), developed by Trimble, calculates and interpolates the correction-parameter with respect to the approximated position of the vehicle, which is transmitted from the user to the data-center. This implementation is currently the most common and also used in this thesis. A big advantage is a user-friendly implementation to get and use the VRS-data. On the other hand, there is no chance to get information from the reference-station about the quality of interpolation. This aspect can complicate the fixing of the double-difference ambiguities for the RTK-Baseline (VRS to Vehicle)

As mentioned before, this thesis uses the VRS-method. The correction-data is transmitted to the vehicle over mobile-communication with a frequency of 1 Hz. *AXIO-NET - Satellite Positioning Services*¹, a company with a reference-station-network in Germany, provides the correction-data for developing the network-RTK. With the help of the RTCM (Radio Technical Commission for Maritime Services)-format and the rough position of the vehicle, the interpolated phase-measurement and pseudorange, the GPS time-stamp and the position of the VRS are transmitted. This additional information will then finally be processed in real-time to improve the joint

¹Homepage: <http://www.axio-net.eu/>

position and attitude determination. The concept and the implementation for this improvement with VRS is closer described in the next chapters.

2.6.4 Limits and future of network-RTK

The limit of network-RTK was demonstrated in the years of 2000-2002 in the last peak of solar-activity. These extremes in the ionosphere caused big problems for the fixing of ambiguities in the reference-network. For such extreme ionospheric conditions, the reference-networks with smaller space between its stations have an advantage [11].

A further method for network-RTK is called State-Space-Representation (SSR). With this technique, there is no need for transmitting the rough vehicle-position, which would helpfully decrease the necessary transmission bandwidth. In the State-Space-Modeling, there are all physical effects with the help of mathematical models represented and are available again with this mathematical models for the user in real-time. The correction-parameters are all valid in the complete reference-network and are usable with models by the user. This relatively new approach is not aimed for precision improvements, but for the simplification of the infrastructure of network-RTKs (distance of reference-stations: 200 km) and for better integration-concepts in a user-system.

Also with a joint multi-satellite system of GPS, Glonass and Galileo, resulting in a huge number of satellites, are networks of reference-stations necessary. The satellite-individual modeling, especially for the ionosphere, improves the fixing of ambiguities for the baseline of user and reference-station. It will be faster and also more reliable.

Chapter 3

State of the Art

This chapter describes similar products and technologies on the market and compares them with the solution of the low-cost tight-coupled GPS/INS-system with virtual reference-station (VRS) from the company *Advanced Navigation Solutions – ANavS GmbH*, which is developed and also improved in this thesis. After the "State of the Art"-consideration of RTK-systems, the autonomous driving is also analyzed. Especially the current stage of development is described and the road-map becomes explained. An important point of view in this field is the role of joint position and attitude determination especially for the autonomous driving.

3.1 Consideration of a low-cost GPS/INS-system

The tight-coupling of GPS/INS with VRS in a low-cost equipment as in the present case, is rarely developed. RTK-systems in consideration of the same tight-coupling and precision uses mainly geodetic receivers coupled with ring-laser IMU's, whereby the application in an autonomous driving is not more cost-effective with such an equipment. In figure 3.1, a schematic market positioning of the tight-coupled *ANavS-Solution* is shown. Following is stated an overview about some developed systems, comparable with the low-cost solution in this thesis.

3.1.1 Piksi by the company Swift-Navigation

A system, comparable with the *ANavS-Solution*, is *Piksi* developed by Swift-Navigation¹. The hardware is based on a similar low-cost RTK-system as the *ANavS-Solution*, with only single-frequency receivers and an open-source software to process the raw-measurement data of GPS. The hardware-costs of this system are around 1.000 \$. It additionally provides a bluetooth-link for a data-link between the two receivers (reference-station and vehicle) of the RTK-system. A maximum accuracy of relative positioning with the help of phase-measurement is given with a few centimeters. After an initial hype by means of the crowd-funding platform Kickstarter² and newfound supporters for the project of this low-cost RTK-system, it's more quiet in the meantime.

The company *Swift-Navigation* is focusing by *Piksi* only on GPS-data without coupling with an IMU. In dynamic conditions, there are several disadvantages without an INS:

- the cycle-slip detection and correction is not reliable

¹Swift Navigation: San Francisco, CA 94107, USA, <http://www.swiftnav.com>

²<https://www.kickstarter.com/projects/swiftnav/piksi-the-rtk-gps-receiver?lang=de>

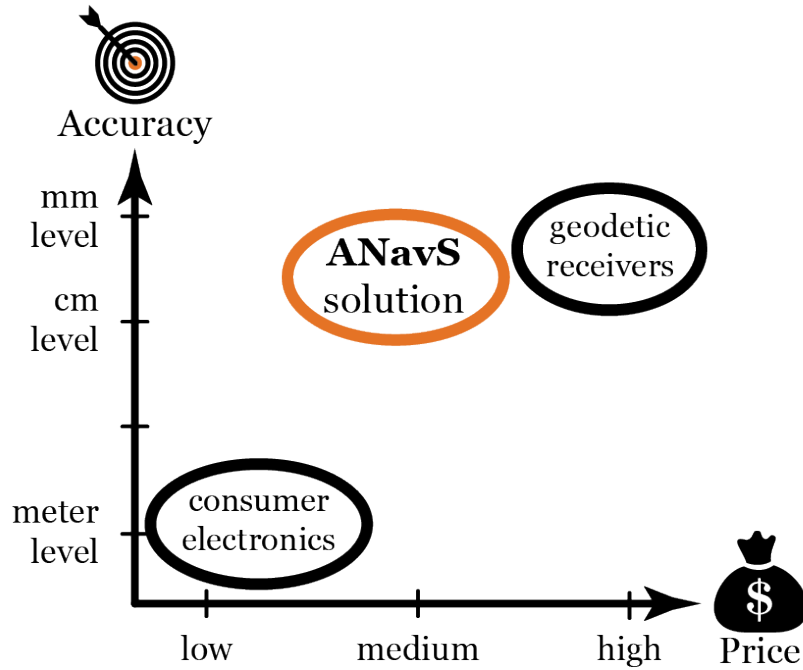


Figure 3.1: Market positioning of *Advanced Navigation Solutions – ANavS GmbH* plotted in a schematic sense

- the update-rate of states like the position and attitude without sensor-fusion by an IMU is lower
- no continuous respectively jump-free solution of the attitude and position is possible

As we see, the solution can't be so stable as with a tight-coupled system provided by *ANavS*, which is extended and improved for this work.

3.1.2 $i\mu$ VRU-01 by the company iMAR

iMAR³ is a leading company for inertial navigation systems (INS) for the military and aviation sector. Besides the expensive inertial systems for this special cases, there are also low-cost IMUs with a possible support for GPS, magnetometer, barometer and odometry. One of this modules is called $i\mu$ VRU-01. The data is also merged with a Kalman Filter and provides the parameters position, velocity and attitude.

Looking at the drift of the IMU with respect to rotation-rate, the system guarantees a high reliability and performance. Besides, the way of coupling is nearly the same as in this thesis. However, by consideration of the typical 1-sigma-values in the datasheet for position and heading, there is no chance to get the same performance as with the explained solution in this work and especially not enough accuracy and reliability for the implementation in the autonomous driving [13].

The reason for this discrepancy in accuracy and reliability lies on the processing of the data in the tight-coupling. As it is still common in the today's market-segment of low-cost navigation-systems, they don't process the real raw-data of the GNSS-receivers, but only the

³St. Ingbert, D-66386 Deutschland, <http://www.imar-navigation.de>

position-solution determined of the GNSS-chips alone without fixed ambiguities and therefore without phase-measurements. In a further step, the imprecise position-solution is given to the tight-coupled Kalman Filter (KF). A precise position-solution of the tight-coupled navigation-system in centimeter-range is not reachable with this approach.

3.1.3 Validation

The search for a comparable system with that from the company *Advanced Navigation Solutions – ANavS GmbH* has been proved to be very difficult. Especially the aspect of a low-cost equipment, what makes this system suitable for the mass market, excludes a huge amount of comparable (in terms of accuracy and reliability) systems. The described systems were deliberately chosen to show other possibilities realized in other systems. Following the detailed analysis of the market, one can say there is no comparable product respectively software developed till now, which reaches the required performance in accuracy and reliability for the joint position and attitude determination for the autonomous driving.

3.2 Consideration of the autonomous driving

As mentioned before, the main application of this thesis with the topic *Joint RTK and Attitude Determination* is for the autonomous driving. The question is now, why one needs the precise position in centimeter-level and also the attitude of the vehicle.

At the beginning, the terminology is explained: the road-map, communicated from the automobile manufacturers, describes the way to the autonomous driving (see figure 3.2). The important point is, how far the driver is needed to control the car. The next goal for series production is the semi-autonomous driving, which should come in the next few years. In this case, the driver must always be able to interfere. In other words, the driver has both hands on the steering and can react respectively over-steer the system in special cases. This assistant would be usable mainly on the highway. In case of the high-autonomous driving, the driver is allowed to do other things like phoning or tuning the radio. However there is also a way given to over-steer the system, or to enable the driver to react in a limited time-range to steer the car, in a case where the system detects difficulties. A course through the city should be no problem with a high-autonomous system. If the automobile manufacturers reach the full-autonomous system, the driver must not sit behind the steering wheel. A possibility to over-steer the system is not given from the system to the operator.

According to the automobile manufacturers, the semi-autonomous driving is mature in technological sense and in the year 2016 ready for series production. For the last two steps, the high- and full-autonomous, are still technological questions to be answered. Prognoses, like the ones created by the manufacturers, are not reliable and can't be treated as fix time-stamps.

In the first technological step of developing a semi-autonomous car, the environmental conditions were treated and modeled. With the help of laser-scanners to measure the distance, several video-cameras and also a lot of ultrasonic- and radar-sensors, the nearest environment of the car is analyzed and actions like braking, steering and accelerating are done by the semi-autonomous system. For reaction and interaction with other road users, this sensor-system is obviously essential. Also to detect and interpret traffic signs, these sensors are needed.

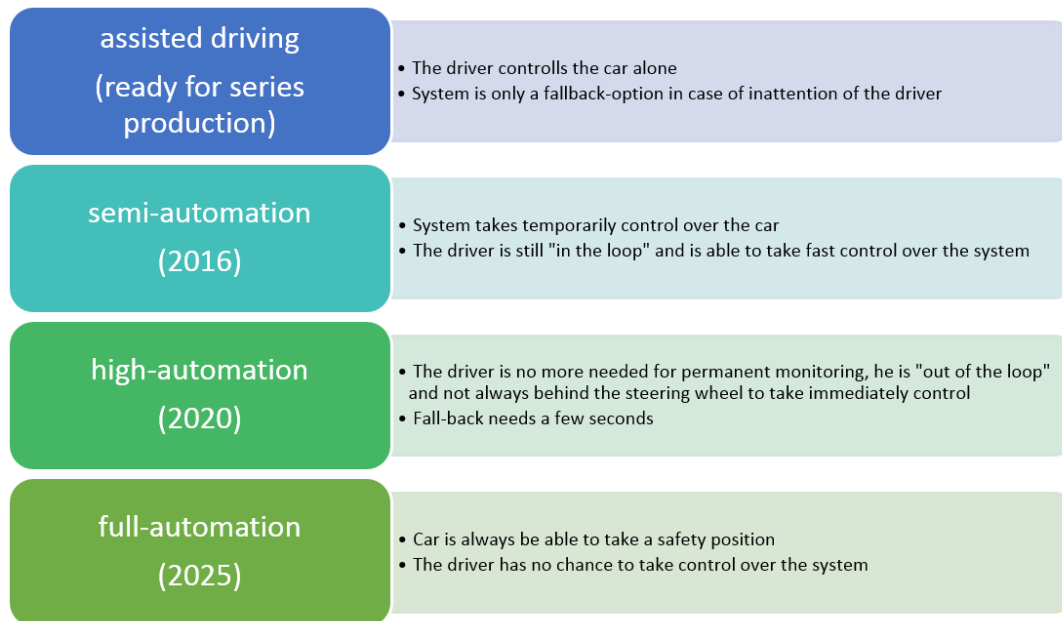


Figure 3.2: Roadmap to the autonomous driving. Especially the distribution of tasks between human and machine is given here. [14]

Now to the question why a precise absolute position for the high- and full-autonomous driving is needed and will also take an important role in the future:

- Every sensor-system respectively parameter in such a safety-application, as the autonomous driving surely is, must be proven with redundancy. Let's take the example of a lane departure warning system (LDW). In the current technology, the information for this system comes only from the lane-markings. But what happens, if there is a new street without markings or if the markings are not detectable in case of snow, rain or sun. A solution respectively a redundant and independent information for this parameter provides the precise absolute position. This state can (only) be determined with a satellite-system, which is explained in this thesis. With the information of the true and accurate position, the track on the road can be determined with the help of (offline-)maps. Liu et al. described in [15] an approach for vehicle lane-change estimation based on GNSS/INS. The assistance-system shows a great potential in application for the autonomous driving.
- If the precise absolute position of the car is known, a feature is also the transmission of additional information over the mobile-network. The information contains, for example, the different traffic signs along the track or on crossroads. This leads to an easier matching of the environment or to an easier detection of traffic-signs in terms of processing power and reliability.
- There is a better chance to get reliable models of prediction. To get an usable high- or full-autonomous system for long roads, an information of the roadway is hereby necessary. With an (online) data-link to infrastructure-systems, with other cars or in the best case with both, this can be improved.
- Critical situations can be detected and solved with the help of Car-to-Car communication. The known absolute position of all cars in an area helps, for example, to plan a secure overtaking maneuver. The optical systems, like cameras, have in such situations the problem, that they can't detect oncoming cars in front of the vehicle, which is part of the

overtaking maneuver. Hazard points behind curves, which are not detectable by optical sensor-systems, can be disarmed with such a communication-link.

- Ultra-precise maps can be automatically measured or created in consideration of lane-separation with the help of data for the precise absolute position of the whole traffic. Through this, map-updates could be done in real-time, which is a great benefit for the autonomous system.

3.2.1 Validation

In this chapter, important aspects for introducing the parameters of absolute position and attitude in an autonomous car have been explained. The question is now, is the GPS/INS sensor-system with correction-data a perfect deal for the autonomous driving. The relation between price and performance is a critical point of view. For a mass-market application in the automotive sector, there is no chance to use geodetic receivers and ring-laser IMUs. Low-cost sensor-systems, paired with intelligent, innovative sensor-fusion, special algorithms to improve the accuracy and real-time management can close this technological gap and make it usable for a mass market like the automotive sector is.

Chapter 4

Modeling and concept of a joint RTK and Attitude determination

The company *Advanced Navigation Solutions – ANavS GmbH* is developing software for a precise position- and attitude determination with low-cost GNSS-receivers (ublox) and low-cost inertial-sensors. The measurements of both sensors are tightly coupled in an (extended) Kalman filter. A special feature of the *ANavS*-solution is the estimation of multipath in static conditions, what leads to higher accuracy and reliability for fixing the attitude- and RTK-baseline.

This thesis deals with the integration of phase-measurements and pseudo-ranges of a virtual reference station (VRS) in a tightly coupled GPS/INS-system with position and attitude determination and also describes improvements of the existing tight-coupling. The VRS-data makes the error-correction of the ionosphere, troposphere, satellite-orbit and satellite-clock-offset possible. With such a system, one can get a precise absolute position determination only with low-cost receivers. A centimeter accuracy should be achievable under normal conditions. The goal of this work is to gain a correct position in the range of 1 m at any time. This should be given in a test-drive through the inner city and also along the highway. The termination of 1 m is for the reason of detecting the correct lane along the road. For comparison, Schubert et al. showed in [16] a position accuracy of 2.19 m with nearly the same test-equipment, the use of an extended Kalman filter and the help of DGPS.

The developed algorithms were tested with recorded datasets from Volkswagen on 11.11.2014. The setup is shown in figure 4.1: two low-cost patch-antennas were attached on the roof along the longitudinal axis of the car and connected with two u-blox LEA 6T-receivers. The distance between both antennas was 1.20 m. In addition, the corrected pseudo-range and phase-measurement of a virtual reference station is received. In the car trunk was stowed the IMU-SARA, which records the acceleration- and rotation-rate-measurements.

The following chapter explains the concept of the tight-coupling of GPS, VRS and IMU measurements to get a joint RTK and attitude determination. As mentioned before, the measurements of all sensors are coupled in an extended Kalman filter. This means, the absolute position and attitude is directly derived from the raw-data of all measurements (i.e. pseudo-range, phase-measurement, Doppler-measurement, acceleration- and rotation-rate-measurement). The GPS- and INS raw-data are measured with different update-rates and with different timestamps, i.e. not triggered in a synchronized way. If a measurement is available, the algorithm takes it to update the parameters of the state-vector (position, velocity, acceleration, attitude, rotation-rate, etc.). Figure 4.2 describes the alternating update-steps of the state-vector in a schematic sense. The correction-data are used as additional measurements in the GPS update-step.

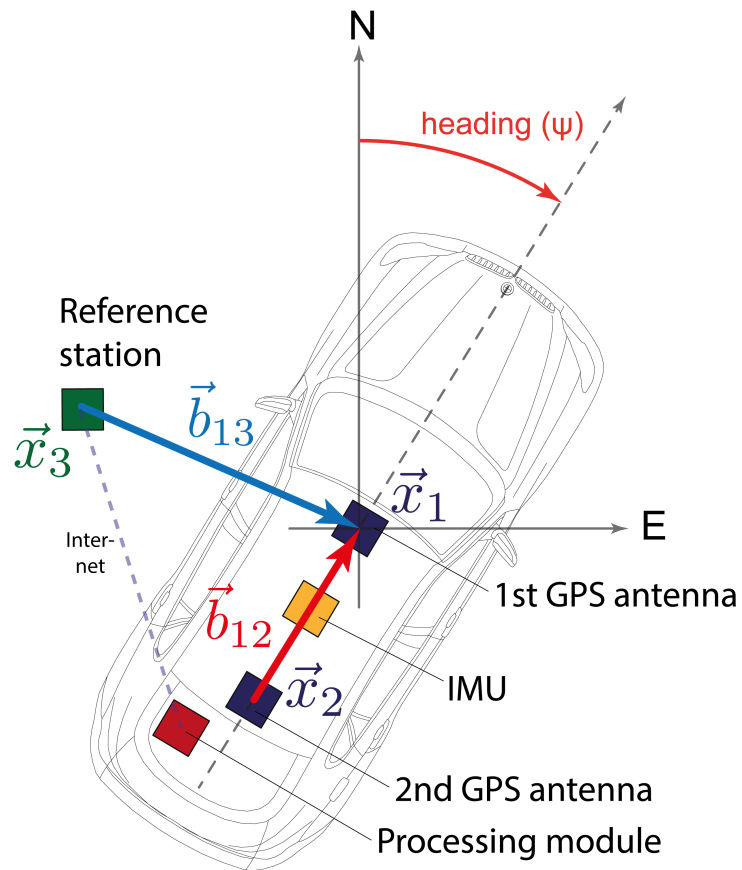


Figure 4.1: The setup of the test-drives with a virtual reference-station in a schematic sense

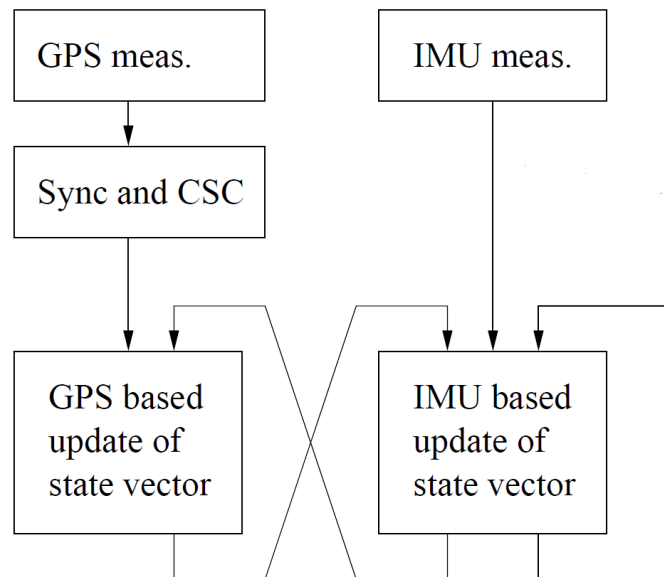


Figure 4.2: Flow-chart of the tight-coupling with GPS and IMU measurements

The measurements of the inertial sensors support the coupling in different ways: First of all, the IMU provides the possibility of detection and correction of phase-jumps. INS-measurements also allow the determination of position and attitude in conditions, where no GNSS-signal can be received. The last advantage is the significantly higher update-rate of IMU-measurements against the raw-data of GPS.

4.1 Modeling with an extended Kalman filter (EKF)

To link measurement-data and a-priori information with the help of movement-models, one can use an extended Kalman filter. Within the mathematical estimation theory, the Kalman Filter is a Bayesian minimum variance estimator for linear stochastic systems in state-space formulation. A big advantage of this filter is the real-time ability. The states, which change hereby continuously, are estimated respectively updated for every epoch with the help of the measurements. To get optimal estimates, deterministic and statistic properties of the system and the measurements are taken into account.

The basics of Kalman filters are described in the following. Hereby we already set the special models of the tight-coupled GPS/INS-system with VRS for explanations into account. The choice of the approximated models is not arbitrary, but depends especially on the (stochastic) distribution of the sensor measurements. Basics for statistics are required in this thesis, but not further explained. A good introduction in this topic is given by the papers of Maybeck in [17]. Jekeli shows in [10] the basic formulations of an extended Kalman filter.

4.1.1 State-space-model

The modeling of a movement-equation describes the transition between two subsequent epochs. The descriptive function for the change in every iteration is a linear function, which is dependent on the state-vector.

In a matrix-vector notation, the state-space-model is given as

$$x_n^- = \Phi_{n-1} x_{n-1}^+ + w_n \quad (4.1)$$

with x_{n-1}^+ as state-vector in epoch $n-1$, Φ_{n-1} as transition-matrix in epoch $n-1$, x_n^- as predicted state-vector and w_n as process-noise. The process-noise is assumed to be Gaussian distributed, white and mean-free (eqn. 4.2).

$$w_n \sim \mathcal{N}(0, Q_n) \quad (4.2)$$

The covariance-matrix of the process-noise for epoch n is given as

$$Q_n = E[w_n w_n^T] \quad (4.3)$$

The model for the transition-matrix is most of the time constant, only the different time-integrations can vary.

For example, in eqn. 4.4 the state-vector for the tight-coupling of GPS/INS with VRS is given:

$$x = \left(\begin{array}{c} \vec{b}_{13} \\ \vec{v}_1 \quad (= \dot{\vec{b}}_{13}) \\ \vec{a}_1 \quad (= \ddot{\vec{b}}_{13}) \\ \hline \psi \\ \dot{\psi} \\ \theta \\ \dot{\theta} \\ \varphi \\ \dot{\varphi} \\ \hline N_3^{kl} - I^{kl} + \beta^{kl} \\ N_{13}^{kl} \\ N_{12}^{kl} \\ \hline \Delta\rho_{MP,1}^{kl} + I^{kl} + b^{kl} \\ \Delta\rho_{MP,2}^{kl} + I^{kl} + b^{kl} \\ \Delta\rho_{MP,3}^{kl} + I^{kl} + b^{kl} \\ \hline b_\omega \\ b_a \end{array} \right) \quad (4.4)$$

The meaning of the different states and the dimensionality:

\vec{b}_{13}	relative position (RTK-baseline) of receiver 1 and 3 (VRS) [m]	3x1
\vec{v}_1	velocity of receiver 1 [m/s]	3x1
\vec{a}_1	acceleration of receiver 1 [m/s ²]	3x1
ψ	heading of the vehicle [rad]	1x1
$\dot{\psi}$	heading-rate of the vehicle [rad/s]	1x1
θ	pitch of the vehicle [rad]	1x1
$\dot{\theta}$	pitch-rate of the vehicle [rad/s]	1x1
φ	roll of the vehicle [rad/s]	1x1
$\dot{\varphi}$	roll-rate of the vehicle [rad/s]	1x1
$N_3^k - I^{kl} + \beta^{kl}$	SD ambiguities of the receiver 3 (VRS) (combined with ionosphere-delay and bias) [Cycles]	32x1
N_{13}^{kl}	DD ambiguities of receiver 1 and 3 (VRS) [Cycles]	32x1
N_{12}^{kl}	DD ambiguities of receiver 1 and 2 [Cycles]	32x1
$\Delta\rho_{MP,1}^{kl} + I^{kl} + b^{kl}$	SD code-multipath of receiver 1 (combined with ionosphere-delay and bias)) [m]	32x1
$\Delta\rho_{MP,2}^{kl} + I^{kl} + b^{kl}$	SD code-multipath of receiver 2 (combined with ionosphere-delay and bias)) [m]	32x1
$\Delta\rho_{MP,3}^{kl} + I^{kl} + b^{kl}$	SD code-multipath of receiver 3 (combined with ionosphere-delay and bias)) [m]	32x1
b_ω	bias of the gyroscope [rad/s]	3x1
b_a	bias of the accelerometer [m/s ²]	3x1

The state-vector includes all states, which are relevant for the tight-coupled system respectively for the modeling of the measurement-models. A closer look at the parameters follows in the next chapter. The dimensionality of 32 for the ambiguities and multipath is the result of the maximum count of visible satellites. By extending to a multi-GNSS-system (GPS, Glonass, Galileo), in accordance with the higher count of satellites, the vector of ambiguities and multipath is increasing.

In case of different update-rates of the measurements of GPS, VRS and IMU, and, also not interrupt-triggered, not all states can be updated in every epoch. It depends on the available measurements for the current epoch. To describe the selection, which states and measurements are updated respectively used, the notation with $s_n^x(y_n, x_n)$ is introduced. Measurements from GPS get the identifier $y_n = 1$ and from the IMU $y_n = 2$. With this specification, the state-update can be clearly defined for every epoch (see the eqn. 4.5 and eqn. 4.6).

$$s_n^x(1, x_n) = \left[\vec{b}_{13}, \vec{v}_1, \vec{a}_1, \psi, \dot{\psi}, \theta, \dot{\theta}, \varphi, \dot{\varphi}, N_3^k - I^{kl} + \beta^{kl}, \Delta\rho_{MP,1}^{kl} + I^{kl} + b^{kl}, \Delta\rho_{MP,2}^{kl} + I^{kl} + b^{kl}, \Delta\rho_{MP,3}^{kl} + I^{kl} + b^{kl}, b_\omega, b_a \right]^T \quad (4.5)$$

$$s_n^x(2, x_n) = \left[\vec{b}_{13}, \vec{v}_1, \vec{a}_1, \psi, \dot{\psi}, \theta, \dot{\theta}, \varphi, \dot{\varphi}, b_\omega, b_a \right]^T \quad (4.6)$$

4.1.2 The observation-model

The observation-model describes the dependency of each measurement of the sensors in comparison with the state-vector. This includes the modeled parameters and the unpredictable measurement-noise. If one uses a Kalman filter, the noise must be uncorrelated, mean-free and

Gaussian distributed. The modeled measurements, the observation equation, is defined as

$$z_n = h_n(x_n) + v_n \quad (4.7)$$

with $h_n(x_n)$ as observation-matrix and v_n as the measurement-noise. The matrix is, as mentioned before, defined in dependency of the state-vector. An extended Kalman filter is hereby used in case of non-linear parameters in the observation-matrix and must be linearized around the involved states.

The measurement-noise is defined as

$$v_n \sim \mathcal{N}(0, R_n) \quad (4.8)$$

whereby the covariance-matrix of the measurement-noise is given as

$$R_n = E[v_n v_n^T] \quad (4.9)$$

In the tight-coupling with GPS/INS and VRS the following measurements can be integrated in the Kalman filter:

$$z_n = \left[\lambda \tilde{\varphi}_1^{kl}, \lambda \tilde{\varphi}_2^{kl}, \lambda \tilde{\varphi}_3^{kl}, \tilde{\rho}_1^{kl}, \tilde{\rho}_2^{kl}, \tilde{\rho}_3^{kl}, \tilde{f}_{D1}^{kl}, \tilde{f}_{D2}^{kl}, \dot{\psi}^b, \dot{\theta}^b, \dot{\varphi}^b, \vec{a}^b \right]^T \quad (4.10)$$

The meanings of each parameter and their dimensionality:

$\lambda \tilde{\varphi}_1^{kl}$	raw-data of the SD phase-measurement of receiver 1 [m]	32x1
$\lambda \tilde{\varphi}_2^{kl}$	raw-data of the SD phase-measurement of receiver 2 [m]	32x1
$\lambda \tilde{\varphi}_3^{kl}$	raw-data of the SD phase-measurement of receiver 3 [m]	32x1
$\tilde{\rho}_1^{kl}$	raw-data of the SD pseudo-range measurement of receiver 1 [m]	32x1
$\tilde{\rho}_2^{kl}$	raw-data of the SD pseudo-range measurement of receiver 2 [m]	32x1
$\tilde{\rho}_3^{kl}$	raw-data of the SD pseudo-range measurement of receiver 3 [m]	32x1
\tilde{f}_{D1}^{kl}	raw-data of the Doppler measurement of receiver 1 [Hz]	32x1
\tilde{f}_{D2}^{kl}	raw-data of the Doppler measurement of receiver 2 [Hz]	32x1
$\dot{\psi}^b$	heading-rate measurement in body-fixed frame [rad/s]	1x1
$\dot{\theta}^b$	pitch-rate measurement in body-fixed frame [rad/s]	1x1
$\dot{\varphi}^b$	roll-rate measurement in body-fixed frame [rad/s]	1x1
\vec{a}^b	3D-accelerometer-measurements in body-fixed frame	3x1

Here, one can also use the previous described selection-method, which measurements are available in the current epoch. Notations for the selection are nearly identical with the previous. The operator is defined with $s_n^z(y_n, z_n)$. Now one can set the variable y_n for GPS to 1 and for IMU to 2. The described selection is given as follows:

$$s_n^z(1, z_n) = \left[\lambda \tilde{\varphi}_1^{kl}, \lambda \tilde{\varphi}_2^{kl}, \lambda \tilde{\varphi}_3^{kl}, \tilde{\rho}_1^{kl}, \tilde{\rho}_2^{kl}, \tilde{\rho}_3^{kl}, \tilde{f}_{D1}^{kl}, \tilde{f}_{D2}^{kl} \right]^T \quad (4.11)$$

$$s_n^z(2, z_n) = \left[\dot{\psi}^b, \dot{\theta}^b, \dot{\varphi}^b, \vec{a}^b \right]^T \quad (4.12)$$

The dimension of the measurement-vector in a GPS-epoch depends here on two different things. First of all, the SD-measurements are only available, if the satellites are over a defined elevation-mask and the signal is stable (continuous and high SNR). Furthermore, the raw-data of the virtual reference-station is also available and received for the selected satellites considered of the rover. In contrast to the GPS-epoch, the size of the measurement-vector in the IMU-epoch is always constant.

4.2 Algorithm of an extended Kalman filter

In a dynamic system like in this thesis, a big amount of variables must be estimated. Also the solution should be based on the past observations and estimations in a recursive way. Another point is the real-time ability for the system. Especially in applications like the autonomous driving is this a crucial point.

The basic idea behind the Kalman filter is now to formulate the estimations of epoch n as linear combinations of all estimations in the past with the newest measurement z_n . That is possible, because the estimation at epoch $n - 1$ contains all information of the measurement series $z_{n-1}, z_{n-2} \dots z_1$. This formulation in a recursive way allows a highly-efficient mathematical implementation.

The Kalman filter dispose in addition to the recursive structure an alternating prediction-correction-structure. In the first step, the state-space-model is used for the prediction-step of the system. This happens on basis of a-priori information and a well describing movement-model. A second step updates the states. For this step, the predicted states are compared with the true measurements and a trade-off between both state-vectors will be found. This optimum is based on the stochastic properties of the models and also on the measurements created with the help of the Bayesian statistic on the basis of MMSE (minimum mean square error). It should be noted, that all states in a Kalman filter are modeled as Gaussian distributed random values, i.e. no statistical correlation between the different states is given.

In terms of the alternating structure and the corresponding notation, all variables concerning the prediction take a superscript minus and variables in the update-step are marked with a superscript plus.

4.2.1 The prediction

The prediction-step tries to make an estimation for epoch n only with the help of the state-space-model. The state-space-model describes a linear movement-model. The equation for the prediction is given as following:

$$\hat{x}_n^- = \Phi_{n-1} \hat{x}_{n-1}^+ \quad (4.13)$$

With \hat{x}_{n-1}^+ as the state-update of the previous epoch, Φ_{n-1} as the transition-matrix for the movement-model and \hat{x}_n^- as the prediction of the states for the current epoch n .

Besides the state-vector, the corresponding covariance-matrix must also be updated. The covariance is defined as the expected value of the state-vector-residual, what is nothing else then the error between the true value (x) and the estimated states (\hat{x}) (see eqn. 4.14).

$$P = \mathbf{E} [(x - \hat{x})(x - \hat{x})^T] \quad (4.14)$$

The a-priori covariance-matrix P_n^- for the prediction is defined as

$$P_n^- = \Phi_{n-1} P_{n-1}^+ \Phi_{n-1}^T + Q_{n-1} \quad (4.15)$$

with P_{n-1}^+ as a-posteriori covariance-matrix for epoch $n - 1$. One can see, that the equation for P_n^- can only increase its values against P_{n-1}^+ . On a closer look, this concept is totally clear, because only prognoses with the state-prediction were made, which are not based on real measurement data. The increase of uncertainty in the a-priori covariance-matrix is thus justified in this context.

4.2.2 The state-update

In this step also the measurement-data is used for the estimation of the states. The relation between the states and the measurements is described as

$$z_n = h_n(x_n) + v_n \quad (4.16)$$

with $h_n(x_n)$ as function of measurements in relation to the states and the measurement-noise v_n . The non-linear function $h_n(x_n)$ is linearized to the measurement-matrix H_n :

$$h_n(x_n) \approx H_n x_n \quad (4.17)$$

This linearization is needed later for the calculation of the Kalman-Gain K_n and also for the a-posteriori covariance-matrix P_n^+ . The derivation of the measurement-matrix is given as follows:

$$H_n(x_n^-) = \left. \frac{\partial h_n(x_n)}{\partial x} \right|_{x=x_n^-} \quad (4.18)$$

The state-update is given as

$$\hat{x}_n^+ = x_n^- + K_n (z_n - h_n(\hat{x}_n^-)) \quad (4.19)$$

with $z_n - h_n(\hat{x}_n^-)$ as the so-called measurement-innovation. This value corresponds to the difference of predicted value to the measurement-data. With the help of the Kalman-Gain, this discrepancy between the sensors and the linear movement-model is weighted and finally added to the predicted state-vector at epoch n .

The a-posteriori covariance-matrix is updated as

$$P_n^+ = (I - K_n H_n) P_n^- \quad (4.20)$$

with I as the identity-matrix.

The last equation for the Kalman filter is the calculation of the Kalman Gain, which takes the measurement-innovation with a weighting in relation to be able to update the state-vector.

$$K_n = P_n^- H_n^T (H_n P_n^- H_n^T + R_n)^{-1} \quad (4.21)$$

The state-vector \hat{x}_n^+ contains now the best trade-off in terms of the measurements and predicted states. This procedure is used for every epoch as long as the measurements are available. [18]

4.3 Concept of the joint RTK and Attitude determination

In this section, the rough concept and processing steps of the tightly coupled GPS/INS-system with correction-data is described. Important steps or improvements are explained more detailed in further chapters.

At the beginning one introduces notations, which are maybe unclear but important in this context: For example the notation *fixed-solution* is used, when the double-difference ambiguities are determined with integer-values. Only after this *fixing* the tight-coupled solution with correction-data is used. Logically, in inverse conclusion, a *float-solution* describes a filtered solution for double-difference ambiguities as real-valued.

The concept of tight-coupling is grouped in the following processing-steps:

1. Position-determination with iterative code-only LS-solution

In this step, the rough position and clock-offset is determined with the pseudo-range for each receiver iteratively with least-squares (ILS). Besides this parameters, the elevation, the troposphere-delay, the LOS-vector (\vec{e}) and the residuals of the rough position are determined. The tropospheric-error is calculated with the help of the MOPS-model. This approach uses meteorological data, depending on the rough latitude and seasonal environment.

2. Velocity-determination with iterative Doppler-only LS-solution

As in the first step, the receiver-velocity and clock-drift is determined here with Doppler-measurements iteratively with least-squares (ILS).

3. Synchronization-correction between receivers

In case of double-difference (DD) measurements, for the RTK-baseline as well as for the attitude-baseline, a synchronization-correction is necessary. This term eliminates the error of the receiver- and satellite-movement within the time-difference between each clock-errors of the receivers. To get the fixed ambiguities of the double-difference, this synchronization is also necessary. A zero-baseline-test shows the impact of non-synchronized DD-measurements in terms of integer-values of DD-ambiguities.

4. Selection of (reference-) satellites

This step determines all available satellites and also the reference-satellite for subtracting the GPS-measurements to form SD- and DD- measurements. After a pre-selection with an elevation-mask (10 degrees), the continuity of the tracked phase of the satellite over the last epochs is considered. If the standard deviation is lying under a maximum of allowed noise, the satellite is added to the list of available satellites. The check is based on the phase-measurement with corrected cycle-slips. The selection of the reference-satellite is based on the highest elevation in the list of available satellites.

5. Determination of SD-measurement

The estimation of the fixed-solution state-vector with the help of an extended Kalman filter uses SD-measurements of phase, pseudo-range and Doppler. For determination of the SD-measurements are all a-priori information of satellite-position, clock-offset of the satellites, tropospheric-error and the position of the virtual reference-station removed for each epoch.

6. Determination of measurement- and process-noise

A realistic modeling of measurement- and process-noise is a basic requirement for a well performing Kalman filter. In this work, the assumption of the process-noise is a constant, excluding the multipath. A greater attention gets the measurement-noise, which is adapted with its true standard-deviation for every epoch in static conditions. In dynamic conditions, an elevation dependent model (see appendix B) must be used for measurements-noise adaption.

7. Detection and correction of cycle-slips for attitude-baseline

By detection of cycle-slips for the attitude-baseline, one uses the higher data-rate of the IMU. With integration of the rotation-rates and a calculated change of the baseline, a reliable detection of cycle-slips of half a wavelength is reachable.

8. Detection and correction of cycle-slips for RTK-baseline

The detection of cycle-slips for the RTK-baseline represents a large hurdle. With the help of triple-differences (TD), the change of phase-measurement between the last two epochs could be determined. Hereby, the estimated velocity of the IMU is considered. From the residuals, one can do a prediction in terms of phase-jumps of the RTK-baseline, which is so reliably as precise the IMU works.

9. Float-solution of the attitude-baseline in static conditions

In this Kalman filter, the DD-ambiguities (float) and the pseudo-range multipath is estimated.

10. Float-solution of the RTK-baseline in static conditions

As in the previous step, an additional Kalman filter estimates the RTK-baseline (float), the DD-ambiguities and the pseudo-range multipath.

11. Fixing of the DD-ambiguities for the attitude-baseline

With the help of the float-solution for the attitude-baseline, a LAMBDA-decorrelation is performed. Based on this solution, a sequential tree-search starts. After this step, the found integer-candidates for the ambiguities are validated with the SSE-values of the baseline-length and measurement-residuals.

12. Fixing of the DD-ambiguities for the RTK-baseline

As described in the previous processing-step, with the help of the float-solution for the RTK-baseline, a LAMBDA-decorrelation is performed. Based on this solution, a sequential tree-search starts. After this step, the found integer-candidates for the ambiguities are validated with the SSE-value of the measurement-residuals and the baseline-deviation. An a-priori information for the baseline-length is not given in this case, what makes this step more difficult.

13. Float-solution of the RTK-baseline in dynamic conditions

The RTK-baseline, the velocity of the vehicle and the DD-ambiguities (float-solution) are estimated during the test-drive with a Kalman filter. In dynamic conditions, there is no chance to differentiate the multipath from other error-terms. The reason is given by the time-correlation of the error-term, which can't be considered in dynamic conditions. The float-solution of this Kalman filter is also used as a point of entry for an instantaneous re-fixing of the ambiguities for the RTK-baseline as a fall-back solution in harsh environments (integrity-check for the fixed tight-coupled solution).

14. The tightly coupled fixed solution

In the tight-coupled fixed solution (GPS, IMU and correction data), the DD-ambiguities of the attitude- and RTK-baseline have been fixed in a previous step. The following parameters are provided by the extended Kalman filter:

RTK-baseline, velocity, acceleration, heading, pitch, roll, rotation-rates, SD ambiguities of the VRS (float-solution), SD pseudo-range multipath, SD ionospheric-delay of the VRS and of both receivers on the vehicle and the bias of the accelerometer and gyroscope. For more information, see the state-vector in eqn. 4.4.

15. Integrity-check of tightly coupled fixed solution

To check especially parameters like RTK-baseline, velocity and heading of the state-update in the tight-coupled Kalman filter, an integrity-check as fall-back routine is implemented. Hereby, the estimated residuals between float-solution and fixed-solution are used to make a decision, whether in cases of discrepancy the float-solution is set as reference for a new instantaneous re-fixing. This decision is important especially after tunnel-sections with long GPS-outages, to re-fix the DD-ambiguities of the tight-coupled fixed solution.

The shown steps don't take place in a sequential or parallel way for each epoch. Some proceedings could be done only after fixed solutions in a previous step. Figure 4.3 shows the schematic flow-chart of each GPS-epoch and which steps are done after each possible constellation.

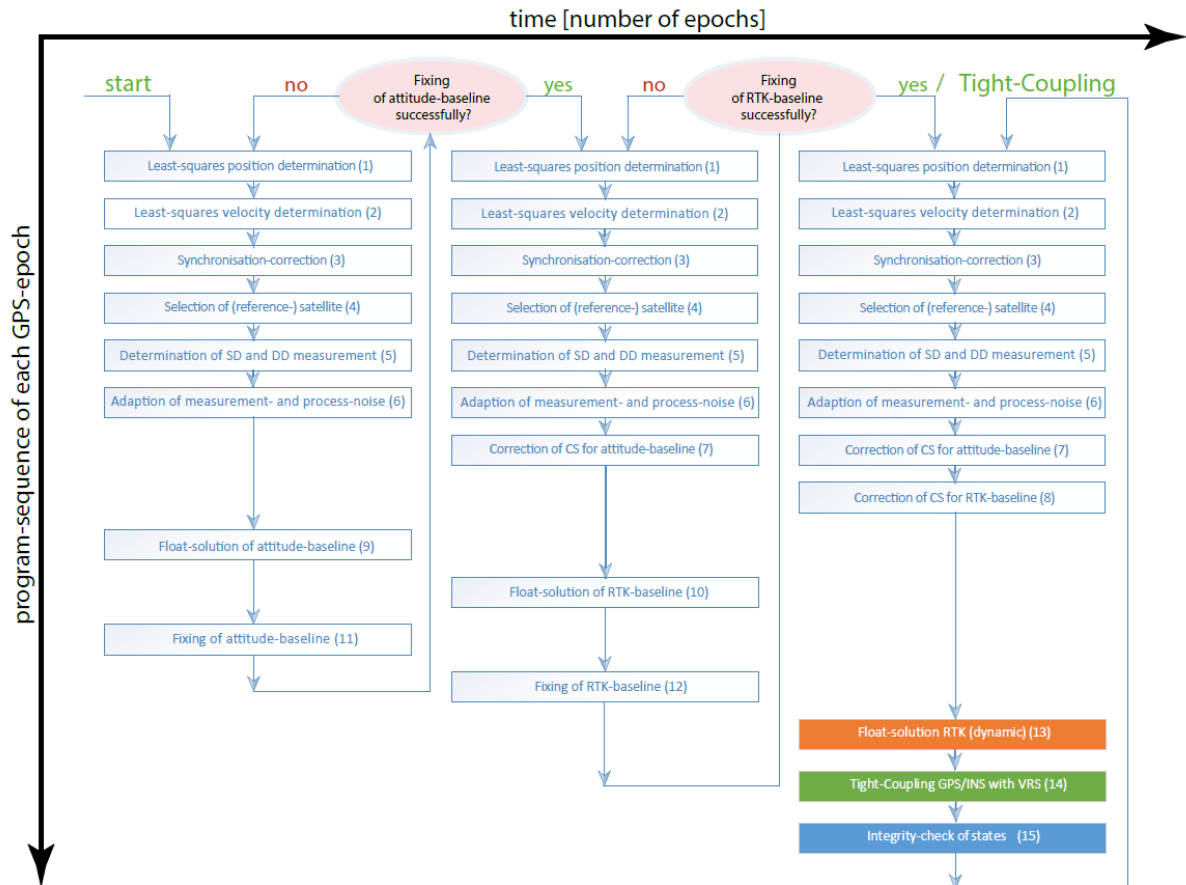


Figure 4.3: Schematic flow-chart for each GPS-epoch. The x-axis shows the initialization-steps till the tight-coupling is reached, the y-axis the sequential processing-steps for each GPS-epoch (depends on the current stage of initialization)

Chapter 5

Joint fixing of attitude- and RTK-baseline

To get a centimeter positioning-accuracy for the tight-coupling of GPS/INS with VRS, the double-difference (DD) ambiguities of both the attitude and RTK-baselines have to be fixed correctly. For this, a Kalman filter parameterized for static conditions is used to get an estimated ambiguity-solution of both baselines. After convergence of the filter and based on the filtered parameter, a fixing of the ambiguities for both baselines is tried. This chapter explains the float-filter of the attitude-baseline, which is the basis for the fixing of these ambiguities. Next, the fixing of the attitude ambiguities itself is described. After this, the float-filter for the RTK-baseline is explained and with this the fixing of the DD-ambiguities of the RTK-baseline.

5.1 The float Kalman filter of the attitude-baseline

This section describes the used models in detail. The parametrization of the Kalman filter is also explained here. The basic function of a Kalman filter was shown in a previous chapter.

5.1.1 The synchronization-correction

The Kalman filter for the float-ambiguities is based on double-difference measurements, shown in eqn. 2.10 and 2.11. But first of all, if one wants to use this measurement-model respectively to fix the ambiguities to integers, a determination of the synchronization-correction $c_{12}^{kl}(t_n)$ between receiver 1 and 2 is needed.

The clock-offset of the receiver distorted not directly the double-difference measurement, because the mistake in the difference between both receiver-measurements eliminates this error-term. However there is still an indirect influence on the double-difference measurement: In such a case of high velocity of the satellites (4 km/s), the error between both receiver-clocks is around 1 millisecond. A previous model of synchronization-correction for double-difference measurements of low-cost GPS-receivers comes also from the company *Advanced Navigation Solutions – ANavS GmbH* and is described by Cardenas in [19]. In the preceding approach, the satellite-movement between the receiver-clocks is extrapolated over 50 epochs, what leads to the need of much processing power. A further disadvantage gets attention in the later described RTK-baseline. Here we get the problem of non-parallel LOS-vectors (\vec{e}_1^{kl} and \vec{e}_3^{kl}) of both receivers (1 and VRS), what is un-modeled in the present DD-measurement-description.

The new synchronization-correction provides the satellite- and receiver-movement within the difference of both receiver clock-offsets $\delta t_1(t_n) - \delta t_2(t_n)$ instantaneously and without extrapolation for each epoch. For this, the LOS-vector and the baseline for double-differences, is shown in more detail:

$$\begin{aligned} \Delta \mathbf{r}_{12}^{kl} = & \vec{e}_1^k(t_n)(\vec{x}_1(t_n) - \vec{x}_1^k(t_n)) - \vec{e}_2^k(t_n + \Delta t_n)(\vec{x}_2(t_n) - \vec{x}_2^k(t_n + \Delta t_n)) - \\ & \vec{e}_1^l(t_n)(\vec{x}_1(t_n) - \vec{x}_1^l(t_n)) - \vec{e}_2^l(t_n + \Delta t_n)(\vec{x}_2(t_n) - \vec{x}_2^l(t_n + \Delta t_n)) \end{aligned} \quad (5.1)$$

In eqn. 5.1 the formulation $\vec{x}_1(t_n) = \vec{x}_2(t_n) + \vec{b}_{12}(t_n)$ is integrated:

$$\begin{aligned} \Delta \mathbf{r}_{12}^{kl} = & \vec{e}_1^k(t_n)(\vec{x}_2(t_n) + \vec{b}_{12}(t_n) - \vec{x}_1^k(t_n)) - \vec{e}_2^k(t_n + \Delta t_n)(\vec{x}_2(t_n) - \vec{x}_2^k(t_n + \Delta t_n)) - \\ & (\vec{e}_1^l(t_n)(\vec{x}_2(t_n) + \vec{b}_{12}(t_n) - \vec{x}_1^l(t_n)) - \vec{e}_2^l(t_n + \Delta t_n)(\vec{x}_2(t_n) - \vec{x}_2^l(t_n + \Delta t_n))) \end{aligned} \quad (5.2)$$

Then the LOS-vector is re-arranged:

$$\begin{aligned} \Delta \mathbf{r}_{12}^{kl} = & \vec{e}_1^{kl}(t_n)\vec{b}_{12}(t_n) + \vec{e}_1^k(t_n)(\vec{x}_2(t_n) - \vec{x}_1^k(t_n)) - \vec{e}_2^k(t_n + \Delta t_n)(\vec{x}_2(t_n) - \vec{x}_2^k(t_n + \Delta t_n)) - \\ & (\vec{e}_1^l(t_n)(\vec{x}_2(t_n) - \vec{x}_1^l(t_n)) - \vec{e}_2^l(t_n + \Delta t_n)(\vec{x}_2(t_n) - \vec{x}_2^l(t_n + \Delta t_n))) \end{aligned} \quad (5.3)$$

The second part on the right side is summarized to the synchronization-correction:

$$\begin{aligned} c_{12}^{kl}(t_n) = & \vec{e}_1^k(t_n)(\vec{x}_2(t_n) - \vec{x}_1^k(t_n)) - \vec{e}_2^k(t_n + \Delta t_n)(\vec{x}_2(t_n) - \vec{x}_2^k(t_n + \Delta t_n)) - \\ & \vec{e}_1^l(t_n)(\vec{x}_2(t_n) - \vec{x}_1^l(t_n)) - \vec{e}_2^l(t_n + \Delta t_n)(\vec{x}_2(t_n) - \vec{x}_2^l(t_n + \Delta t_n)) \end{aligned} \quad (5.4)$$

There is now the following relation for the modeled measurements:

$$\Delta \mathbf{r}_{12}^{kl} = \vec{e}_1^{kl}(t_n)\vec{b}_{12}(t_n) + c_{12}^{kl}(t_n) \quad (5.5)$$

A big advantage of this form of synchronization-correction lies in the instantaneous calculation for every epoch (see figure 5.1). The processor intensive extrapolation of the satellite-movement is not necessary anymore. The RTK-baseline takes the same method for synchronization-correction, only the index from receiver 2 to receiver 3 (VRS) changes.

Furthermore, a mistake, caused by the relation between $\vec{e}_1^{kl}(t_n)\vec{b}_{12/3}(t_n)$, is eliminated. When using the LOS-vector just by considering the first receiver, there is only a negligible error in case of the attitude-baseline due to the small gap between the receivers. However, in case of the RTK-baseline, the parallelism of the LOS-vectors can't be assumed here. A new error-term would be brought into the measurement model. With the help of the new synchronization-correction, this error-term is already compensated and must not be further considered.

5.1.2 The parametrization of the Kalman filter

After the determination of the synchronization-correction, it will be subtracted from the double-difference pseudo-range and phase-measurement. The measurement-equations are described as following:

$$\begin{aligned} \lambda \tilde{\varphi}_{12}^{kl}(t_n) = & \lambda \varphi_{12}^{kl}(t_n) - c_{12}^{kl}(t_n) \\ = & \vec{e}_1^{kl}(t_n)\vec{b}_{12}(t_n) + \lambda N_{12}^{kl} + \frac{\lambda}{2} \Delta N_{12}^{kl}(t_n) + \lambda \Delta \varphi_{MP,12}^{kl}(t_n) + \varepsilon_{12}^{kl}(t_n) \end{aligned} \quad (5.6)$$

The half cycle-slips $\Delta N_{12}^{kl}(t_n)$ are corrected in a pre-processing step before estimating the unknown states in the Kalman filter.

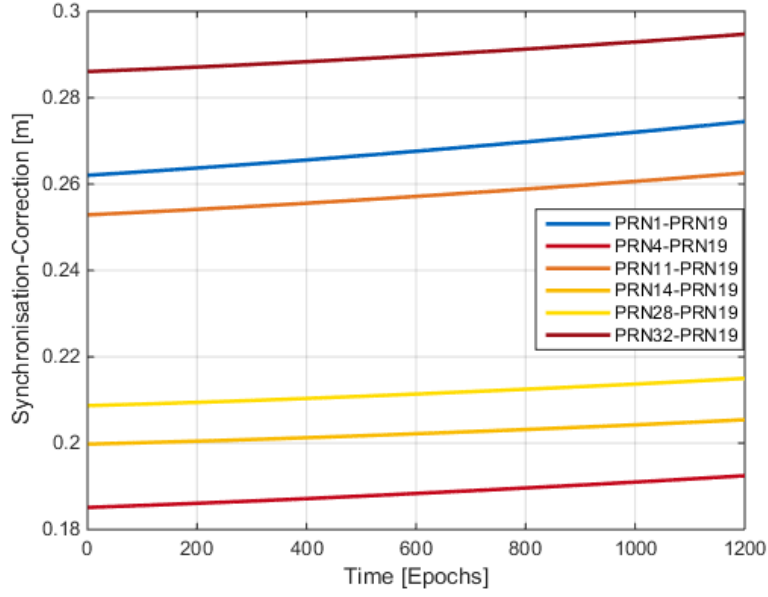


Figure 5.1: The synchronization-correction c_{12}^{kl} of the DD phase-measurement. The continuous drift is the result from the movement of the satellites

The pseudo-range measurement for the filter is given as:

$$\begin{aligned}\tilde{\rho}_{12}^{kl}(t_n) &= \rho_{12}^{kl}(t_n) - c_{12}^{kl}(t_n) \\ &= \vec{e}_1^{kl}(t_n)\vec{b}_{12}(t_n) + \Delta\rho_{MP,12}^{kl}(t_n) + \eta_{12}^{kl}(t_n)\end{aligned}\quad (5.7)$$

The remaining unknowns are stacked in the state-vector:

$$x = \begin{pmatrix} \vec{b}_{12} \\ N_{12}^{kl} \\ \Delta\rho_{MP,12}^{kl} \end{pmatrix}\quad (5.8)$$

with the attitude-baseline \vec{b}_{12} in the navigation-frame NED (North-East-Down).

The corresponding measurement-vector of the state-vector is given by:

$$z = \begin{pmatrix} \lambda\tilde{\varphi}_{12}^{kl} \\ \tilde{\rho}_{12}^{kl} \\ \bar{x} \end{pmatrix}\quad (5.9)$$

The count of measurements depends on the available satellites minus the reference-satellite. In this measurement-vector is also given an additional information with \bar{x} . This a-priori information constrains the up-component in the Kalman filter. One assumes a flat baseline (pitch ~ 0 degrees) for this assumption, so the height can deviate not much around zero. C3ias et al.

shows in [3] a further possibility for constraining the up-component in the fixing-process.

The transition-matrix is given in this context as identity-matrix. The reason for this lies in the static environment for this float Kalman filter, which makes an integration of velocity respectively acceleration over time unnecessary.

The observation-matrix for 32 satellites is given as follows:

$$H = \begin{pmatrix} \vec{e}_{132 \times 3, NED}^{kl} & I_{32 \times 32} \cdot \lambda & 0_{32 \times 32} \\ \vec{e}_{132 \times 3, NED}^{kl} & 0_{32 \times 32} & I_{32 \times 32} \\ (0, 0, 1) & 0_{1 \times 32} & 0_{1 \times 32} \end{pmatrix} \quad (5.10)$$

A subset is used in the actual Kalman filter. The variable $\vec{e}_{132 \times 3, NED}^{kl}$ describes the single-difference (SD) LOS-vector in the navigation (NED) frame.

Correct process- and measurement-noise covariance matrices are essential for a good functionality of the Kalman filter. False values could lead to a divergence of the filter. Moreover, the state estimation errors are larger in case of inappropriate process- and measurement-noises. This leads to a false mapping of measurement-errors to the states, what makes especially the fixing of the double-difference (DD) ambiguities probably erroneous.

So far, the measurement-noise was determined with the help of an elevation depend model of each satellite (see appendix B). This means, the signal of a low elevation satellite is weighted higher than the signal of a high-elevation satellite in the Kalman filter. A big disadvantage is the missing adaption to the true signal-quality of the measurements. After analyses of the signal-quality against the elevation, a definite connection of both parameters (measurement-noise/satellite-elevation) could not always be verified. Figure 5.2 shows, despite of a big discrepancy of elevation of both measurements, only marginal differences in the noise level of the measurement. This weakness leads to a false weighting of the measurements, i.e. a mismatch of the error-mapping to the states could happen, what leads especially in the ambiguity fixing to wrong solutions respectively to integer-candidates without the correct one.

The new adaptive method uses a linear least-squares (LS) fitting of the double-difference measurements. A measurement-model is given as

$$\underbrace{\begin{pmatrix} z_1 \\ z_2 \\ z_3 \\ \vdots \end{pmatrix}}_z = \underbrace{\begin{pmatrix} 1 & t_1 - t_1 \\ 1 & t_1 - t_2 \\ 1 & t_1 - t_3 \\ \vdots & \vdots \end{pmatrix}}_H \begin{pmatrix} h_0 \\ h_1 \end{pmatrix} + \begin{pmatrix} \eta_1 \\ \eta_2 \\ \eta_3 \\ \vdots \end{pmatrix} \quad (5.11)$$

with the parameter z as the measurement-vector and H as the coefficient-matrix (h_0 and h_1) of the linear fitting in dependency of the timestamps. The minimization-problem is solved without a weighting-matrix as following:

$$\begin{pmatrix} h_0 \\ h_1 \end{pmatrix} = (H^T H)^{-1} H^T z \quad (5.12)$$

In case of phase-measurements, with the help of the residual-vector Δr of the linear-fitting against

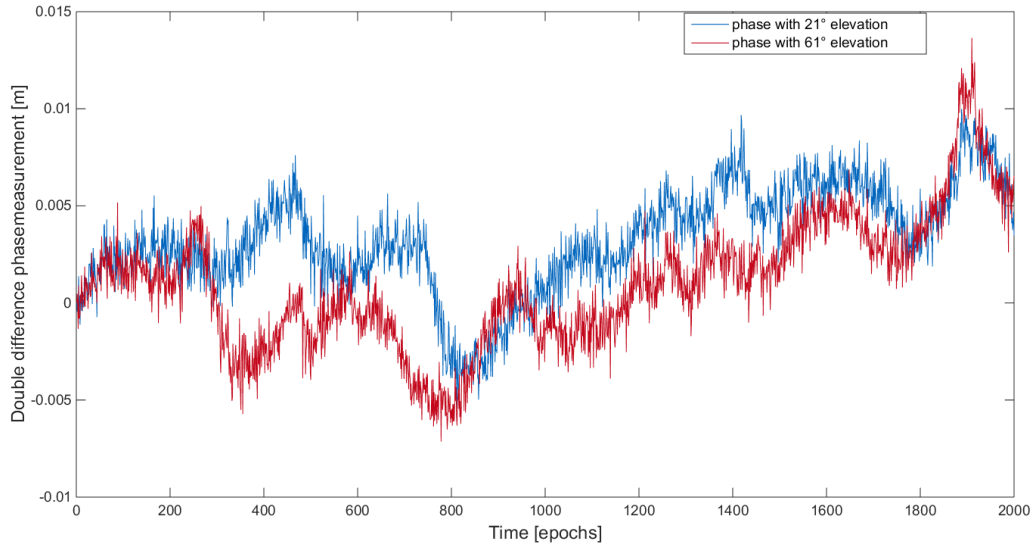


Figure 5.2: Comparison of DD phase-measurement (subtracting the phase-measurement from the first epoch) in terms of the elevation of the satellite. The standard-deviation of the blue curve is 2.7 mm and of the red curve 3.3 mm. Short-term variation indicates noise, mid-term variation phase multipath and long-term variation change in geometry (\bar{e}^{*l})

the true measurements, the variance of the phase-noise is given by:

$$\sigma^2 = \frac{1}{N} \sum_i^N \Delta r_i^2 \quad (5.13)$$

The measurement-noise for the pseudo-range is determined in the same way. Besides this, the multipath for the process-noise must also be estimated and can't be negligible as for the phase-measurement. The multipath is in static conditions as a timely correlated oscillation detectable. Unlikely, this trend is first seen only after several hundred epochs. To estimate this unknown, the use of special multipath limiting antennas (i.e., choke ring or multi-beam antennas) [20], the carrier smoothing to reduce code multipath, and the code tracking algorithms based on receiver internal correlation technique are the most prominent approaches [21], [22], [23].

In this approach, the multipath is modeled with the help of a Kalman filter. Sahmoudi in [24] and Bourdeau in [25] describes an approach for estimating the multipath with a filter. In this thesis, one models a suitable slope for estimating the multipath. Hereby one searches the minimum and the maximum of the measurements in the recent past epochs and normalizes this value to get the potential change of the multipath within one epoch. Finally this value is modeled to the process-noise of the state-prediction in the Kalman filter.

Figure 5.3 shows the estimated multipath with the described parametrization of measurement- and process-noise for the pseudo-range measurement with 26 degree elevation. The curve of the estimated state (red dashed) follows clearly the correct multipath (blue), what gives feedback for a right modeling of multipath. The correct multipath is determined as DD pseudo-range measurement subtracted by the precise attitude-baseline (see eqn. 5.7).

In this adaptive approach, the measurement-noise for all satellites is adapted in every epoch, what leads to right valuation of measurements and to stable and more precise states. Excepted

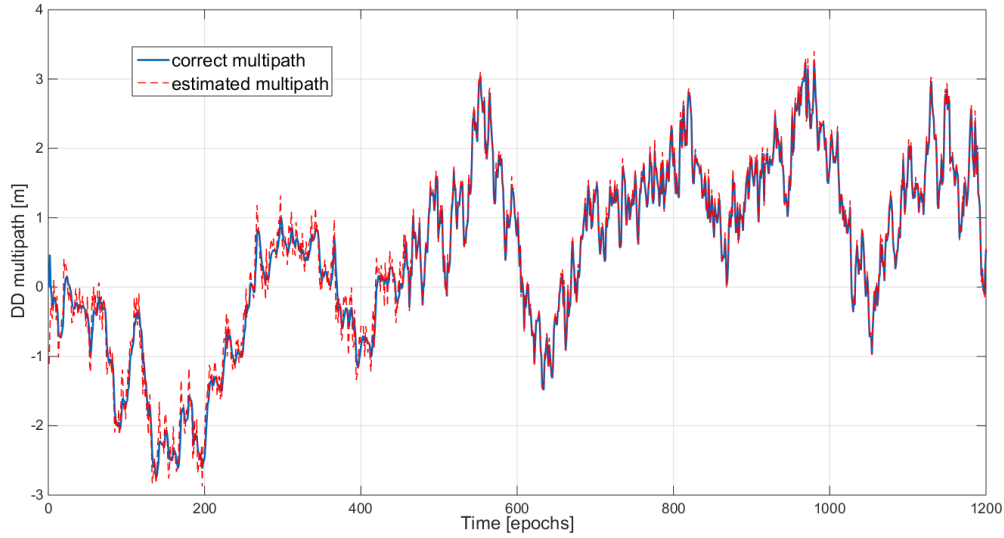


Figure 5.3: Comparison of the correct multipath for the DD pseudo-range measurement (blue) with the estimated multipath of the static float Kalman filter (red dashed). The elevation is 26 degrees.

here is the a-priori (pseudo-)measurement of the height, which has a static initialization of $\sigma_{\bar{h}} = 2$ cm. In the process-noise, the multipath is also set in an adaptive way. The maximum change of the baseline in every epoch is set to zero in this static behavior of the system. The process-noise for the ambiguities has also a low value of $\sigma_N = 0.001$ Cycles. This setting constraints the Kalman filter for the change of this state for every epoch. The filter has this way no chance to correct errors in the measurements only with the state of ambiguity. A meaningful and correct state for the ambiguities is given with the later described fixing to integers.

An overview of the complete measurement-noise matrix (eqn. 5.14):

$$\Sigma_R = \begin{pmatrix} \Sigma_{\varphi_{12}^{kl}} & \mathbf{0}_{32 \times 32} & \mathbf{0}_{32 \times 1} \\ \mathbf{0}_{32 \times 32} & \Sigma_{\rho_{12}^{kl}} & \mathbf{0}_{32 \times 1} \\ \mathbf{0}_{1 \times 32} & \mathbf{0}_{1 \times 32} & \Sigma_{\bar{h}} \end{pmatrix} \quad (5.14)$$

The process-noise matrix is given as (eqn. 5.15)

$$\Sigma_Q = \begin{pmatrix} \mathbf{0}_{3 \times 3} & \mathbf{0}_{3 \times 32} & \mathbf{0}_{3 \times 32} \\ \mathbf{0}_{32 \times 3} & \Sigma_{N_{12}^{kl}} & \mathbf{0}_{32 \times 32} \\ \mathbf{0}_{32 \times 3} & \mathbf{0}_{32 \times 32} & \Sigma_{\Delta \rho_{MP,12}^{kl}} \end{pmatrix} \quad (5.15)$$

5.2 Ambiguity-fixing of the attitude-baseline

The determination of integer ambiguities is the most important step for the initialization of the tight-coupled GPS/INS-system with correction-data (VRS). Without this step, there is no chance to get a centimeter precise and reliable position estimation as well as a precise attitude of the vehicle. In case of a false fixing of the ambiguities, it will result in a big error in position and attitude, what leads to the need of a high reliability.

The derivation is subdivided in two steps. First of all, the modeling to solve the ambiguities is introduced and explained. Then the thesis shows the practical implementation of the shown derivation.

5.2.1 The mathematical model

The fixing of the ambiguities to integers is done for double-difference measurements. For the deviation of the models is hence the synchronized DD measurement of the phase of eqn. 5.6 considered. First of all, this equation is described in matrix-vector notation:

$$z = H\vec{b}_{12} + AN_{12} + \eta \quad (5.16)$$

Teunissen developed in [26] the LAMBDA-method to solve the least-square (LS) problem in eqn. 5.16. In [27] Teunissen discussed the a-priori information of the baseline-length, which is also used in this thesis. With the help of the MAP(Maximum A Posteriori Probability)-estimator and the assumptions of the Gaussian distributed measurement-noise, the minimization-problem is given as follows:

$$\min_{\vec{b}_{12}, N_{12}} \left(\|z - H\vec{b}_{12} - AN_{12}\|_{\Sigma_z^{-1}}^2 + (\|\vec{b}_{12}\| - \bar{l})^2 / \sigma_l^2 \right) \quad (5.17)$$

The first term in eqn. 5.17 is decomposed according to Teunissen in [26] with an orthogonal projector P_H^\perp of H :

$$\|z - H\vec{b}_{12} - AN_{12}\|_{\Sigma_z^{-1}}^2 = \|(P_H + P_H^\perp)(z - H\vec{b}_{12} - AN_{12})\|_{\Sigma_z^{-1}}^2 \quad (5.18)$$

With the rule:

$$P_H + P_H^\perp = 1 \quad (5.19)$$

Now, the decomposition is considered as follows:

$$\|z - H\vec{b}_{12} - AN_{12}\|_{\Sigma_z^{-1}}^2 = \|P_H(z - H\vec{b}_{12} - AN_{12})\|_{\Sigma_z^{-1}}^2 + \|P_H^\perp(z - H\vec{b}_{12} - AN_{12})\|_{\Sigma_z^{-1}}^2 \quad (5.20)$$

As first step we are looking to the baseline-residuals. With the help of the terms $P_H H = H$ and $P_H(z - AN_{12}) = H\vec{b}_{12}(\check{N}_{12})$ (see appendix C) are further simplifications done:

$$\begin{aligned} \|P_H(z - H\hat{\vec{b}}_{12} - A\check{N}_{12})\|_{\Sigma_z^{-1}}^2 &= \|P_H(z - A\check{N}_{12}) - H\hat{\vec{b}}_{12}\|_{\Sigma_z^{-1}}^2 \\ &= \|H\check{\vec{b}}_{12}(\check{N}_{12}) - H\hat{\vec{b}}_{12}\|_{\Sigma_z^{-1}}^2 \\ &= \left\| H \left(\check{\vec{b}}_{12}(\check{N}_{12}) - \hat{\vec{b}}_{12} \right) \right\|_{\Sigma_z^{-1}}^2 \\ &= \left(\check{\vec{b}}_{12}(\check{N}_{12}) - \hat{\vec{b}}_{12} \right)^T H^T \Sigma_z^{-1} H \left(\check{\vec{b}}_{12}(\check{N}_{12}) - \hat{\vec{b}}_{12} \right) \\ &= \left\| \left(\check{\vec{b}}_{12}(\check{N}_{12}) - \hat{\vec{b}}_{12} \right) \right\|_{\Sigma_{\check{\vec{b}}_{12}}^{-1}}^2 \end{aligned} \quad (5.21)$$

The used baseline $\vec{\tilde{b}}_{12}(\check{N}_{12})$ refers to the fixed least-squares (LS) solution, based on the possible integer ambiguity vector \check{N}_{12} . The calculation is described in eqn. 5.22. The baseline \hat{b}_{12} defines the float-solution for the baseline.

$$\vec{\tilde{b}}_{12}(\check{N}_{12}) = (H^T \Sigma_z^{-1} H)^{-1} H^T \Sigma_z^{-1} (z - A \check{N}_{12}) \quad (5.22)$$

In the second term in eqn. 5.20, which regards the ambiguity-residuals, an orthogonal projector $P_{\bar{A}}^\perp$ ($\bar{A} = P_H^\perp A$) is used in the same way as before. With the help of the condition $P_{\bar{A}}^\perp P_H^\perp z = \bar{A} \hat{N}_{12}$ (see appendix C) the ambiguity-residual term is simplified as follows:

$$\begin{aligned} \|P_H^\perp(z - H\vec{\tilde{b}}_{12} - AN_{12})\|_{\Sigma_z^{-1}}^2 &= \|P_H^\perp(z - AN_{12})\|_{\Sigma_z^{-1}}^2 && \text{with } P_H^\perp H = 0 \\ &= \|(P_{\bar{A}} + P_{\bar{A}}^\perp)P_H^\perp(z - AN_{12})\|_{\Sigma_z^{-1}}^2 \\ &= \|P_{\bar{A}}P_H^\perp(z - AN_{12})\|_{\Sigma_z^{-1}}^2 + \|P_{\bar{A}}^\perp P_H^\perp(z - AN_{12})\|_{\Sigma_z^{-1}}^2 \\ &= \|P_{\bar{A}}P_H^\perp z - \bar{A}N_{12}\|_{\Sigma_z^{-1}}^2 + \underbrace{\|P_{\bar{A}}^\perp P_H^\perp z\|_{\Sigma_z^{-1}}^2}_{\text{irreducible noise}} \\ &= \|\bar{A}(\hat{N}_{12} - N_{12})\|_{\Sigma_z^{-1}}^2 + \|P_{\bar{A}}^\perp P_H^\perp z\|_{\Sigma_z^{-1}}^2 \\ &= (\hat{N}_{12} - N_{12})^T \bar{A}^T \Sigma_z^{-1} \bar{A} (\hat{N}_{12} - N_{12}) + \|P_{\bar{A}}^\perp P_H^\perp z\|_{\Sigma_z^{-1}}^2 \\ &= \|\hat{N}_{12} - N_{12}\|_{\Sigma_{\hat{N}_{12}}^{-1}}^2 + \|P_{\bar{A}}^\perp P_H^\perp z\|_{\Sigma_z^{-1}}^2 \end{aligned} \quad (5.23)$$

with the variable \hat{N}_{12} as float least-squares (LS) solution of the ambiguities, whereby the calculation is described in eqn. 5.24. The float-solution, estimated with a Kalman filter, is named as N_{12} .

$$\hat{N}_{12} = (\bar{A}^T \Sigma_z^{-1} \bar{A})^{-1} \bar{A}^T \Sigma_z^{-1} P_H^\perp z \quad (5.24)$$

In summary, the decomposition of the minimization-problem in eqn. 5.17 is given by:

$$\begin{aligned} \min_{\vec{b}_{12}, N_{12}} \left(\|z - H\vec{b}_{12} - AN_{12}\|_{\Sigma_z^{-1}}^2 + (\|\vec{b}_{12}\| - \bar{l})^2 / \sigma_l^2 \right) &= \left\| \left(\vec{\tilde{b}}_{12}(\check{N}_{12}) - \vec{b}_{12} \right) \right\|_{\Sigma_{\vec{b}_{12}}^{-1}}^2 \\ &+ \|\hat{N}_{12} - N_{12}\|_{\Sigma_{\hat{N}_{12}}^{-1}}^2 \\ &+ (\|\vec{\tilde{b}}_{12}\| - \bar{l})^2 / \sigma_l^2 \\ &+ \|P_{\bar{A}}^\perp P_H^\perp z\|_{\Sigma_z^{-1}}^2 \end{aligned} \quad (5.25)$$

After this steps, a sequential tree-search is started to find all possible integer-candidates for the DD ambiguities within a search-space. A detailed description of the search-process is not necessary in this context and only referred to the method of Henkel et al. in [2].

5.2.2 The practical implementation

After the theoretical background is described, the practical implementation for selecting the right ambiguity-vector is shown. To get a correct fixing, we need static conditions for this initialization. Besides, the Kalman filter has to be converged (minimum 50 epochs) and the phase-residuals

have to be low enough. Furthermore, the DD phase-measurement is smoothed with a low-pass filter:

$$\varphi_{filtered}(n) = \frac{1}{\tau}\varphi_{measured}(n) + \left(1 - \frac{1}{\tau}\right)\varphi_{filtered}(n - 1) \quad (5.26)$$

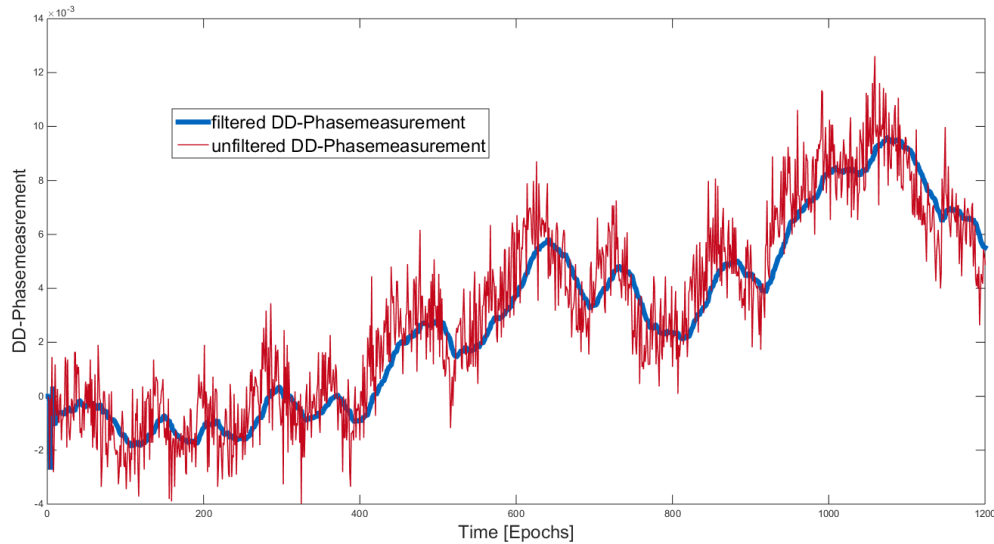


Figure 5.4: Comparison of a smoothed (blue) and noisy (red) DD phase-measurement.

After converging the Kalman float-filter, a sequential tree-search is started. This search-process is based on the solution of the float filter. At this point, the float-ambiguities and the uncertainty flow into the determination of possible ambiguity-candidates within a search-space. For all of this integer ambiguity-vectors, a baseline is calculated with the least-squares (LS) method (see eqn. 5.22). After this tree-search, the right ambiguity-vector must be selected, which minimizes the SSE-Value of eqn. 5.25. For this selection, one can use different approaches, which are shown next. Coias et al. shows in [3] besides this a constraint selection based on the up-component for flat baselines, what is not necessary in this approach because of already limited up-component in the float Kalman filter.

Candidate-selection based on ambiguity-residuals

As shown in eqn. 5.25, the ambiguity-residuals can influence the minimization-problem. The residuals are determined as

$$SSE_{\check{N}_{12}} = (\check{N}_{12} - \hat{N}_{12})^T \Sigma_{\hat{N}_{12}}^{-1} (\check{N}_{12} - \hat{N}_{12}) \frac{1}{K} \quad (5.27)$$

with K as normalization-parameter for the count of available double-difference (DD) measurements, \check{N}_{12} as an ambiguity integer-candidate determined through the tree-search and \hat{N}_{12} as the Kalman filter float solution for the ambiguities.

Now one has to check, if the selection based on the SSE-values for each candidate is the best approach for selecting the right candidate of the fixed ambiguity-vector. Figure 5.5 describes a typical distribution of residuals with 200 determined candidates. To select now the right candidate, one needs enough discrimination from the right fixed ambiguities to the rest of the choices.

The attempt to fix the ambiguity-residuals is tried after the first 50 epochs of the float filter. A further condition for the attempt to fix the ambiguities are stable states of the Kalman filter. After the convergence-process, the fixing is tried in a constant interval to get a correct fixing. In case of a insufficient fixing over a long period of time, the Kalman filter is reseted and the convergence-process restarts again (see figure 5.12).

The candidates are sorted based on the residuals, i.e. the smallest SSE-value is on the left side. Figure 5.5 shows a logarithmic distribution for the best candidates, a relatively high discrimination to other candidates is also given in this case. After analyzing the candidates, the second best is here the right one, what leads to a wrong fixing. With analyzing a huge amount of datasets, there is no chance to get a reliable fixing with the criterion of ambiguity-residuals.

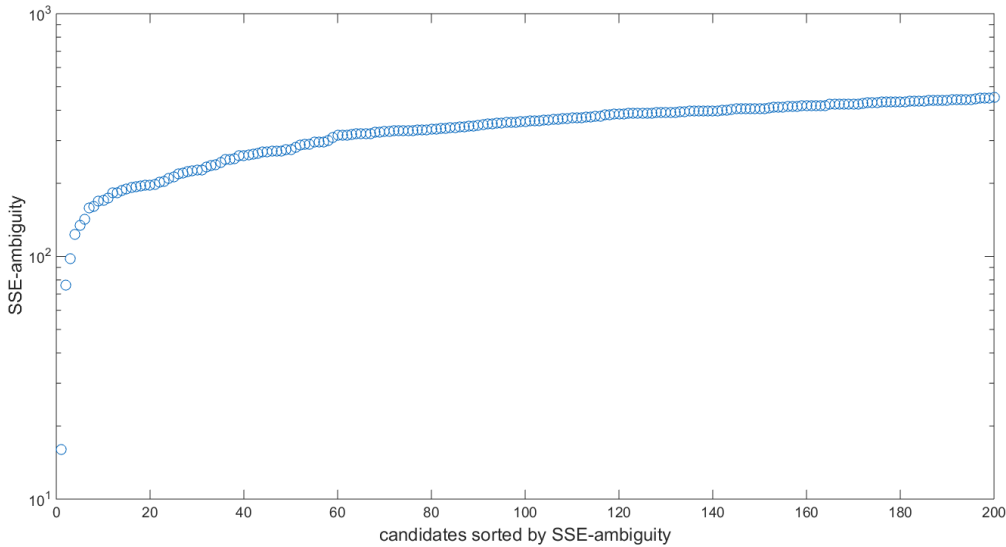


Figure 5.5: Logarithmic distribution of ambiguity-residual candidates. The false candidate has the lowest SSE-value, this by high candidate-discrimination.

Candidate-selection based on baseline-residuals

Also the baseline-residuals influence the minimization-problem in eqn. 5.25. The SSE-value is given as follows:

$$SSE_{\tilde{b}_{12}} = \left(\tilde{b}_{12}(\tilde{N}_{12}) - \hat{b}_{12} \right)^T \Sigma_{\tilde{b}_{12}}^{-1} \left(\tilde{b}_{12}(\tilde{N}_{12}) - \hat{b}_{12} \right) \frac{1}{3} \quad (5.28)$$

with $1/3$ as the normalization-term considering all three components in the navigation-frame, $\tilde{b}_{12}(\tilde{N}_{12})$ as the LS-solution of the baseline in terms of the integer-candidate for the fixed ambiguity and \hat{b}_{12} as the Kalman filter float-solution of the attitude baseline.

As shown before, a typical distribution of 200 determined candidates with baseline-residuals is given in figure 5.6. After analyzing the candidates, the best candidate is also the correct one. Further tests show no clear discrimination of the candidates after only a short convergence-time of the attitude-baseline Kalman filter. But one also detected, that the right candidate is always in the near of the first best positions. As longer the filter converged, the reliability of selecting the correct integer-candidate increases.

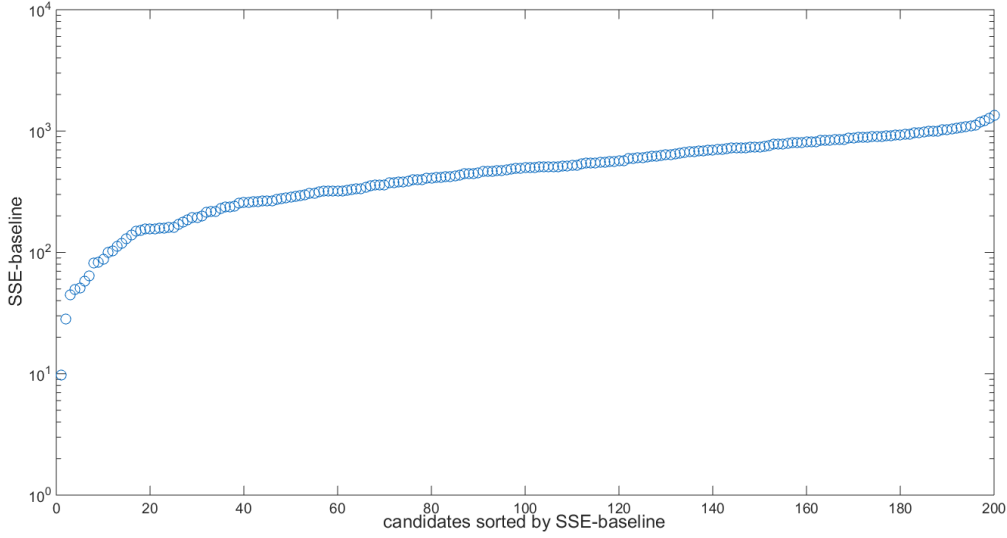


Figure 5.6: Logarithmic distribution of baseline-residual candidates. Best candidate is also the correct one, but shows no clear discrimination after short convergence-time.

Candidate-selection based on measurement-residuals

A further criterion for candidate-selection is given with the measurement-residuals. The residuals are given by:

$$\Delta r_\varphi = \lambda \tilde{\varphi}_{12}^{kl} - c_{12}^{kl} - \tilde{e}_1^{kl} \tilde{b}_{12}(\tilde{N}_{12}) - \lambda \tilde{N}_{12} \quad (5.29)$$

After subtraction of attitude baseline and ambiguities from the phase-measurement, whereby the phase multipath is negligible, the residual-vector should contain only the left phase-noise and the error caused by incorrect ambiguity-fixing. Next the SSE-value is calculated:

$$SSE_\varphi = \Delta r_\varphi^T \Sigma_z^{-1} \Delta r_\varphi \frac{1}{K} \quad (5.30)$$

with K as normalization-parameter for the count of available double-difference (DD) measurements and Σ_z as covariance-matrix of the measurement-noise.

Figure 5.7 describes again the SSE-values in terms of the measurement-residuals. If one analyzes the distribution, there is no reliable chance to select the correct fixing only with this information. However, help can be provided with this criterion in cases where the selection (based on another criterion) is not safe enough and one supports this decision with the SSE-value of the measurement-residuals.

Candidate-selection based on length-residuals

With the help of an a-priori information about the length between receiver 1 and 2, a statement of candidate-correctness can be given. The residuals are given by:

$$SSE_{Length} = \left(\|\tilde{b}_{12}\| - \tilde{l} \right)^2 / \sigma_{\tilde{l}}^2 \quad (5.31)$$

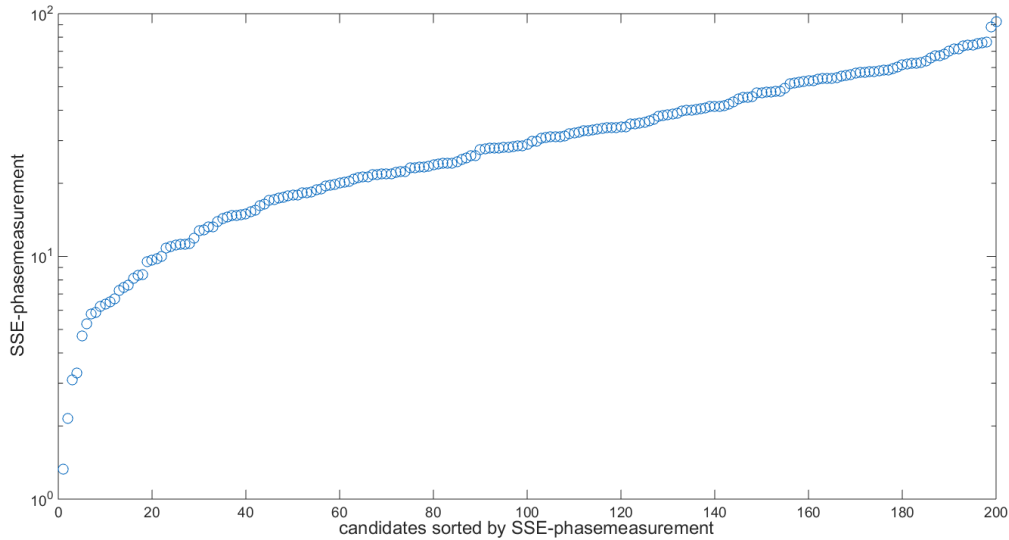


Figure 5.7: Logarithmic distribution of phase-measurement-residual candidates. The best candidate is most of the time the correct one, in this shown case also. Nevertheless required reliability is not given with this criterion.

with the length of a baseline-candidate $\|\vec{b}_{12}\|$, the a-priori information \bar{l} and the uncertainty of the a-priori information of the baseline-length $\sigma_{\bar{l}}$, which is set with 1 cm in this application.

Considering figure 5.8, there is a clear classification of the best candidate against the rest of the possibilities. The first candidate is also the right one, the ambiguities are solved correct in this case. After analyzing a large amount of datasets, one can give a extremely reliable selection of the fixed ambiguity-vector with the help of this criterion. With a good satellite-constellation, a well parameterized float Kalman filter and the constraint of a sufficient discrimination of best to second best candidate, the reliability of ambiguity fixing for the attitude-baseline is nearly 100 percent. The fixing-duration is below 20 seconds in conditions without multipath and good satellite-constellation.

To show the reliability of this method, figure 5.9 shows a continuous fixing of the DD ambiguities. The Kalman filter is restarted after each fixing for an independent solution. For 91 attempts in a good satellite constellation, there is no incorrect fixing. A successful ambiguity-fixing happens nearly all 60 epochs (12 seconds). The count of available satellites with good signal reception (low noise) and above elevation-mask was most of the time ten.

In comparison to an ambiguity-fixing with bad satellite-constellation (see figure 5.9), there are less fixings in the same time. Furthermore a false fixing happens here. The count of available satellites with good signal reception (low noise) and above elevation-mask was most of the time 6.

In figure 5.10 the accuracy of the fixed baseline-length is shown. With a good satellite-constellation, the length-error is within the sigma-value of 1 cm by a true length of 50 cm. One can see, in a bad satellite-constellation, the deviation of the baseline-length is much higher.

The next figure 5.11 gives on overview of the stability of the baseline in the navigation- (NED) frame. As previous, there is a big contrast between the solution for good and bad satellite-

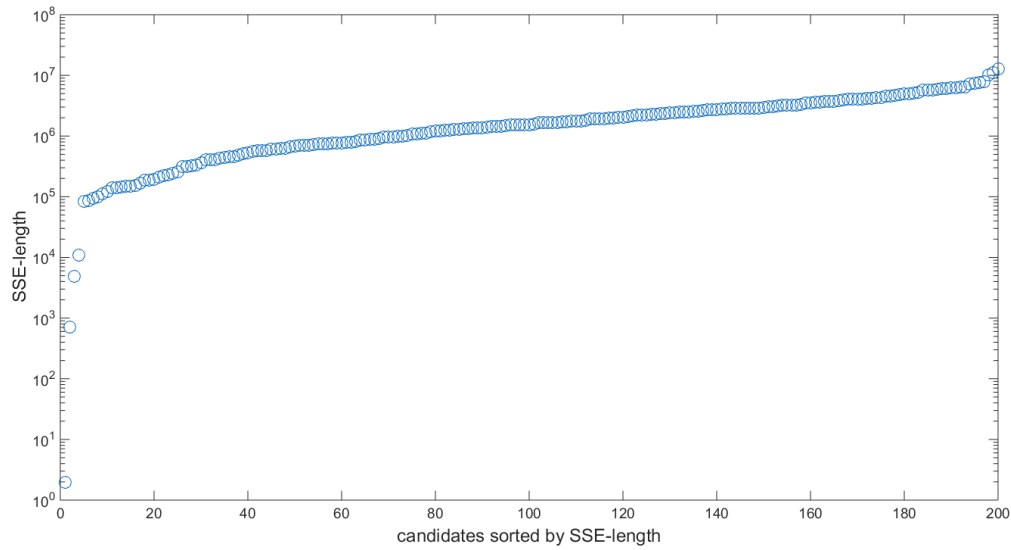


Figure 5.8: Logarithmic distribution of length-residual candidates. A high discrimination (factor 353) of best to second-best candidate is given.

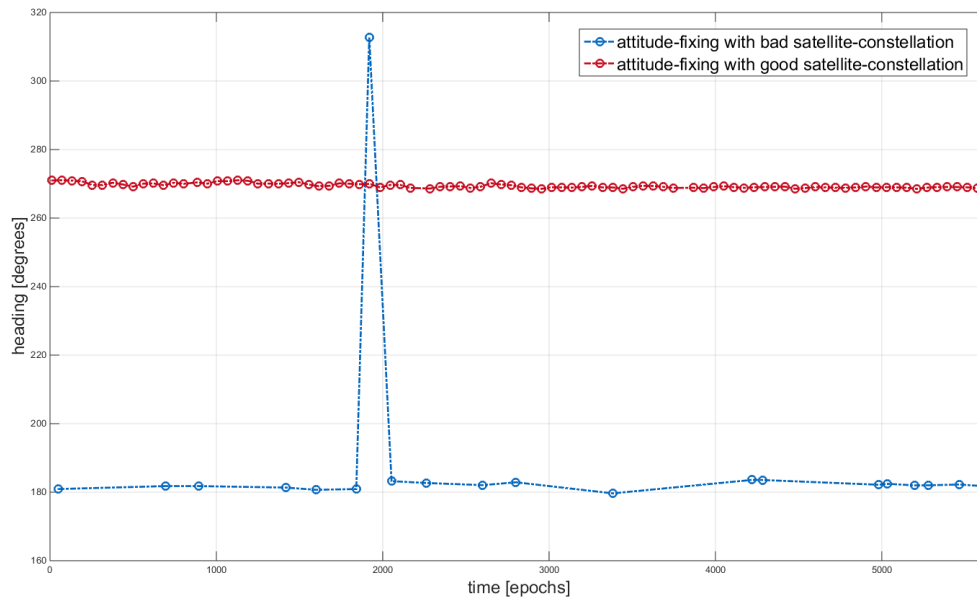


Figure 5.9: Continuous re-fixing of ambiguities with length-residuals. The correct heading was rough 270 degrees for the red curve and nearly 180 degrees for the blue curve. The red one has a good satellite-constellation, the blue a bad one.

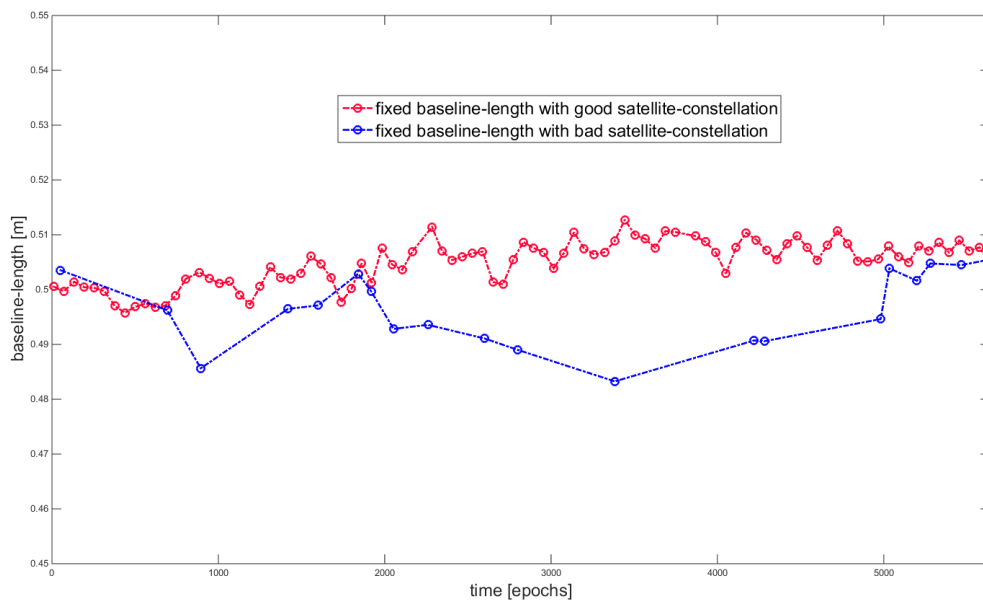


Figure 5.10: Comparison of the fixed baseline-length with good (red) and bad (blue) satellite-constellation. fixing of ambiguities with length-residuals. The correct is 50 cm with a sigma of 1 cm.

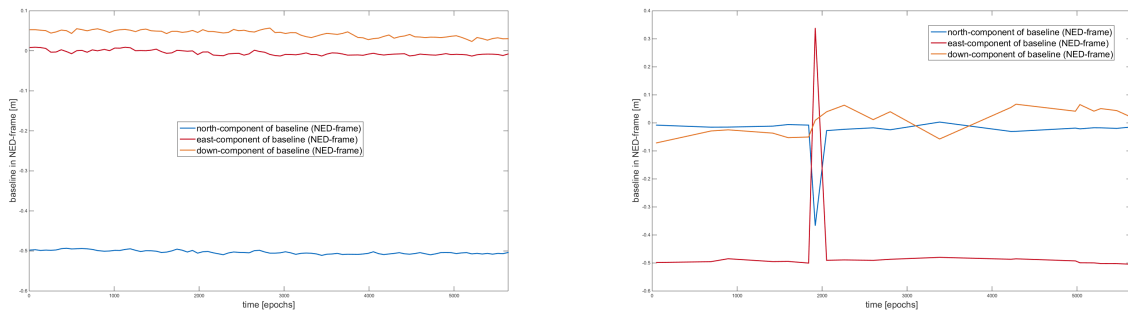
constellations. The peaks of the right plot overlaps with the false fixing in this time.

At the moment, there are still problems in cases with extremely bad satellite-constellations (≤ 5 satellites in bad constellation) and in conditions with high phase multipath. The reliability would increase in such cases, if one takes also the satellite-systems GLONASS and Galileo into account.

In figure 5.12, the coarse progress of ambiguity-fixing for the attitude-baseline is finally shown. The diagram gives reasons for restarts and also constellations with bad fixing, what leads to a next try of ambiguity-fixing after 20 epochs. An important constrain is that the SSE-value of the best candidate is smaller then 10. In dimensions, this means that the fixed baseline-length differs of a maximum of 3 cm in comparison to the a-priori length-information. In cases of more candidates fall below this limit, the SSE-values depending on the measurement-residuals for the best length-residual candidates are included in the decision. If there is again not enough discrimination between the best two candidates a new try of ambiguity-fixing is performed.

5.3 The float Kalman filter of the RTK-baseline

The basic measurement-models are already described. For a system with two low-cost receivers at the rover and a VRS with correction-data, the models are once again transformed respectively extended to benefit from the advantages of the additional reference-station. To describe the fixing of the RTK-baseline, first of all the parametrization of the Kalman filter is defined. Especially the differences to the attitude float Kalman filter. After this, the fixing of the RTK-baseline is described briefly.



(a) Fixed baseline-vector in the navigation- (NED) frame with good satellite-constellation (b) Fixed baseline-vector in the navigation- (NED) frame with bad satellite-constellation

Figure 5.11: Comparison of the fixed baseline in the navigation- (NED) frame with good (left) and bad (right) satellite-constellation. The peaks on the right plot are in same time as the false fixing of the double-difference ambiguities.

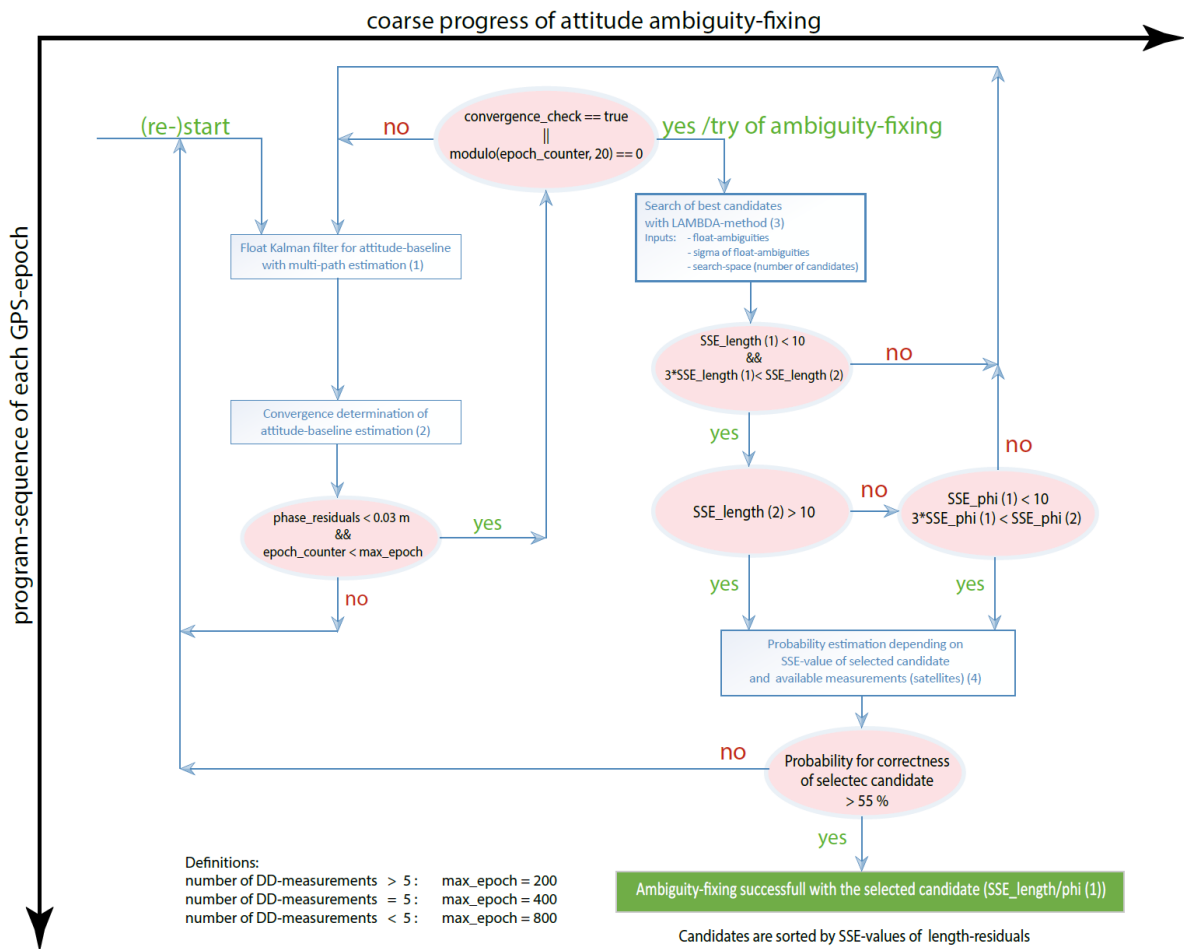


Figure 5.12: Schematic representation of the ambiguity-fixing for the attitude-baseline

5.3.1 The parametrization of the float Kalman filter

The measurements of the float Kalman filter are used as double-differences. Also a synchronization-correction is needed, which is determined in the same way as in eqn. 5.1 till 5.4. The phase-measurements are used in the following way:

$$\begin{aligned}\lambda\tilde{\varphi}_{13}^{kl}(t_n) &= \lambda\varphi_{13}^{kl}(t_n) - c_{13}^{kl}(t_n) \\ &= \vec{e}_1^{kl}(t_n)\vec{b}_{13}(t_n) + \lambda N_{13}^{kl} + \varepsilon_{13}^{kl}(t_n)\end{aligned}\quad (5.32)$$

The multipath error $\lambda\Delta\varphi_{MP,13}^{kl}(t_n)$ is negligible. Also the half cycle-slips $\Delta N_{13}^{kl}(t_n)$ are not considered till the fixing of double-difference ambiguities of the RTK-baseline.

The pseudo-range measurements are given by:

$$\begin{aligned}\tilde{\rho}_{13}^{kl}(t_n) &= \rho_{13}^{kl}(t_n) - c_{13}^{kl}(t_n) \\ &= \vec{e}_1^{kl}(t_n)\vec{b}_{13}(t_n) + \Delta\rho_{MP,13}^{kl}(t_n) + \eta_{13}^{kl}(t_n)\end{aligned}\quad (5.33)$$

The amount of measurements is doubled with a simple relation. As shown in figure 5.13, one can set a further baseline-vector \vec{b}_{23} , which is usable with a simple vector-addition. For the associated phase-measurement the following relation is given:

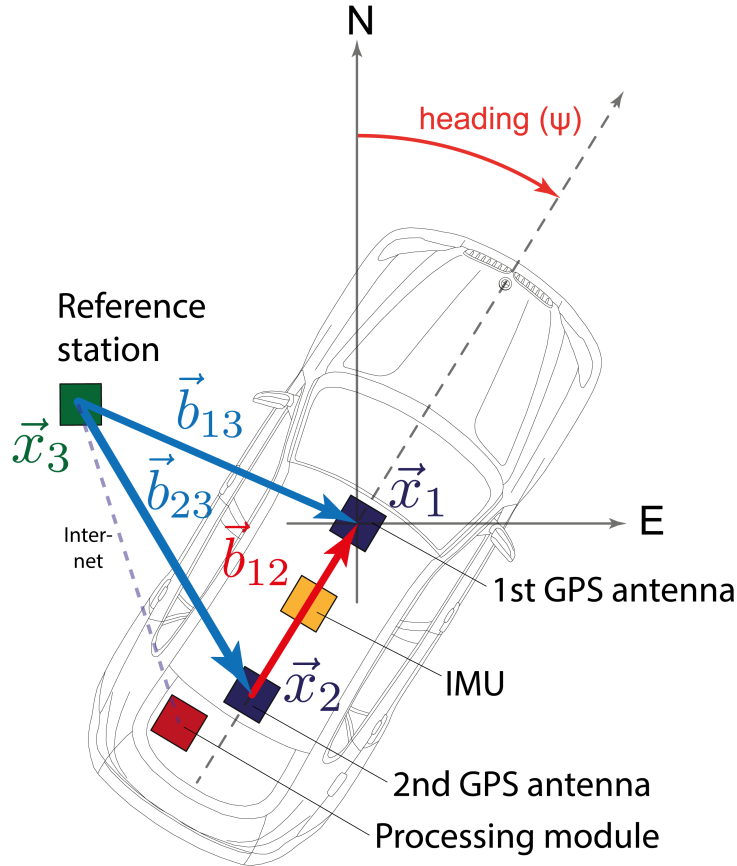


Figure 5.13: The schematic measurement-setup with three baseline-vectors

$$\begin{aligned}\lambda\varphi_{23}^{kl}(t_n) &= \lambda\tilde{\varphi}_{13}^{kl}(t_n) - \lambda\tilde{\varphi}_{12}^{kl}(t_n) \\ &= \vec{e}_1^{kl}(t_n)(\vec{b}_{13}(t_n) - \vec{b}_{12}(t_n)) + \lambda N_{13}^{kl} - \lambda N_{12}^{kl} + \varepsilon_{13}^{kl}(t_n) - \varepsilon_{12}^{kl}(t_n)\end{aligned}\quad (5.34)$$

To get the advantages of doubling the amount of measurements, the previous fixing of the attitude-baseline is required. With the help of this condition, the known terms are brought to the left-hand side.

$$\begin{aligned}\lambda\tilde{\varphi}_{23}^{kl}(t_n) &= \lambda\varphi_{23}^{kl}(t_n) + \vec{e}_1^{kl}(t_n)\vec{b}_{12}(t_n) + \lambda N_{12}^{kl} \\ &= \vec{e}_1^{kl}(t_n)\vec{b}_{13}(t_n) + \lambda N_{13}^{kl} + \varepsilon_{13}^{kl}(t_n) - \varepsilon_{12}^{kl}(t_n)\end{aligned}\quad (5.35)$$

According to the phase-measurement, the pseudo-range measurements are also doubled for the Kalman filter.

$$\begin{aligned}\rho_{23}^{kl}(t_n) &= \rho_{13}^{kl}(t_n) - \rho_{12}^{kl}(t_n) \\ &= \vec{e}_1^{kl}(t_n)(\vec{b}_{13}(t_n) - \vec{b}_{12}(t_n)) + \Delta\rho_{MP,13}^{kl}(t_n) - \Delta\rho_{MP,12}^{kl}(t_n) + \eta_{13}^{kl}(t_n) - \eta_{12}^{kl}(t_n)\end{aligned}\quad (5.36)$$

To get all known terms on the left-hand side, the multipath for the attitude-baseline should also be determined:

$$\Delta\rho_{MP,12}^{kl}(t_n) = \rho_{12}^{kl}(t_n) - \vec{e}_1^{kl}(t_n)\vec{b}_{12}(t_n)\quad (5.37)$$

Finally, the measurement-model of the pseudo-range in terms of the baseline \vec{b}_{23} is given by

$$\begin{aligned}\tilde{\rho}_{23}^{kl}(t_n) &= \rho_{23}^{kl}(t_n) + \vec{e}_1^{kl}(t_n)\vec{b}_{12}(t_n) + \Delta\rho_{MP,12}^{kl}(t_n) \\ &= \vec{e}_1^{kl}(t_n)\vec{b}_{13}(t_n) + \Delta\rho_{MP,13}^{kl}(t_n) + \eta_{13}^{kl}(t_n) - \eta_{12}^{kl}(t_n)\end{aligned}\quad (5.38)$$

It should be borne in mind, that the measurements in eqn. 5.35 and 5.38 are strongly correlated with the measurements of $\lambda\tilde{\varphi}_{13}^{kl}$ respectively $\tilde{\rho}_{13}^{kl}$. This aspect is treated in the noise-statistics. Finally, there are only the unknowns on the right-hand side of the measurement equations, which are estimated in the state-vector. The states are given in vector-notation:

$$x = \begin{pmatrix} \vec{b}_{13} \\ N_{13} \\ \Delta\rho_{MP,13}^{kl} \end{pmatrix}\quad (5.39)$$

The baseline-vector \vec{b}_{13} is given in the geocentric coordinate-system ECEF (Earth-Centered, Earth-Fixed).

The measurement-vector for the float Kalman filter is given by

$$z = \begin{pmatrix} \lambda\tilde{\varphi}_{13}^{kl} \\ \lambda\tilde{\varphi}_{23}^{kl} \\ \tilde{\rho}_{13}^{kl} \\ \tilde{\rho}_{23}^{kl} \end{pmatrix}\quad (5.40)$$

The additional described measurements of the RTK-baseline \vec{b}_{23} are added to the measurement vector. An a-priori information about the height can't be done for the RTK-baseline, because there is no information given about a flat baseline between the big space of the rover

and the virtual reference-station (VRS).

As introduced in the float-filter of the attitude-baseline, the transition-matrix is set with the identity-matrix. The condition for a static rover within the initialization-phase till the fixing is also given here.

The observation-matrix is given as follows:

$$H = \begin{pmatrix} \vec{e}_{132 \times 3}^{kl} & I_{32 \times 32} \cdot \lambda & 0_{32 \times 32} \\ \vec{e}_{132 \times 3}^{kl} & I_{32 \times 32} \cdot \lambda & 0_{32 \times 32} \\ \vec{e}_{132 \times 3}^{kl} & 0_{32 \times 32} & I_{32 \times 32} \\ \vec{e}_{132 \times 3}^{kl} & 0_{32 \times 32} & I_{32 \times 32} \end{pmatrix} \quad (5.41)$$

The parameters for process- and measurement-noise are here also a limiting-factor for the functionality of the float Kalman filter. An estimation of the parameters is tried in the same adaptive way as for the attitude-baseline.

Finally, the process-noise of the RTK-baseline and of the double-difference ambiguities is chosen static. The maximum change of the baseline in one epoch is initialized with $\sigma_{b_{13}}^- = 0.5$ cm. For a clear separation of the state-parameters, the process-noise for the double-difference ambiguities is chosen very small ($\sigma_{N_{13}} = 0.001$ Cycles). The right DD-ambiguities are determined in the fixing-step.

The following overview shows the complete matrix of measurement-noise (Gl. 5.42):

$$\Sigma_R = \begin{pmatrix} \Sigma_{\vec{\varphi}_{13}^{kl}} & 0_{32 \times 32} & 0_{32 \times 32} & 0_{32 \times 32} \\ 0_{32 \times 32} & \Sigma_{\vec{\varphi}_{23}^{kl}} & 0_{32 \times 32} & 0_{32 \times 32} \\ 0_{32 \times 32} & 0_{32 \times 32} & \Sigma_{\vec{\rho}_{13}^{kl}} & 0_{32 \times 32} \\ 0_{32 \times 32} & 0_{32 \times 32} & 0_{32 \times 32} & \Sigma_{\vec{\rho}_{23}^{kl}} \end{pmatrix} \quad (5.42)$$

The chosen process-noise is given by (Gl. 5.43):

$$\Sigma_Q = \begin{pmatrix} \Sigma_{b_{13}} & 0_{32 \times 32} & 0_{32 \times 32} \\ 0_{32 \times 32} & \Sigma_{N_{13}} & 0_{32 \times 32} \\ 0_{32 \times 32} & 0_{32 \times 32} & \Sigma_{\Delta \rho_{MP,13}^{kl}} \end{pmatrix} \quad (5.43)$$

Thereby the process-noise of the RTK-baseline is first of all rotated in the ECEF-frame to the corresponding phase-measurement and pseudo-range:

$$\Sigma_{b_{13}} = R_n^e \begin{pmatrix} \Sigma_{b_{13X}} & 0 & 0 \\ 0 & \Sigma_{b_{13Y}} & 0 \\ 0 & 0 & \Sigma_{b_{13Z}} \end{pmatrix} (R_n^e)^T \quad (5.44)$$

with R_n^e as rotation-matrix of the navigation- (NED) frame to the ECEF-frame and with $\Sigma_{b_{13}^{x/y/z}}$ as process-noise in navigation-frame.

5.4 Ambiguity-fixing of the RTK-baseline

In this section, we describe the ambiguity fixing method of our RTK. We start with a motivation, i.e. it is explained that the widely used standard LAMBDA method cannot give a reliable solution as it fully relies on the float ambiguity covariance matrix and does not consider any errors in this covariance matrix.

- The temporal correlation of the measurement noise (due to phase multipath or due to receiver-internal coupling of tracking loops) is not known. The Kalman filter (or any least-squares block processing) of the float solution assumes a white Gaussian measurement noise, which is not realistic. Therefore, the statistics of the float ambiguity solution are not trustworthy.
- An integer error in the float ambiguity solution results in the same integer error of the fixed solution and cannot be recognized from the ambiguity residuals $\hat{N}_r^k - \check{N}_r^k$. Thus, an erroneous candidate might be chosen from the ambiguity residuals.

We have extended the LAMBDA method to overcome the previous disadvantages. The method includes three phases:

- The first phase is the *candidate collection phase*. The integer candidates are obtained from the float solution using the classical integer decorrelation and sequential tree search of the LAMBDA method. As the float solution might be biased, we determine sets of candidates in a regular interval (every 50 epochs) from the float solution, and merge these candidates. This candidate collection phase is triggered once the baseline of the float solution is sufficiently stable. We have chosen a baseline stability requirement of 40 cm/200 epochs to obtain a reasonable trade-off between convergence time and probability of including the correct candidate in the set of candidates.
- The second phase is the *candidate tracking phase*. We determine a *single-epoch* least-squares baseline estimate for *every* integer candidate vector at *every* epoch and store the fixed phase measurement residuals. As the solution is computed on a single epoch basis, the temporal correlation of the measurements does not need to be considered.
- The third phase is the *candidate selection phase*. We use two criteria for candidate selection: the accumulated sum of squared phase residuals and the baseline stability. The *accumulation* of the sum of squared phase residuals *over time* improves the reliability. The analysis of the baseline stability further enhances the success rate as the fixed baseline starts to drift for all erroneous candidates. This drift of the baseline can be explained from the mapping of the integer error into the baseline. As the integer error is constant but $\vec{e}_r k$ is changing with time, the baseline estimate has to change to compensate for the change of $\vec{e}_r k$. Thus, the baseline stability is a valuable information for candidate selection.

The subsequent figures and tables show the performance of our fixing, i.e. a millimeter-level positioning accuracy is obtained despite code multipath errors of up to 100 m. For this test campaign with long RTK-baselines, we introduced in datasets with good conditions an artificial code multipath in a random-walk process (see figure 5.15). Besides this, we removed satellites randomly. Finally, figure 5.16 shows the performance of the RTK ambiguity fixing. The solutions are given in cases with quite bad satellite constellation and with less/much code multipath.

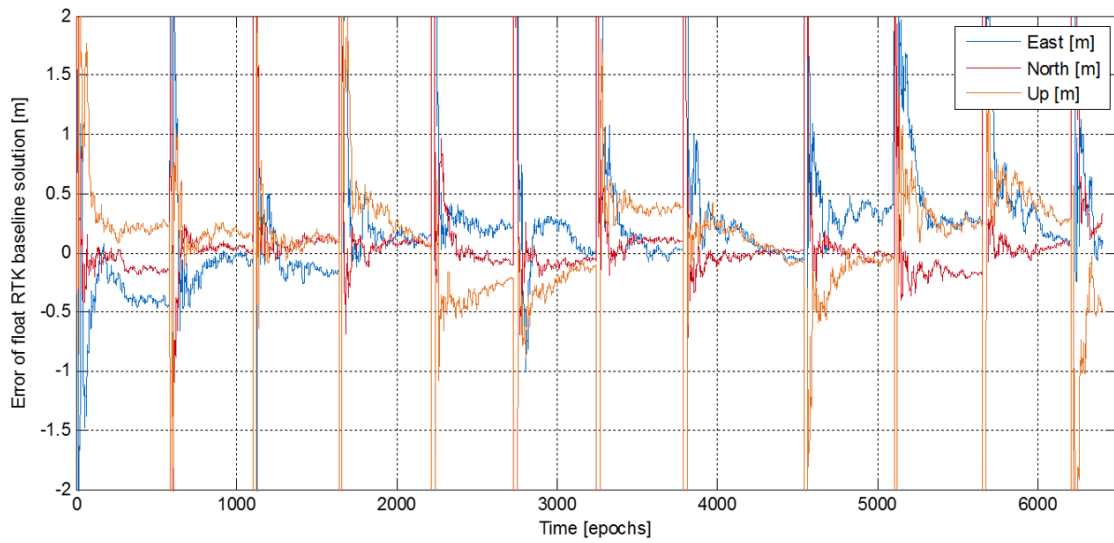


Figure 5.14: Float-solution of the RTK-baseline. The Kalman filter converges under 0.5 m. Restarts are performed after achieved fixing (peaks in the baseline estimation).

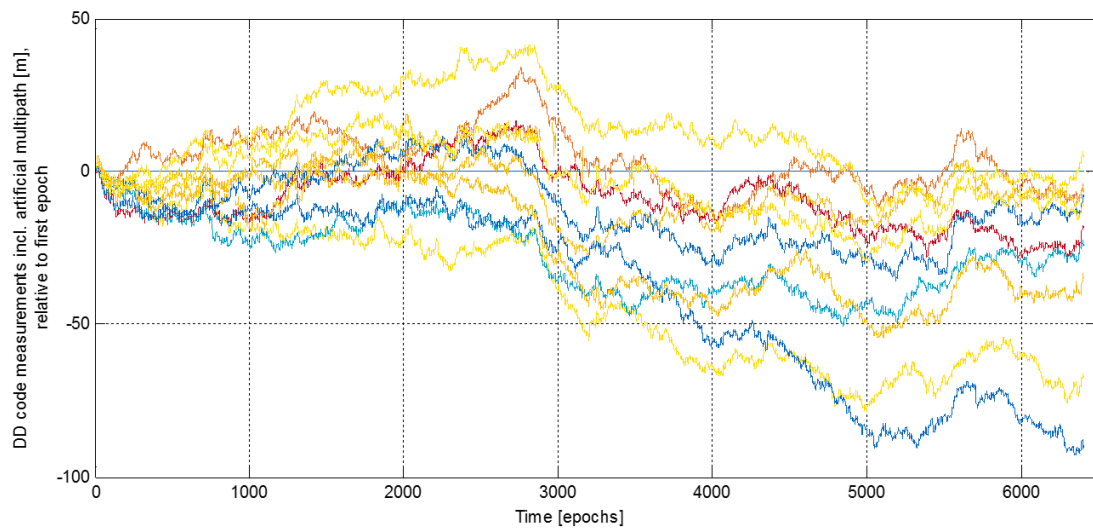


Figure 5.15: Double-difference measurements with artificial added code multipath with the help of a random-walk process

2015-07-20 - Asdheim - Long range static RTK (Receiver_South_104m_2015_07_20_22_10 (SVN code revision: 694, Artificial multipath (random walk, sigma_init = 3m, sigma_delta = 0.2 m. PRN 23, 1 and 19 artificially removed.)																	
Further parameters: ncands = 500, t_ep = 1000 (>6 DD), else 2000.																	
Index	Fixed RTK baseline estimate [m]			Error of fixed RTK baseline estimate [m]			Length [m]	Heading [deg]	Pitch [deg]	Epochs to stable float solution (0.4 m/ 200 ep.)	Total num. of epochs to final fixing (ratio of 2 for basel. drift)	Ambiguity index of chosen candidate	Filtered SSE of fixed phase resid. over 10 epochs	Baseline drift [m/s]	Ratio of baseline drifts	Number of used sat. for fixing	Result code
	East	North	Up	East	North	Up											
1	12,894	103,323	-0,368	-0,002	-0,003	-0,011	104,125	7,113	-0,202	431	1481	1	1,587	0,0000439	2,07	6	40
2015-07-20 - Asdheim - Long range static RTK (Receiver_South_104m_2015_07_20_22_10 (SVN code revision: 695, Artificial multipath (random walk, sigma_init = 3m, sigma_delta = 0.2 m. PRN 19, 1 and 32 artificially removed.)																	
Further parameters: ncands = 500, t_ep = adaptive with number of DD.																	
Index	Fixed RTK baseline estimate [m]			Error of fixed RTK baseline estimate [m]			Length [m]	Heading [deg]	Pitch [deg]	Epochs to stable float solution (0.4 m/ 200 ep.)	Total num. of epochs to final fixing (ratio of 2 for basel. drift)	Ambiguity index of chosen candidate	Filtered SSE of fixed phase resid. over 10 epochs	Baseline drift [m/s]	Ratio of baseline drifts	Number of used sat. for fixing	Result code
	East	North	Up	East	North	Up											
1	12,887	103,443	-0,154	-0,009	0,117	0,203	104,242	7,102	-0,085	476	1326	353	0,749	0,00004190	1,18	6	40
2	12,900	103,323	-0,361	0,004	-0,003	-0,004	104,126	7,117	-0,199	367	1317	2	1,528	0,00003170	1,21	6	40
2015-07-20 - Asdheim - Long range static RTK (Receiver_South_104m_2015_07_20_22_10 (SVN code revision: 695, Artificial multipath (random walk, sigma_init = 3m, sigma_delta = 0.2 m. PRN 17, 19 and 28 artificially removed.)																	
Further parameters: ncands = 500, t_ep = adaptive with number of DD.																	
Index	Fixed RTK baseline estimate [m]			Error of fixed RTK baseline estimate [m]			Length [m]	Heading [deg]	Pitch [deg]	Epochs to stable float solution (0.4 m/ 200 ep.)	Total number of epochs to final fixing (ratio of 2 for baseline drift)	Ambiguity index of chosen candidate	Filtered SSE of fixed phase resid. over 10 epochs	Baseline drift [m/s]	Ratio of baseline drifts	Number of used sat. for fixing	Result code
	East	North	Up	East	North	Up											
1	12,892	103,331	-0,348	-0,004	0,005	0,009	104,133	7,112	-0,191	382	682	9	8,467	0,00005260	2,73	7	40
2	12,896	103,333	-0,354	0,000	0,007	0,003	104,135	7,114	-0,195	344	644	7	6,512	0,00002020	8,11	7	40
3	12,897	103,323	-0,370	0,001	-0,003	-0,013	104,126	7,115	-0,204	384	684	1	1,015	0,00012700	1,47	7	40
2015-07-20 - Asdheim - Long range static RTK (Receiver_South_104m_2015_07_20_22_10 (SVN code revision: 695, Artificial multipath (random walk, sigma_init = 3m, sigma_delta = 0.2 m. PRN 4, 23 and 19 artificially removed.)																	
Further parameters: ncands = 500, t_ep = adaptive with number of DD.																	
Index	Fixed RTK baseline estimate [m]			Error of fixed RTK baseline estimate [m]			Length [m]	Heading [deg]	Pitch [deg]	Epochs to stable float solution (0.4 m/ 200 ep.)	Total number of epochs to final fixing (ratio of 2 for baseline drift)	Ambiguity index of chosen candidate	Filtered SSE of fixed phase resid. over 10 epochs	Baseline drift [m/s]	Ratio of baseline drifts	Number of used sat. for fixing	Result code
	East	North	Up	East	North	Up											
1	12,897	103,321	-0,374	0,001	-0,005	-0,017	104,123	7,115	-0,206	384	984	1	2,097	0,00004680	2,07	6	40
2	12,898	103,323	-0,367	0,002	-0,003	-0,010	104,126	7,115	-0,202	368	868	1	0,237	0,00001900	6,98	6	40
3	12,899	103,324	-0,354	0,003	-0,002	0,003	104,127	7,116	-0,195	399	899	2	0,269	0,00008800	1,08	6	40
4	12,901	103,320	-0,364	0,005	-0,006	-0,007	104,122	7,117	-0,200	322	822	1	0,398	0,00004390	2,72	6	40
2015-07-20 - Asdheim - Long range static RTK (Receiver_South_104m_2015_07_20_22_10 (SVN code revision: 695, Artificial multipath (random walk, sigma_init = 3m, sigma_delta = 0.2 m. PRN 4, 17 and 22 artificially removed.)																	
Further parameters: ncands = 500, t_ep = adaptive with number of DD.																	
Index	Fixed RTK baseline estimate [m]			Error of fixed RTK baseline estimate [m]			Length [m]	Heading [deg]	Pitch [deg]	Epochs to stable float solution (0.4 m/ 200 ep.)	Total number of epochs to final fixing (ratio of 2 for baseline drift)	Ambiguity index of chosen candidate	Filtered SSE of fixed phase resid. over 10 epochs	Baseline drift [m/s]	Ratio of baseline drifts	Number of used sat. for fixing	Result code
	East	North	Up	East	North	Up											
1	12,895	103,328	-0,352	-0,001	0,002	0,005	104,130	7,113	-0,194	393	693	39	12,974	0,00005760	2,88	7	40
2	12,897	103,331	-0,355	0,001	0,005	0,002	104,133	7,115	-0,195	333	633	11	7,764	0,00002340	11,46	7	40
3	12,896	103,325	-0,367	0,000	-0,001	-0,010	104,127	7,114	-0,202	335	685	1	3,152	0,00009950	1,47	7	40

Figure 5.16: Solutions of the RTK ambiguity fixing in cases with artificial code multipath and artificially removed satellites. The RTK-baseline estimation has an accuracy in centimeter-level in all sufficient fixings.

Chapter 6

Joint RTK and attitude determination in a tight-coupled system

After the description of the sequential conditional fixing of the attitude- and RTK ambiguities in the previous chapter, the tight coupling of GPS/INS with correction-data from a virtual reference-station (VRS) is described in this section. Once both RTK and attitude ambiguities are fixed and the respective baselines are known with millimeter-level accuracy and the IMU is calibrated, one can switch to the tight coupling for the dynamic system. Compare here again with figure 4.3 to see the relationships of the processing-steps. One reaches now the last program-loop in this figure. As well as in the float-filters, a further extended Kalman filter is needed.

6.1 The measurement-model of the tight-coupled EKF

The measurement-model for the tightly coupled extended Kalman filter (EKF) is not the same as for the float filters due to the usage of single-difference (SD) measurements. The reason for this implementation is the high expandability of the software in cases with no complete measurements by reference-stations, but only with models and correction-parameters for calculating the error-terms. The performance is not affected by the other way of differentiation (SD against DD).

It must be noted, that the VRS transmits its phase-measurement and pseudo-range with an update-rate of 1 Hz. Besides this, the absolute position of the VRS is transferred in the ECEF-frame. Doppler-measurements are logically not provided by the reference-station.

The basic measurement-models are described in the beginning of this thesis. For a system with two low-cost GNSS receivers at the rover and a VRS, the models can be once again re-modeled respectively extended. Through this step, the advantages of an additional reference-station can be taken into account to estimate the states in the extended Kalman filter (EKF) more accurately. First of all, the model of the single-difference (SD) phase in the general derivation in eqn. 2.7 is considered, here in the special case for the first receiver. Known terms such as satellite position, clock offset and tropospheric delay are already subtracted in the next formulations:

$$\lambda\varphi_1^{kl}(t_n) = \vec{e}_1^{kl}(t_n)\vec{x}_1(t_n) - I^{kl}(t_n) + \lambda N_1^{kl} + \lambda\beta^{kl}(t_n) + \varepsilon_1^{kl}(t_n) \quad (6.1)$$

An ionospheric-delay with a dependency of a special receiver is forgone in this case. Receivers within a space of 5 km have nearly an identical influence of ionospheric-delay. The half cycle-slips ΔN_1^{kl} are assumed to be known. The determination of such cycle-slips is described in a later step in this thesis.

The integer property of the double difference ambiguities shall be exploited. Therefore, we express the single difference ambiguities of each receiver in terms of the single difference ambiguities of the reference station and the double difference integer ambiguities (attitude and RTK). The ionosphere delay satellite phase bias is mapped to the single difference ambiguity, which is treated as a real-valued term.

Next, the measurement is introduced in dependency of the state-vector. For this, compare the unknown states in eqn. 6.1 with the complete state-vector of the tight-coupled system in eqn. 4.4. With the help of $\vec{e}_1^{kl}(t_n)\vec{x}_1(t_n) = \vec{e}_1^{kl}(t_n)\vec{b}_{13}(t_n) + \vec{e}_1^{kl}(t_n)\vec{x}_3(t_n)$ and $\lambda N_1^{kl} = \lambda N_{13}^{kl} + \lambda N_3^{kl}$ one gets an equation in dependency of only to be estimated parameters in the tight-coupled fixed Kalman filter.

$$\begin{aligned}\lambda\tilde{\varphi}_1^{kl}(t_n) &= \lambda\varphi_1^{kl}(t_n) - \lambda N_{13}^{kl} - \vec{e}_1^{kl}(t_n)\vec{x}_3(t_n) \\ &= \vec{e}_1^{kl}(t_n)\vec{b}_{13}(t_n) + \lambda N_3^{kl} - I^{kl}(t_n) + \lambda\beta^{kl}(t_n) + \varepsilon_1^{kl}(t_n)\end{aligned}\quad (6.2)$$

Now, one can consider the phase-measurement of the second receiver. With the rearrangement of $\vec{e}_1^{kl}(t_n)\vec{x}_2(t_n) = \vec{e}_1^{kl}(t_n)(\vec{b}_{13}(t_n) - \vec{b}_{12}(t_n)) + \vec{e}_1^{kl}(t_n)\vec{x}_3(t_n)$ and $\lambda N_2^{kl} = \lambda(N_{13}^{kl} - N_{12}^{kl} + N_3^{kl})$, the measurement is again described in relation to the state-vector. It should be kept in mind that the synchronization-correction $c_{12}^{kl}(t_n)$ between the receivers, whereby the first receiver is given as reference, is also needed in this model. This means in context, the measurements of the second receiver are synchronized with the first receiver.

$$\begin{aligned}\lambda\tilde{\varphi}_2^{kl}(t_n) &= \lambda\varphi_2^{kl}(t_n) + c_{12}^{kl}(t_n) - \lambda N_{13}^{kl} + \lambda N_{12}^{kl} - \vec{e}_1^{kl}(t_n)\vec{x}_3(t_n) \\ &= \vec{e}_1^{kl}(t_n)(\vec{b}_{13}(t_n) - \vec{b}_{12}(t_n)) + \lambda N_3^{kl} - I^{kl}(t_n) + \lambda\beta^{kl}(t_n) + \varepsilon_2^{kl}(t_n)\end{aligned}\quad (6.3)$$

The last single difference (SD) phase-measurement describes the virtual reference-station (VRS). There are no further simplifications needed, only the synchronization-correction $c_{13}^{kl}(t_n)$ must be noted. The exact position of the reference-station is transmitted with the correction-data.

$$\begin{aligned}\lambda\tilde{\varphi}_3^{kl}(t_n) &= \lambda\varphi_3^{kl}(t_n) + c_{13}^{kl}(t_n) - \vec{e}_1^{kl}(t_n)\vec{x}_3(t_n) \\ &= \underbrace{\lambda N_3^{kl} - I^{kl}(t_n) + \lambda\beta^{kl}(t_n)}_{\text{single state parameter}} + \varepsilon_3^{kl}(t_n)\end{aligned}\quad (6.4)$$

Next, the model for the single-difference pseudo-range in eqn. 2.5 is considered. First of all, in general for receiver one:

$$\rho_1^{kl}(t_n) = \vec{e}_1^{kl}(t_n)\vec{x}_1(t_n) + I^{kl}(t_n) + b^{kl}(t_n) + \Delta\rho_{MP,1}^{kl}(t_n) + \eta_1^{kl}(t_n)\quad (6.5)$$

The ionospheric-delay is again not specified for a single receiver. The special measurement-models of the single-difference pseudo-range in dependency of the state-parameters are set in the same way as for the phase-measurements. For completeness, here are the three measurement-models for the single-difference (SD) pseudo-range:

$$\begin{aligned}\tilde{\rho}_1^{kl}(t_n) &= \rho_1^{kl}(t_n) - \vec{e}_1^{kl}(t_n)\vec{x}_3(t_n) \\ &= \vec{e}_1^{kl}(t_n)\vec{b}_{13}(t_n) + \Delta\rho_{MP,1}^{kl}(t_n) + I^{kl}(t_n) + b^{kl}(t_n) + \eta_1^{kl}(t_n)\end{aligned}\quad (6.6)$$

$$\begin{aligned}\tilde{\rho}_2^{kl}(t_n) &= \rho_2^{kl}(t_n) + c_{12}^{kl}(t_n) - \vec{e}_1^{kl}(t_n)\vec{x}_3(t_n) \\ &= \vec{e}_1^{kl}(t_n)(\vec{b}_{13}(t_n) - \vec{b}_{12}(t_n)) + \Delta\rho_{MP,2}^{kl}(t_n) + I^{kl}(t_n) + b^{kl}(t_n) + \eta_2^{kl}(t_n)\end{aligned}\quad (6.7)$$

$$\begin{aligned}\tilde{\rho}_3^{kl}(t_n) &= \rho_3^{kl}(t_n) + c_{13}^{kl}(t_n) - \vec{e}_1^{kl}(t_n)\vec{x}_3(t_n) \\ &= \Delta\rho_{MP,3}^{kl}(t_n) + I^{kl}(t_n) + b^{kl}(t_n) + \eta_3^{kl}(t_n)\end{aligned}\quad (6.8)$$

As mentioned before, the Doppler-measurement is not given for the virtual reference-station (VRS). With the general measurement model in eqn. 2.9, the Doppler-measurement for the first receiver is given by

$$\tilde{f}_{D1}^{kl}(t_n) = -\frac{f_T}{c} \tilde{e}_1^{*kl}(t_n) \vec{v}_1(t_n) + \eta_{D1}^{kl}(t_n) \quad (6.9)$$

Note that the receiver clock drift was eliminated by single differencing. The satellite clock drift is below the noise level and, therefore not treated as additional parameter.

The Doppler-measurement for the second receiver is again described in dependency of the state-vector of the fixed extended Kalman filter. With the relation $\vec{v}_2 = \vec{v}_1 - \dot{\vec{b}}_{12}$, the Doppler-measurement of the second receiver is given by

$$\tilde{f}_{D2}^{kl}(t_n) = -\frac{f_T}{c} \tilde{e}_2^{*kl}(t_n) (\vec{v}_1 - \dot{\vec{b}}_{12}) + \eta_{D2}^{kl}(t_n) \quad (6.10)$$

The described measurement-models for all three receivers include in this application eight measurements for each available satellite-satellite single-difference (SD). On the right-hand side of all measurement-equations are only the unknown states left, which are estimated in the fixed extended Kalman filter. The whole measurement-model for the fixed filter is given in eqn. 6.11. On the left-hand side of the equations are all parameters, which are determined with models or are included in the navigation-sequence of the satellites. These states must not be estimated by the fixed extended Kalman filter.

$$\left(\begin{array}{l}
\lambda \tilde{\varphi}_1^{kl} = \lambda \varphi_1^{kl} - \bar{e}_1^{*kl} \bar{x}_3 + \bar{e}_1^* \bar{x}^k - \bar{e}_1^l \bar{x}^l + c \delta t^{kl} - T_1^{kl} - \lambda N_{13}^{kl} - \frac{\lambda}{2} \Delta N_{13}^{kl} \\
\lambda \tilde{\varphi}_2^{kl} = \lambda \varphi_2^{kl} - \bar{e}_1^{*kl} \bar{x}_3 + \bar{e}_1^* \bar{x}^k - \bar{e}_1^l \bar{x}^l + c \delta t^{kl} - T_1^{kl} + c_{12}^{kl} - \lambda N_{13}^{kl} - \frac{\lambda}{2} \Delta N_{13}^{kl} + \lambda N_{12}^{kl} + \frac{\lambda}{2} \Delta N_{12}^{kl} \\
\lambda \tilde{\varphi}_3^{kl} = \lambda \varphi_3^{kl} - \bar{e}_1^{*kl} \bar{x}_3 + \bar{e}_1^* \bar{x}^k - \bar{e}_1^l \bar{x}^l + c \delta t^{kl} - T_1^{kl} + c_{13}^{kl} \\
\hline
\tilde{\rho}_1^{kl} = \rho_1^{kl} - \bar{e}_1^{*kl} \bar{x}_3 + \bar{e}_1^* \bar{x}^k - \bar{e}_1^l \bar{x}^l + c \delta t^{kl} - T_1^{kl} \\
\tilde{\rho}_2^{kl} = \rho_2^{kl} - \bar{e}_1^{*kl} \bar{x}_3 + \bar{e}_1^* \bar{x}^k - \bar{e}_1^l \bar{x}^l + c \delta t^{kl} - T_1^{kl} + c_{12}^{kl} \\
\tilde{\rho}_3^{kl} = \rho_3^{kl} - \bar{e}_1^{*kl} \bar{x}_3 + \bar{e}_1^* \bar{x}^k - \bar{e}_1^l \bar{x}^l + c \delta t^{kl} - T_1^{kl} + c_{13}^{kl} \\
\hline
\tilde{f}_{D1}^{kl} = f_{D1}^{kl} - \frac{f_r}{c} \left((\bar{e}_1^* \bar{v}^k - \bar{e}_1^l \bar{v}^l) + c \dot{\delta} t^{kl} \right) \\
\tilde{f}_{D2}^{kl} = f_{D2}^{kl} - \frac{f_r}{c} \left((\bar{e}_1^* \bar{v}^k - \bar{e}_1^l \bar{v}^l) + c \dot{\delta} t^{kl} \right)
\end{array} \right) = \left(\begin{array}{l}
\bar{e}_1^{*kl} \bar{b}_{13} + \lambda N_3^{kl} - I^{kl} + \lambda \beta^{kl} + \varepsilon_1^{kl} \\
\bar{e}_1^{*kl} (\bar{b}_{13} - \bar{b}_{12}) + \lambda N_3^{kl} - I^{kl} + \lambda \beta^{kl} + \varepsilon_2^{kl} \\
\lambda N_3^{kl} - I^{kl} + \lambda \beta^{kl} + \varepsilon_3^{kl} \\
\hline
\bar{e}_1^{*kl} \bar{b}_{13} + \Delta \rho_{MP,1}^{kl} + I^{kl} + b^{kl} + \eta_1^{kl} \\
\bar{e}_1^{*kl} (\bar{b}_{13} - \bar{b}_{12}) + \Delta \rho_{MP,2}^{kl} + I^{kl} + b^{kl} + \eta_2^{kl} \\
\Delta \rho_{MP,3}^{kl} + I^{kl} + b^{kl} + \eta_3^{kl} \\
\hline
-\frac{f_r}{c} \bar{e}_1^{*kl} \bar{v}_1 + \eta_{D1}^k \\
-\frac{f_r}{c} \bar{e}_1^{*kl} (\bar{v}_1 - \bar{b}_{12}^l) + \eta_{D2}^k
\end{array} \right) \quad (6.11)$$

6.2 The parametrization of the fixed tight-coupled EKF

The used measurement-models were exactly described in the last section, also how they are used in the fixed tight-coupled filter. Besides this, a priori information on some state parameter is in the measurement-vector. The a priori information on the pitch and roll angles is 0, as these angles are close to 0 for automotive applications. This a priori information is beneficial as the pitch and roll angles are only weakly observable and the Kalman filter to diverge. Further, a priori information for the baseline \vec{b}_{13} and a priori information for the velocity of the rover are integrated in the measurement-vector. In total are following (pseudo-) measurements available:

$$z = \begin{pmatrix} \lambda\tilde{\varphi}_1^{kl} \\ \lambda\tilde{\varphi}_2^{kl} \\ \lambda\tilde{\varphi}_3^{kl} \\ \hline \tilde{\rho}_1^{kl} \\ \tilde{\rho}_2^{kl} \\ \tilde{\rho}_3^{kl} \\ \hline \tilde{f}_{D1}^{kl} \\ \tilde{f}_{D2}^{kl} \\ \hline \bar{\theta} = 0 \\ \bar{\varphi} = 0 \\ \hline \vec{b}_{13} \\ \vec{v}_1 \end{pmatrix} \quad (6.12)$$

As mentioned before, the low-cost GNSS receivers (5 Hz) and the virtual reference-station (VRS) (1 Hz) have different update-rates. This aspect should be clearly considered in the measurement-vector. The first try for integrating this different update-rates was the extrapolation of the VRS-measurements to get the same measurement rate as for the receivers on the rover. But such a processing-intensive effort is not needed, if one keeps the single-difference (SD) measurement in mind and also that the position of the VRS doesn't change. It's in this case enough to update the satellite-position, the satellite clock-offset, the synchronization-correction and the tropospheric-delay with the calculation for the first receiver on the rover at 5 Hz. The correction is given by

$$\Delta c_{\text{VRS}}^{kl} = \vec{e}_1^k \vec{x}^k - \vec{e}_1^l \vec{x}^l + c\delta t^{kl} - T_1^{kl} \quad (6.13)$$

With this correction, all measurements of all three receivers can be processed with the same update-rate.

The complete state-vector was already defined in eqn. 4.4 and also the meanings of the parameters have been described. The measurement-equations were modeled in dependency of all unknowns in the state-vector. To provide an overview, the complete state vector is given by:

$$x = \left(\begin{array}{c} \vec{b}_{13} \\ \vec{v}_1 \\ \vec{a}_1 \\ \hline \psi \\ \dot{\psi} \\ \theta \\ \dot{\theta} \\ (\varphi) \\ (\dot{\varphi}) \\ \hline N_3^k - I^{kl} + \beta^{kl} \\ (N_{13}^{kl}) \\ (N_{12}^{kl}) \\ \hline \Delta\rho_{MP,1}^{kl} + I^{kl} + b^{kl} \\ \Delta\rho_{MP,2}^{kl} + I^{kl} + b^{kl} \\ \Delta\rho_{MP,3}^{kl} + I^{kl} + b^{kl} \\ \hline b_\omega \\ b_a \end{array} \right) \quad (6.14)$$

The variables in brackets are not updated from the fixed tightly coupled extended Kalman filter. In this configuration, there is no chance to estimate the roll-angle (φ) with GPS. By using three receivers on the rover, the possibility for determining this state would be given then. Also the double-difference ambiguities N_{13}^{kl} and N_{12}^{kl} are not updated for each epoch in the EKF, as it is generally known, that they are initially set in static conditions. Although the values of the fixed ambiguities are transferred to the EKF, changes of both states are only done in cases of changing a reference-satellite or by resetting the EKF to the dynamic float filter, what is particularly described in the integrity-check. The state b_ω , which describes the bias of the gyroscope, is not updated in all cases. Only in situations with moderate dynamics this parameter could be estimated, but in conditions with high dynamics there is no reliable estimation of the bias-state possible.

As previously said, the conditions for the fixed tightly coupled EKF are not constrained to a static environment. Immediately after fixing the double-difference (DD) ambiguities of the phase-measurements for the attitude- and RTK-baseline, a dynamic process is allowed. The transition-matrix is adapted as follows:

$$\Phi = \left(\begin{array}{cccccccccccc} I_{3 \times 3} & I_{3 \times 3} \cdot \Delta t & I_{3 \times 3} \cdot \frac{\Delta t^2}{2} & 0_{3 \times 1} & 0_{(3 \times 32) \cdot 6} & 0_{(3 \times 3) \cdot 2} \\ 0_{3 \times 3} & I_{3 \times 3} & I_{3 \times 3} \cdot \Delta t & 0_{3 \times 1} & 0_{(3 \times 32) \cdot 6} & 0_{(3 \times 3) \cdot 2} \\ 0_{3 \times 3} & 0_{3 \times 3} & I_{3 \times 3} & 0_{3 \times 1} & 0_{(3 \times 32) \cdot 6} & 0_{(3 \times 3) \cdot 2} \\ 0_{1 \times 3} & 0_{1 \times 3} & 0_{1 \times 3} & 1 & \Delta t & 0 & 0 & 0 & 0 & 0 & 0_{(1 \times 32) \cdot 6} & 0_{(1 \times 3) \cdot 2} \\ 0_{1 \times 3} & 0_{1 \times 3} & 0_{1 \times 3} & 0 & 1 & 0 & 0 & 0 & 0 & 0 & 0_{(1 \times 32) \cdot 6} & 0_{(1 \times 3) \cdot 2} \\ 0_{1 \times 3} & 0_{1 \times 3} & 0_{1 \times 3} & 0 & 0 & 1 & \Delta t & 0 & 0 & 0 & 0_{(1 \times 32) \cdot 6} & 0_{(1 \times 3) \cdot 2} \\ 0_{1 \times 3} & 0_{1 \times 3} & 0_{1 \times 3} & 0 & 0 & 0 & 1 & 0 & 0 & 0 & 0_{(1 \times 32) \cdot 6} & 0_{(1 \times 3) \cdot 2} \\ 0_{1 \times 3} & 0_{1 \times 3} & 0_{1 \times 3} & 0 & 0 & 0 & 0 & 1 & 0 & 0 & 0_{(1 \times 32) \cdot 6} & 0_{(1 \times 3) \cdot 2} \\ 0_{1 \times 3} & 0_{1 \times 3} & 0_{1 \times 3} & 0 & 0 & 0 & 0 & 0 & 1 & 0 & 0_{(1 \times 32) \cdot 6} & 0_{(1 \times 3) \cdot 2} \\ 0_{(32 \cdot 6) \times 3} & 0_{(32 \cdot 6) \times 3} & 0_{(32 \cdot 6) \times 3} & 0_{(32 \cdot 6) \times 1} & I_{(32 \times 32) \cdot 6} & 0_{(32 \cdot 6) \times (3 \cdot 2)} \\ 0_{(2 \cdot 3) \times 3} & 0_{(2 \cdot 3) \times 3} & 0_{(2 \cdot 3) \times 3} & 0_{(2 \cdot 3) \times 1} & 0_{(2 \cdot 3) \times (32 \cdot 6)} & I_{(3 \times 3) \cdot 2} \end{array} \right)$$

The transition-matrix treats the whole state-vector, and also the parameters which are not updated with GPS-measurements. It can be seen, that the later prediction of a state depends also on further states. For example, the RTK-baseline \vec{b}_{13} is predicted by the integration in time of velocity and acceleration of the previous epoch. The prediction of the current heading and pitch is also done by the integration in time of the rotation-rates of the gyroscope in the previous epoch. The double-difference (DD) ambiguities, the multipath and the biases remain unchanged in the state-prediction.

The assumptions of the process-noise are determined with the rover-dynamics, the temporal variation of the multipath and also with the sensor-characteristics as given in the table 6.1. Single-difference (SD) ambiguities of the phase-measurements of the VRS are in principal temporal constant and are not influenced by cycle-slips. But here are additionally the phase-bias and the ionospheric-delay mapped to the SD, what leads to a process-noise of $\sigma_N = 0.005$ cycles per epoch. The pseudo-range multipath of the virtual reference-station (VRS) is also negligible. As same as before, the bias of the pseudo-range and the ionospheric-delay are mapped to the parameter, whereat the noise standard deviation is initialized with $\sigma_{\Delta\rho_{MP,3}} = 0.005$ m.

Table 6.1: Process Noise Assumptions

position	$\sigma_{b_{13x}}^{(n)} = 0.50$ m
	$\sigma_{b_{13y}}^{(n)} = 0.50$ m
	$\sigma_{b_{13z}}^{(n)} = 0.05$ m
velocity	$\sigma_{v_x}^{(n)} = 0.20$ m/s
	$\sigma_{v_y}^{(n)} = 0.20$ m/s
	$\sigma_{v_z}^{(n)} = 0.02$ m/s
acceleration	$\sigma_{a_x}^{(n)} = 0.50$ m/s ²
	$\sigma_{a_y}^{(n)} = 0.50$ m/s ²
	$\sigma_{a_z}^{(n)} = 0.10$ m/s ²
derivatives of the angular rates	$\sigma_{\ddot{\psi}} = 25$ °/s ²
	$\sigma_{\ddot{\theta}} = 5$ °/s ²
	$\sigma_{\ddot{\varphi}} = 0$ °/s ² (not updated!)
SD ambiguities	$\sigma_{N_3} = 0.005$ cycles
pseudo-range multipath	{2 m, ..., 5 m} depending on satellite elevation
gyroscope biases	$\sigma_{b_{\dot{\psi}}} = 2 \cdot 10^{-7}$ rad/s
	$\sigma_{b_{\dot{\theta}}} = 2 \cdot 10^{-7}$ rad/s
	$\sigma_{b_{\dot{\varphi}}} = 0 \cdot 10^{-7}$ rad/s (not updated!)
accelerometer biases	$\sigma_{b_{a_x}^{(b)}} = 10^{-9}$ m/s ²
	$\sigma_{b_{a_y}^{(b)}} = 10^{-9}$ m/s ²
	$\sigma_{b_{a_z}^{(b)}} = 10^{-9}$ m/s ²

The statistics for phase-measurement, pseudo-ranges and Doppler-measurements are given in table 6.2. There is no possibility to do an adaptive initialization of the noise. For this reason, an elevation-depended model is used (see appendix B). As the dynamical variation of the statistics is very high in urban environments and can hardly be estimated, we keep do a model.

Table 6.2: Measurement Noise Assumptions

phase noise (SD)	$\sigma_\varphi = \{2 \text{ mm} \dots 4 \text{ mm}\}$ depending on satellite elevation
code noise (SD)	$\sigma_\rho = \{0.5 \text{ m} \dots 1.0 \text{ m}\}$ depending on satellite elevation
doppler noise (SD)	$\sigma_{f_D} = \{1 \text{ Hz} \dots 10 \text{ Hz}\}$ depending on satellite elevation
angular rates	$\sigma_{\dot{\psi}} = 0.001 \text{ rad/s}$ $\sigma_{\dot{\theta}} = 0.001 \text{ rad/s}$ $\sigma_{\dot{\varphi}} = 0.001 \text{ rad/s}$
acceleration	$\sigma_{a_x} = 0.1 \text{ m/s}^2$ $\sigma_{a_y} = 0.1 \text{ m/s}^2$ $\sigma_{a_z} = 0.1 \text{ m/s}^2$

6.3 The update-step of the fixed tightly coupled EKF

The prediction of the state-vector and the corresponding state-covariance-matrix is given with the known equations of the standard Kalman filter. This happens with the introduced transition-matrix in eqn. 6.15, the complete state-vector in eqn. 6.14 and the initialized process-noise variances from table 6.1. A state-update is not as easy as the prediction because of the need of precise statistics. First of all, there are some adjustments needed, which are described in the following section.

To get first of all the residuals of the state-prediction, one needs the transformation of the state-prediction to the corresponding measurements. For this step, a modified state-vector is defined:

$$\mathbf{x}_{\text{mod}} = \begin{pmatrix} \vec{b}_{13} \\ \vec{v}_1 \\ \vec{a}_1 \\ \vec{b}_{12,\text{NED}} \\ \dot{\vec{b}}_{12,\text{NED}} \\ N_3^k - I^{kl} + \beta^{kl} \\ \Delta\rho_{MP,1}^{kl} + I^{kl} + b^{kl} \\ \Delta\rho_{MP,2}^{kl} + I^{kl} + b^{kl} \\ \Delta\rho_{MP,3}^{kl} + I^{kl} + b^{kl} \end{pmatrix} \quad (6.16)$$

This vector includes now all known predicted states of position and velocity, and also the single-difference (SD) ambiguities and multipath of the previous epoch. The modification concerns the attitude-baseline $\vec{b}_{12,\text{NED}}$ and the attitude-baseline-rate $\dot{\vec{b}}_{12,\text{NED}}$, which are new in this state-vector. The determination of the baseline is given by:

$$\vec{b}_{12,\text{NED}} = \vec{l} \cdot \begin{pmatrix} \cos(\theta)\cos(\psi) \\ \cos(\theta)\sin(\psi) \\ -\sin(\theta) \end{pmatrix} \quad (6.17)$$

The attitude-baseline is determined with the help of the predicted states of heading and pitch. Also the a-priori information \bar{l} for the length of the attitude-baseline is used. The value for the baseline is given in the local navigation- (NED) frame.

Next the baseline-rate is defined:

$$\dot{\vec{b}}_{12,\text{NED}} = \bar{l} \cdot \begin{pmatrix} -\sin(\theta)\cos(\psi) \\ -\sin(\theta)\sin(\psi) \\ -\cos(\theta) \end{pmatrix} \cdot \dot{\theta} + \bar{l} \cdot \begin{pmatrix} -\cos(\theta)\sin(\psi) \\ \cos(\theta)\cos(\psi) \\ 0 \end{pmatrix} \cdot \dot{\psi} \quad (6.18)$$

Here the baseline $\vec{b}_{12,\text{NED}}$ is differentiated with respect to ψ and also to θ . After that, the predicted values of the state-vector are inserted in the derived equation for the baseline-rate. The calculated value is given in the navigation-frame.

Based on the modified state-vector in eqn. 6.16, one needs also a matching observation-matrix H_{mod} for residual-determination of the prediction-step. With the help of the defined measurement-models in eqn. 6.11, the matrix is given by:

$$H_{\text{mod}} = \begin{pmatrix} \vec{e}_{1\ 32 \times 3}^{kl} & 0_{32 \times 3} & 0_{32 \times 3} & 0_{32 \times 3} & 0_{32 \times 3} & I_{32 \times 32} \cdot \lambda & 0_{32 \times 32} & 0_{32 \times 32} & 0_{32 \times 32} \\ \vec{e}_{1\ 32 \times 3}^{kl} & 0_{32 \times 3} & 0_{32 \times 3} & -\vec{e}_{1,\text{NED}\ 32 \times 3}^{kl} & 0_{32 \times 3} & I_{32 \times 32} \cdot \lambda & 0_{32 \times 32} & 0_{32 \times 32} & 0_{32 \times 32} \\ 0_{32 \times 3} & I_{32 \times 32} \cdot \lambda & 0_{32 \times 32} & 0_{32 \times 32} & 0_{32 \times 32} \\ \hline \vec{e}_{1\ 32 \times 3}^{kl} & 0_{32 \times 3} & 0_{32 \times 3} & 0_{32 \times 3} & 0_{32 \times 3} & 0_{32 \times 32} & I_{32 \times 32} & 0_{32 \times 32} & 0_{32 \times 32} \\ \vec{e}_{1\ 32 \times 3}^{kl} & 0_{32 \times 3} & 0_{32 \times 3} & 0_{32 \times 3} & 0_{32 \times 3} & 0_{32 \times 32} & 0_{32 \times 32} & I_{32 \times 32} & 0_{32 \times 32} \\ 0_{32 \times 3} & 0_{32 \times 32} & 0_{32 \times 32} & 0_{32 \times 32} & I_{32 \times 32} \\ \hline 0_{32 \times 3} & -\vec{e}_{1\ 32 \times 3}^{kl} \cdot \frac{f_c}{c} & 0_{32 \times 3} & 0_{32 \times 3} & 0_{32 \times 3} & 0_{32 \times 32} & 0_{32 \times 32} & 0_{32 \times 32} & 0_{32 \times 32} \\ \vec{e}_{1\ 32 \times 3}^{kl} & -\vec{e}_{1\ 32 \times 3}^{kl} \cdot \frac{f_c}{c} & 0_{32 \times 3} & 0_{32 \times 3} & \vec{e}_{1,\text{NED}\ 32 \times 3}^{kl} & 0_{32 \times 32} & 0_{32 \times 32} & 0_{32 \times 32} & 0_{32 \times 32} \end{pmatrix} \quad (6.19)$$

In the last step to get the predicted measurement-equations, the multiplication of the modified state-vector in eqn. 6.16 and the observation-matrix in eqn. 6.19 is needed:

$$\hat{z}^- = \begin{pmatrix} H_{\text{mod}} \cdot \mathbf{x}_{\text{mod}} \\ \hat{\theta} \\ \hat{\varphi} \\ \hat{b}_{13} \\ \hat{v}_1 \end{pmatrix} \quad (6.20)$$

Besides the calculated phase-measurement, pseudo-range and Doppler-measurement with the help of the predicted states, the values for pitch, roll, RTK-baseline and velocity are integrated

in the measurement-vector. The residuals of the state-prediction are now easily given by

$$\Delta \hat{r}^- = z - \hat{z}^- \quad (6.21)$$

The measurement-model in eqn. 6.11 also includes the non-linear terms \vec{b}_{12} and $\dot{\vec{b}}_{12}$. In a normal Kalman filter, such non-linear terms can't be used in the measurement-model. A linearization around this two states has to be done. The complete derivation of the linearization and further details about the baseline parametrization are given in appendix A. The complete observation-matrix with linearized terms is given in eqn. 6.22.

$$H_{LIN} = \begin{pmatrix} \vec{e}_{1,32 \times 3}^{kl} & 0_{32 \times 3} & 0_{32 \times 3} & 0_{32 \times 1} & 0_{32 \times 1} & 0_{32 \times 1} & 0_{32 \times 1} & 0_{32 \times 2} & I_{32 \times 32} \cdot \lambda & 0_{(32 \times 32) \cdot 2} & 0_{32 \times 32} & 0_{32 \times 32} & 0_{32 \times 32} & 0_{32 \times 3} & 0_{32 \times 3} \\ \vec{e}_{1,32 \times 3}^{kl} & 0_{32 \times 3} & 0_{32 \times 3} & -\vec{e}_{1,NED,32 \times 3}^{kl} \cdot \vec{b}_{12,NED,\psi} & 0_{32 \times 1} & -\vec{e}_{1,NED,32 \times 3}^{kl} \cdot \vec{b}_{12,NED,\theta} & 0_{32 \times 1} & 0_{32 \times 2} & I_{32 \times 32} \cdot \lambda & 0_{(32 \times 32) \cdot 2} & 0_{32 \times 32} & 0_{32 \times 32} & 0_{32 \times 32} & 0_{32 \times 3} & 0_{32 \times 3} \\ 0_{32 \times 3} & 0_{32 \times 3} & 0_{32 \times 3} & 0_{32 \times 1} & 0_{32 \times 1} & 0_{32 \times 1} & 0_{32 \times 1} & 0_{32 \times 2} & I_{32 \times 32} \cdot \lambda & 0_{(32 \times 32) \cdot 2} & 0_{32 \times 32} & 0_{32 \times 32} & 0_{32 \times 32} & 0_{32 \times 3} & 0_{32 \times 3} \\ \vec{e}_{1,32 \times 3}^{kl} & 0_{32 \times 3} & 0_{32 \times 3} & 0_{32 \times 1} & 0_{32 \times 1} & 0_{32 \times 1} & 0_{32 \times 1} & 0_{32 \times 2} & 0_{32 \times 32} & 0_{(32 \times 32) \cdot 2} & I_{32 \times 32} & 0_{32 \times 32} & 0_{32 \times 32} & 0_{32 \times 3} & 0_{32 \times 3} \\ \vec{e}_{1,32 \times 3}^{kl} & 0_{32 \times 3} & 0_{32 \times 3} & -\vec{e}_{1,NED,32 \times 3}^{kl} \cdot \vec{b}_{12,NED,\psi} & 0_{32 \times 1} & -\vec{e}_{1,NED,32 \times 3}^{kl} \cdot \vec{b}_{12,NED,\theta} & 0_{32 \times 1} & 0_{32 \times 2} & 0_{32 \times 32} & 0_{(32 \times 32) \cdot 2} & 0_{32 \times 32} & I_{32 \times 32} & 0_{32 \times 32} & 0_{32 \times 3} & 0_{32 \times 3} \\ 0_{32 \times 3} & 0_{32 \times 3} & 0_{32 \times 3} & 0_{32 \times 1} & 0_{32 \times 1} & 0_{32 \times 1} & 0_{32 \times 1} & 0_{32 \times 2} & 0_{32 \times 32} & 0_{(32 \times 32) \cdot 2} & 0_{32 \times 32} & 0_{32 \times 32} & I_{32 \times 32} & 0_{32 \times 3} & 0_{32 \times 3} \\ 0_{32 \times 3} & \vec{e}_{1,32 \times 3}^{kl} \cdot \frac{f_c}{c} & 0_{32 \times 3} & 0_{32 \times 1} & 0_{32 \times 1} & 0_{32 \times 1} & 0_{32 \times 1} & 0_{32 \times 2} & 0_{32 \times 32} & 0_{(32 \times 32) \cdot 2} & 0_{32 \times 32} & 0_{32 \times 32} & 0_{32 \times 3} & 0_{32 \times 3} & 0_{32 \times 3} \\ 0_{32 \times 3} & \vec{e}_{1,32 \times 3}^{kl} \cdot \frac{f_c}{c} & 0_{32 \times 3} & A & B & C & D & 0_{32 \times 2} & 0_{32 \times 32} & 0_{(32 \times 32) \cdot 2} & 0_{32 \times 32} & 0_{32 \times 32} & 0_{32 \times 3} & 0_{32 \times 3} & 0_{32 \times 3} \\ 0_{1 \times 3} & 0_{1 \times 3} & 0_{1 \times 3} & 0 & 0 & 1 & 0 & 0_{1 \times 2} & 0_{1 \times 32} & 0_{(1 \times 32) \cdot 2} & 0_{1 \times 32} & 0_{1 \times 32} & 0_{1 \times 3} & 0_{1 \times 3} & 0_{1 \times 3} \\ 0_{1 \times 3} & 0_{1 \times 3} & 0_{1 \times 3} & 0 & 0 & 0 & 0 & (1, 0) & 0_{1 \times 32} & 0_{(1 \times 32) \cdot 2} & 0_{1 \times 32} & 0_{1 \times 32} & 0_{1 \times 3} & 0_{1 \times 3} & 0_{1 \times 3} \\ I_{3 \times 3} & 0_{3 \times 3} & 0_{3 \times 3} & 0_{3 \times 1} & 0_{3 \times 1} & 0_{3 \times 1} & 0_{3 \times 1} & 0_{3 \times 2} & 0_{3 \times 32} & 0_{(3 \times 32) \cdot 2} & 0_{3 \times 32} & 0_{3 \times 32} & 0_{3 \times 3} & 0_{3 \times 3} & 0_{3 \times 3} \end{pmatrix} \quad (6.22)$$

$$A : \quad \vec{e}_{1,NED,32 \times 3}^{kl} \cdot \frac{f_c}{c} \cdot \dot{\vec{b}}_{12,NED,\psi}$$

$$B : \quad \vec{e}_{1,NED,32 \times 3}^{kl} \cdot \frac{f_c}{c} \cdot \dot{\vec{b}}_{12,NED,\psi}$$

$$C : \quad \vec{e}_{1,NED,32 \times 3}^{kl} \cdot \frac{f_c}{c} \cdot \dot{\vec{b}}_{12,NED,\theta}$$

$$D : \quad \vec{e}_{1,NED,32 \times 3}^{kl} \cdot \frac{f_c}{c} \cdot \dot{\vec{b}}_{12,NED,\theta}$$

With the help of the introduced formulas for a Kalman filter, a complete update-step of the fixed tightly coupled EKF for one GPS-epoch could be executed. For considering the residuals of the update of the state-vector, the same steps as for the determination of the prediction-residuals must be done.

6.4 Detection and correction of cycle slips

The introduced measurement-model and the precise estimation of the unknown states require previous detection and correction of cycle-slips. Such jumps by a multiple of $\lambda/2$, for geodetic receivers only by a multiple of λ , could occur on the attitude-baseline as well as on the RTK-baseline. Cycle slips are caused by reflexions of trees, buildings, bridges or the like. A critical point in view is the separation of changes in the phase-measurement due to dynamics of the rover and true cycle-slips. In figure 6.1, a typical cycle-slip of $\lambda/2$ in static conditions is shown. The double-difference measurement of the phase should only take a small drift due to the satellite-movement, jumps are not given in correct phase-measurements. Following the correction of cycle-slips for the attitude-baseline is given. Afterwards, the possibilities for cycle-slip corrections for the RTK-baseline are described.

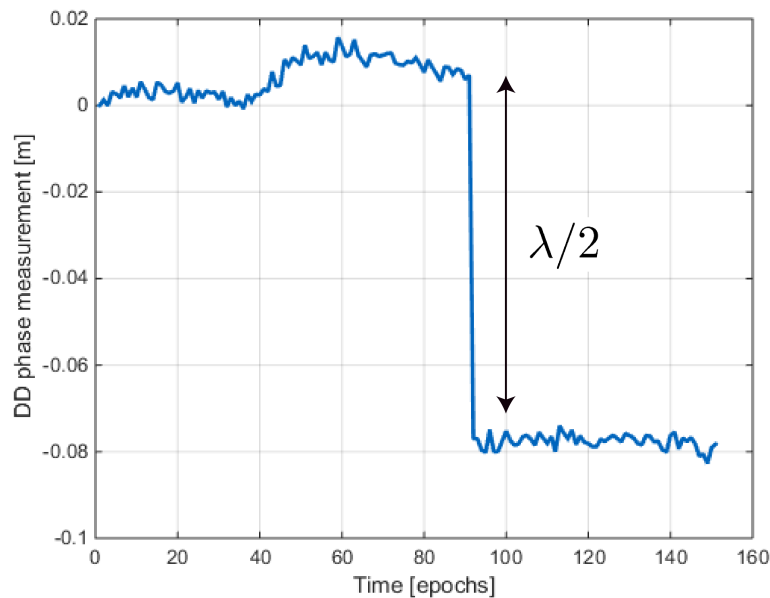


Figure 6.1: Double-difference (DD) phase-measurement of a satellite in static conditions. In epoch 91, a cycle-slip of $\lambda/2$ is occurred.

6.4.1 Cycle-slip on the attitude-baseline

The attitude-baseline possesses the great benefit from the missing relative movement between both receivers, but only changes its attitude, what gives a big advantage for cycle-slip correction. This statement makes the cycle-slip detection and correction highly reliable. For the detection of a cycle-slip on the attitude-baseline, one uses the prediction of the phase-measurement to get the residual and to make a choice, if this phase-change describes a cycle-slip or not. Figure 6.2 shows the difficulty of detection of cycle-slips in dynamic conditions.

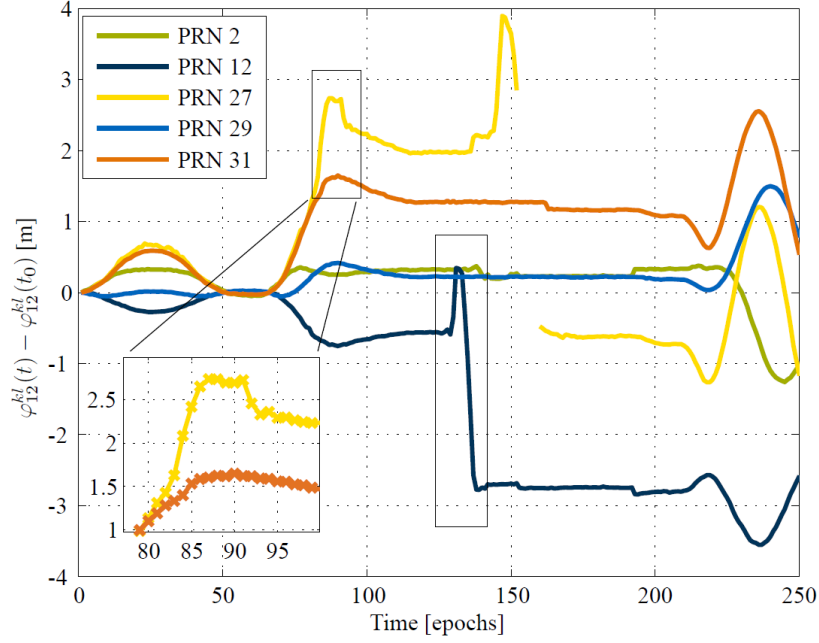


Figure 6.2: Double-difference phase-measurements deducting the phase-measurement in the first epoch of all visible satellites in dynamic conditions [8]

In the following cycle-slip correction several state-information is included:

- the fixed double-difference ambiguities
- the heading of the previous epoch and the resulting prediction of the current epoch
- the baseline-length between both rover-receivers

Initially the first step estimates the attitude-baseline for the current epoch to predict the dynamic of the non-corrected measurement:

$$\hat{b}_{12}(t_n) = \bar{l} \begin{pmatrix} \cos(\theta(t_{n-1}) + \Delta t \cdot \dot{\theta}(t_{n-1})) \cos(\psi(t_{n-1}) + \Delta t \cdot \dot{\psi}(t_{n-1})) \\ \cos(\theta(t_{n-1}) + \Delta t \cdot \dot{\theta}(t_{n-1})) \sin(\psi(t_{n-1}) + \Delta t \cdot \dot{\psi}(t_{n-1})) \\ -\sin(\theta(t_{n-1}) + \Delta t \cdot \dot{\theta}(t_{n-1})) \end{pmatrix} \quad (6.23)$$

The attitude-baseline is, as supplied before, calculated in the navigation- (NED) frame. New in this model is the temporal integration of the rotation-rate of heading and pitch. The temporal integration includes the last update of the parameters, what is in normal case the IMU-update till the current GPS-epoch.

In the next step, the change of phase-measurement is considered:

$$\Delta \lambda \varphi_{12}^{kl}(t_n) = \lambda \varphi_{12}^{kl}(t_n) - \lambda N_{12}^{kl} - R_n^e \cdot \hat{b}_{12}(t_n) \quad (6.24)$$

In eqn. 6.24 the predicted attitude-baseline $\hat{b}_{12}(t_n)$, which is rotated to the ECEF-frame, and the double-difference integer ambiguities N_{12}^{kl} are subtracted from the current phase-measurement

$\varphi_{12}^{kl}(t_n)$. Important for this step is a well calibrated IMU, especially for the baseline-prediction. After the determination of the residuals in the current phase-measurement, a decision is taken with regard to possible cycle-slips:

$$\Delta N_{12}^{kl}(t_n) = \text{round} \left(\Delta \lambda \varphi_{12}^{kl}(t_n) / \frac{\lambda}{2} \right) \quad (6.25)$$

The rounding is performed to the next integer value and thus forms the decision-threshold, if the residual is caused by a cycle-slip or not. A similar approach for a cycle-slip correction is given by Lipp et al. in [28].

6.4.2 Cycle-slip on the RTK-baseline

In a dynamic system, the RTK-baseline could concurrently change its norm and attitude. Nevertheless a cycle-slip correction must be implemented for the DD-ambiguities of the RTK-baseline. The assumption of the VRS, that this station is not influenced by cycle-slips, is furthermore valid. Only receiver 1 is able to induce phase-jumps in the double-difference measurement. As described for the attitude-baseline, again here is tried to predict the phase-measurement as far as possible.

The estimation of the RTK-baseline is given by

$$\hat{\vec{b}}_{13}(t_n) = \vec{b}_{13}(t_{n-1}) + \Delta t \cdot \vec{v}_1(t_{n-1}) \quad (6.26)$$

A temporal integration of the velocity includes the last (IMU-)update until the current GPS-epoch.

The next step is the triple-difference (TD) of the phase-measurement (see eqn. 2.12).

$$\Delta \lambda \varphi_{13}^{kl}(t_n) = \lambda \varphi_{13}^{kl}(t_n) - \lambda \varphi_{13}^{kl}(t_{n-1}) - \left(\vec{e}_1^{kl}(t_n) \cdot \hat{\vec{b}}_{13}(t_n) - \vec{e}_1^{kl}(t_n) \cdot \vec{b}_{13}(t_{n-1}) \right) \quad (6.27)$$

With the help of the triple-difference (TD), the double-difference ambiguity N_{13}^{kl} is eliminated from the equation. Only the baseline-change between both epochs is still in the equation. This term is now tried to become eliminated with the prediction of the baseline $\hat{\vec{b}}_{13}(t_n)$. The condition for functionality of the cycle-slip correction is a much lower drift of $\lambda/2$ within the prediction of the RTK-baseline within 0.2 seconds.

After determination of the residuals in the current phase-measurement, a decision is taken with regard to possible cycle-slips:

$$\Delta N_{13}^{kl}(t_n) = \text{round} \left(\Delta \lambda \varphi_{13}^{kl}(t_n) / \frac{\lambda}{2} \right) \quad (6.28)$$

The rounding is performed to the next integer value and thus forms the decision-threshold, if the residual is caused by an cycle-slip or not. A similar approach for a cycle-slip correction is also given by Lipp et al. in [28].

After this estimation of possible cycle-slips, two further constrains should be valid for a RTK cycle-slip correction:

- The attitude baseline has also detected cycle-slips for the same satellite-receiver constellation

- The single-difference measurement $\lambda\tilde{\varphi}_1^{kl}$ minus the predicted RTK-baseline jumps also by a multiple of half cycle-slips

Only if one of both constrains are valid, we execute a cycle-slip correction for the proven satellite-receiver pair. The second condition excludes here the possibility that receiver 1 and 2 suffer under the same cycle slips in the same epoch, which could prevent the correction in terms of the first condition.

6.5 The integrity-check based on the dynamic float-solution

Besides the solution of the fixed tight-coupled EKF, a further reference for cross-checking and fall-back solution is needed and integrated for critical situations. An example is given by a long tunnel section without GPS-signal, where the only-IMU solution drifts away after time. After this tunnel-section the tight-coupled EKF needs a sufficiently precise re-initialization of the position, whereby also the double-difference ambiguities are re-fixed. At the moment, the float Kalman filter includes only GPS-epochs for updates. A next step is the coupling with IMU-measurements.

6.5.1 The parametrization of the RTK float Kalman filter

This float Kalman filter for the dynamic RTK-baseline is once more based on the double-difference measurements.

The state-vector for the integrity-check respectively for the re-fixing of the RTK double-difference ambiguities is given by

$$x = \begin{pmatrix} \vec{b}_{13} \\ \vec{v}_1 \\ N_{13} \end{pmatrix} \quad (6.29)$$

with the RTK-baseline \vec{b}_{13} and the velocity \vec{v}_1 in ECEF-frame. The double-difference ambiguities are real-valued, even though they are fixed to integers in the initialization. This aspect gives an independent solution as against the fixed tight-coupled one.

The measurement is given as follows

$$z = \begin{pmatrix} \lambda\tilde{\varphi}_{13}^{kl} \\ \lambda\tilde{\varphi}_{23}^{kl} \\ \tilde{\rho}_{13}^{kl} \\ \tilde{\rho}_{23}^{kl} \\ \tilde{f}_{D1}^{kl} \\ 0 \end{pmatrix} \quad (6.30)$$

with the double-difference (DD) measurements for the phase- and pseudo-range and also the single-difference (SD) of the Doppler-measurement of receiver one. Furthermore, a pseudo-measurement for constraining the height-component of the velocity in the ECEF-frame is integrated in the measurement-vector.

After the definition of the state- and measurement-vector, the observation-matrix can be explained in detail. The matrix is given by:

$$H = \begin{pmatrix} \vec{e}_{1\ 32 \times 3}^{kl} & 0_{32 \times 3} & I_{32 \times 32} \cdot \lambda \\ \vec{e}_{1\ 32 \times 3}^{kl} & 0_{32 \times 3} & I_{32 \times 32} \cdot \lambda \\ \vec{e}_{1\ 32 \times 3}^{kl} & 0_{32 \times 3} & 0_{32 \times 32} \\ \vec{e}_{1\ 32 \times 3}^{kl} & 0_{32 \times 3} & 0_{32 \times 32} \\ 0_{32 \times 3} & -\vec{e}_{1\ 32 \times 3}^{kl} \cdot \frac{f_c}{c} & 0_{32 \times 32} \\ 0_{1 \times 3} & R_n^e \cdot (0, 0, 1)^T & 0_{1 \times 32} \end{pmatrix} \quad (6.31)$$

The measurement-model includes only linear terms, what makes a linearization around states not necessary. The matrix R_n^e defines the rotation of the navigation (NED) frame to the ECEF-frame.

For the allowed dynamic conditions of the rover, the transition-matrix can't be given only with an identity-matrix. The matrix is described as following in the filter:

$$\Phi = \begin{pmatrix} I_{3 \times 3} & I_{3 \times 3} \cdot \Delta t & 0_{3 \times 32} \\ 0_{3 \times 3} & I_{3 \times 3} & 0_{3 \times 32} \\ 0_{32 \times 3} & 0_{32 \times 3} & I_{32 \times 32} \end{pmatrix} \quad (6.32)$$

The prediction of the RTK-baseline \vec{b}_{13} is given here by the temporal integration of velocity \vec{v}_1 between two epochs (Δt).

For the process-noise, the adjustments are taken by considering the rover-dynamics as shown in table 6.3. The double-difference ambiguities N_{13}^{kl} are not fixed in this float filter, what leads to a larger process-noise against the selected one in the fixed tight-coupled filter. It should be noted, that this parameter must be nevertheless small enough for a correct adjustment of corrections for all states, to avoid an only adjustment of measurement-variations (movement) with the DD ambiguities. A $\sigma_{N_{13}}$ of 0.005 cycles for each epoch is a good trade-off in this case. The constraint velocity for the hight-component is initialized with a process-noise of $\sigma_{v_{z\text{apriori}}}^{(n)} = 2.5$ m/s for each epoch.

The values for the phase-measurement, pseudo-range and Doppler-measurement noise are described in table 6.4. In dynamic conditions, an elevation-based model (see appendix B) is used for determining the measurement-noise. An adaptive approach, like in the other static float-filter, is not helpful with this condition.

Table 6.3: Process Noise Assumptions

position	$\sigma_{b_{13x}}^{(n)} = 1.00 \text{ m}$
	$\sigma_{b_{13y}}^{(n)} = 1.00 \text{ m}$
	$\sigma_{b_{13z}}^{(n)} = 0.05 \text{ m}$
velocity	$\sigma_{v_x}^{(n)} = 1/3.6 \text{ m/s}$
	$\sigma_{v_y}^{(n)} = 1/3.6 \text{ m/s}$
	$\sigma_{v_z}^{(n)} = 0.2/3.6 \text{ m/s}$
velocity in up-component (a-priori)	$\sigma_{v_z^{\text{apriori}}}^{(n)} = 2.5 \text{ m/s}$
double difference ambiguities	$\sigma_{N_{13}} = 0.005 \text{ cycles}$

Table 6.4: Measurement Noise Assumptions

phase noise (double-difference)	$\sigma_\varphi = \{2 \text{ mm} \dots 4 \text{ mm}\}$ depending on satellite elevation
code noise (double-difference)	$\sigma_\rho = \{0.5 \text{ m} \dots 1.0 \text{ m}\}$ depending on satellite elevation
Doppler noise (double-difference)	$\sigma_{f_D} = \{1 \text{ Hz} \dots 10 \text{ Hz}\}$ depending on satellite elevation

6.5.2 The integrity-check of the RTK-baseline

After the description of parametrization and functionality of the dynamic float Kalman filter, the important step of an integrity-check for the fixed tight-coupled solution is explained. Criteria for using the dynamic float solution as fall-back method for re-initializing the fixed tight-coupled EKF in case of the RTK-baseline state \vec{b}_{13} are given as follows:

- The residuals of the float-solution in comparison to the pseudo-range are sufficiently small
- The difference of the horizontal component of the RTK-baseline \vec{b}_{13} between the fixed- and float-solution is sufficiently large
- The dynamic float-solution has a sufficiently large amount of state-updates available from the past. In case of only state-predictions for an epoch, the dynamic float solution is not that much reliable. A state-prediction without state-update happens in cases with extremely high innovation or with bad satellite-constellation (tunnel, trees, etc.).

After fulfilling all of this three criteria, the RTK-baseline \vec{b}_{13} is re-initialized with an instantaneous re-fixing of the ambiguities, which is based on the dynamic float solution, resulting in the new RTK-baseline. Thus the state-covariance-matrix P_x^+ is also reseted with the appropriate of the dynamic float solution.

But if there is no chance to get a new instantaneous re-fixing of the ambiguities after time (no candidates fulfilling the criteria for re-fixing), one takes the float RTK-baseline estimation as new fixed solution. Besides this, the double-difference (DD) ambiguities N_{13}^{kl} must be adapted for the (new) baseline. For this, the modeling-error of the single-difference (SD) phase-measurement is determined:

$$\Delta\lambda\tilde{\varphi}_1^{kl}(t_n) = \lambda\tilde{\varphi}_1^{kl}(t_n) - \vec{e}_1^{kl}(t_n) \cdot \vec{b}_{13,\text{float}} - \lambda N_3^{kl}(t_n) + I^{kl}(t_n) - \beta^{kl}(t_n) \quad (6.33)$$

Now the residuals $\Delta\lambda\tilde{\varphi}_1^{kl}(t_n)$ can be allocated to the double-difference (DD) ambiguities N_{13}^{kl} . As known from the cycle-slip correction, the values are rounded to integer-values:

$$\Delta N_{13}^{kl} = \text{round} \left(\Delta\lambda\tilde{\varphi}_1^{kl}(t_n) / \frac{\lambda}{2} \right) \quad (6.34)$$

The determined integer-value is finally added to the double-difference (DD) ambiguities:

$$\lambda N_{13}^{kl} = \lambda N_{13}^{kl} + \lambda \Delta N_{13}^{kl} \quad (6.35)$$

6.5.3 The integrity-check of velocity

Besides the testing of the RTK-baseline, the velocity \vec{v}_1 of receiver 1 needs also an integrity-check. At first, the velocity is rotated in the navigation (NED) frame to determine the heading with the help of the velocity-vector:

$$\psi_{\vec{v}_1} = \text{atan2}\left(\frac{\vec{v}_{1E}}{\vec{v}_{1N}}\right) \quad (6.36)$$

Next the offset between the normal heading, which is determined with the attitude-baseline \vec{b}_{12} , and the temporal integration of the rotation-rate and the heading of the velocity-vector is determined. In cases of large offsets, the velocity-vector is re-initialized with the baseline-attitude.

For the integrity-check in case of the norm of the velocity, the dynamic float-solution is used. Criteria for using this solution as fall-back method for re-initialization the velocity-vector \vec{v}_1 are given as following:

- The residuals of the dynamic float-solution in terms of the Doppler-measurements are sufficiently small
- The difference between the norm of velocity for the fixed- and float-solution is sufficiently large
- The dynamic float-solution has a sufficiently large amount of state-updates available from the past. In case of only state-predictions for an epoch, the dynamic float solution is not that much reliable. A state-prediction without state-update happens in cases with extremely high innovation or with bad satellite-constellation (tunnel, trees, etc.).

After fulfilling all of this three criteria, the velocity \vec{v}_1 is re-initialized with the dynamic float solution. Thus the state-covariance-matrix P_x^+ is reseted with the appropriate of the dynamic float solution.

6.5.4 The integrity-check of heading

The process of proving the heading ψ aims also at the adaption of attitude-baseline \vec{b}_{12} and the double-difference (DD) ambiguities N_{12}^{kl} . At first, the current heading is compared with the reference. Used as reference is the Doppler-measurement respectively the Doppler-velocity, with the help of which a heading could be determined in sufficiently high dynamics. The heading is estimated with the same schema as in eqn. 6.36 shown. Criteria for using this solution as fall-back method for re-initializing the heading ψ , the attitude-baseline \vec{b}_{12} and the double-difference (DD) ambiguities N_{12}^{kl} are given as follows:

- The velocity of the rover is sufficiently large
- The residuals of the dynamic float-solution in terms of the Doppler-measurement are sufficiently small

- The residuals of the fixed tight-coupled solution in terms of the attitude-baseline ($\lambda\tilde{\varphi}_1^{kl}(t_n) - \lambda\tilde{\varphi}_2^{kl}(t_n)$) are unusually large
- The difference of the norm of heading between the Doppler-measurement and the current state-heading of the fixed tight-coupled solution is sufficiently large

After fulfilling all of this four criteria, the heading ψ , the attitude-baseline \vec{b}_{12} and the double-difference (DD) ambiguities N_{12}^{kl} are re-initialized. Hereby the heading is initialized with the Doppler-solution, whereby the attitude-baseline \vec{b}_{12} is adjusted. The adaption of the double-difference (DD) ambiguities N_{12}^{kl} is given by:

$$\begin{aligned}\Delta\lambda\tilde{\varphi}_{12}^{kl}(t_n) &= \lambda\tilde{\varphi}_{12}^{kl}(t_n) - \vec{e}_1^{kl}(t_n) \cdot \vec{b}_{13_{\text{updated}}} - c_{12}^{kl} \\ &= \lambda N_{12}^{kl} + \varepsilon_{12}^{kl}\end{aligned}\quad (6.37)$$

The residuals $\Delta\lambda\tilde{\varphi}_{12}^{kl}(t_n)$ are assigned to the double-difference (DD) ambiguities N_{12}^{kl} . A rounding to integer-values is given as follows:

$$\Delta N_{12}^{kl} = \text{round}\left(\Delta\lambda\tilde{\varphi}_{12}^{kl}(t_n)/\frac{\lambda}{2}\right)\quad (6.38)$$

The determined integer-value is finally added to the previous double-difference (DD) ambiguities:

$$\lambda N_{12}^{kl} = \lambda N_{12}^{kl} + \lambda\Delta N_{12}^{kl}\quad (6.39)$$

The introduced proving and redundancy of states in this chapter is exceptionally important for the fixed tight-coupled system. Such an integrity-check provides, also after critical situations, a highly accurate position and attitude determination. Without this arrangement of re-initialization, the fixed tight-coupled EKF would have no chance to come back to a precise position and attitude after tunnel-sections or bridges.

Chapter 7

Measurement results

This chapter contains a detailed evaluation of the recorded data-sets provided by Volkswagen at 11.11.2014. The exact test-setup was described in another chapter. Besides the recorded test-data, reference-data is provided by the company *Applanix*, a Trimble company. With the help of this reliable and highly precise reference-solution, the correctness of the different states is proven.

The verification of the implemented models will be executed in two different environments. To prove the robustness of the system against cycle-slips or signal-outages, a test-drive in an urban environment (Wolfsburg) is performed. Proving the software with regard of high dynamics, a drive on the highway is also evaluated.

7.1 The test-drive in an urban environment

In figure 7.1, the course of the test-drive in the inner city of Wolfsburg is plotted. The route includes narrow streets (e.g. Schiller- / Goethestrasse) with high multipath, long tunnel-sections with signal-outages and crossing under bridges. The developed fixed tight-coupled position- and attitude determination with correction-data shows in all cases a continuous progress, what is also shown in this chapter in more detail.



Figure 7.1: Map section of the driving route (yellow) in the inner-city of Wolfsburg at 11.11.2014

The determination of an ultra-precise absolute position is an important state for the highly automatic driving. Especially for the car-to-car communication or the prediction of the traffic and traffic-environment is this an indispensable state. A further benefit is the possible statement

about the current lane on the road of the rover. Figure 7.2 highlights the absolute position accuracy for the implemented solution of the fixed tight-coupled EKF. It shows a position-accuracy of at least 40 cm in 68 % of time and better than 1 m in more than 95 % of time for the driving-route in the inner-city of Wolfsburg. One should mention, that large tunnel-sections are included in this figure. The figure gives also a statement about the re-initialization after long signal-outages, what seems to be very accurate.

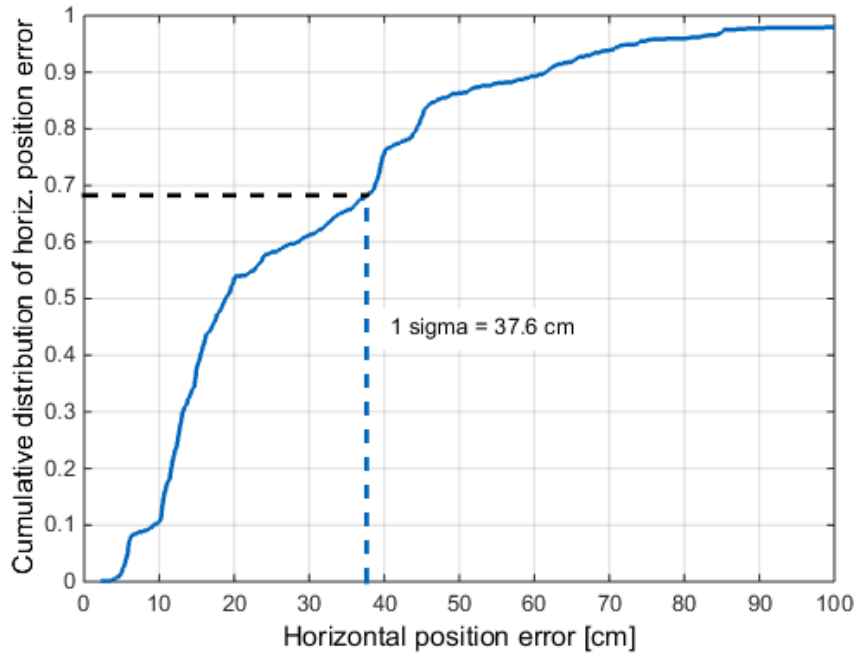


Figure 7.2: Cumulative distribution of the horizontal position-error in the test-driving through the inner-city of Wolfsburg. The position-error is maximum 40 cm in 68 % of time.

The next figure 7.3 shows the absolute position-estimation of the fixed tight-coupled solution against the reference-solution for a section in an urban environment with high buildings, what leads to high multipath. The deviation is less than 10 cm and thus under the resolution of the Google-Earth plot. Next to the fixed tight-coupled solution is also the dynamic float-solution shown, which reaches an accuracy of rough 50 cm in this hard environment.

In figure 7.4 a section with a high rotation-rate within an urban environment with high buildings is shown. The deviation of the fixed tight-coupled solution against the reference-solution is rough 35 cm. Here prevails again high multipath due to the house-walls on both street-sides and also the mentioned high dynamic, what leads to loss of satellites with continuous phase (only 6 of 11 possible satellites). One can also see a continuous offset on the RTK-baseline, what comes from a false evaluation of a possible cycle-slip in the past.

An estimation of the position for the passing of a tunnel-section is given in figure 7.5. The systematic error before the beginning of the tunnel was again performed due to an incorrect cycle-slip correction. The position estimation at the beginning of the tunnel shows a continuous course with state-updates by inertial measurements and the punctual elimination of still available GPS-satellites. Inside the tunnel, the solution began to drift. One can see, the drift happens only in the moving direction in terms of the velocity, the heading of the rover is nearly drift-free through the once-only integration of rotation-rates of the gyroscope. The correction of

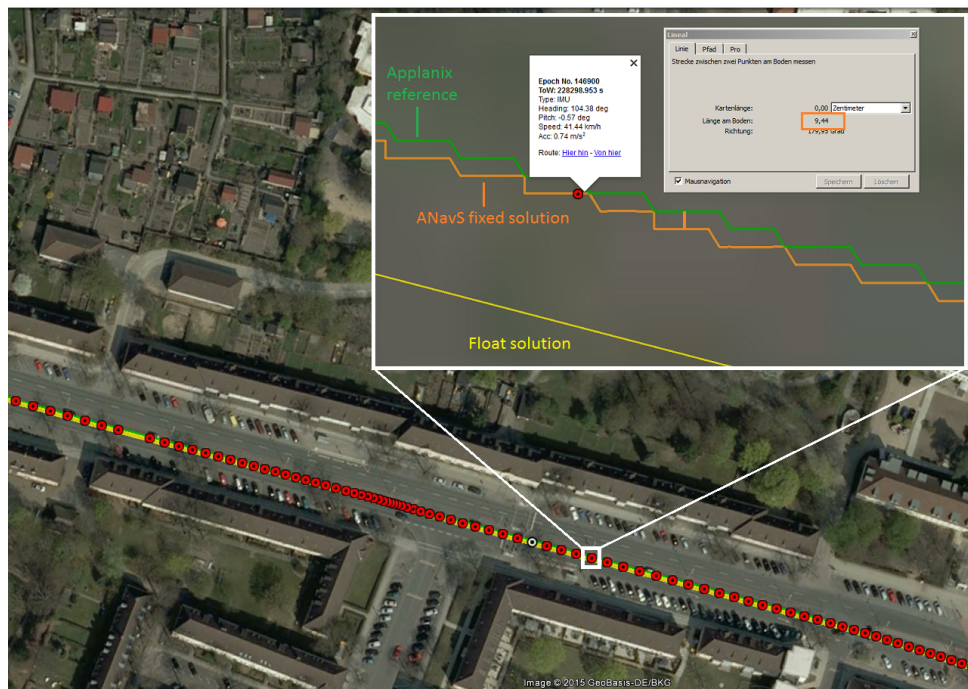


Figure 7.3: Map-section in an urban environment with high buildings. Plotted are the fixed tight-coupled solution (orange), the dynamic float-solution (yellow) and the reference-solution (green)

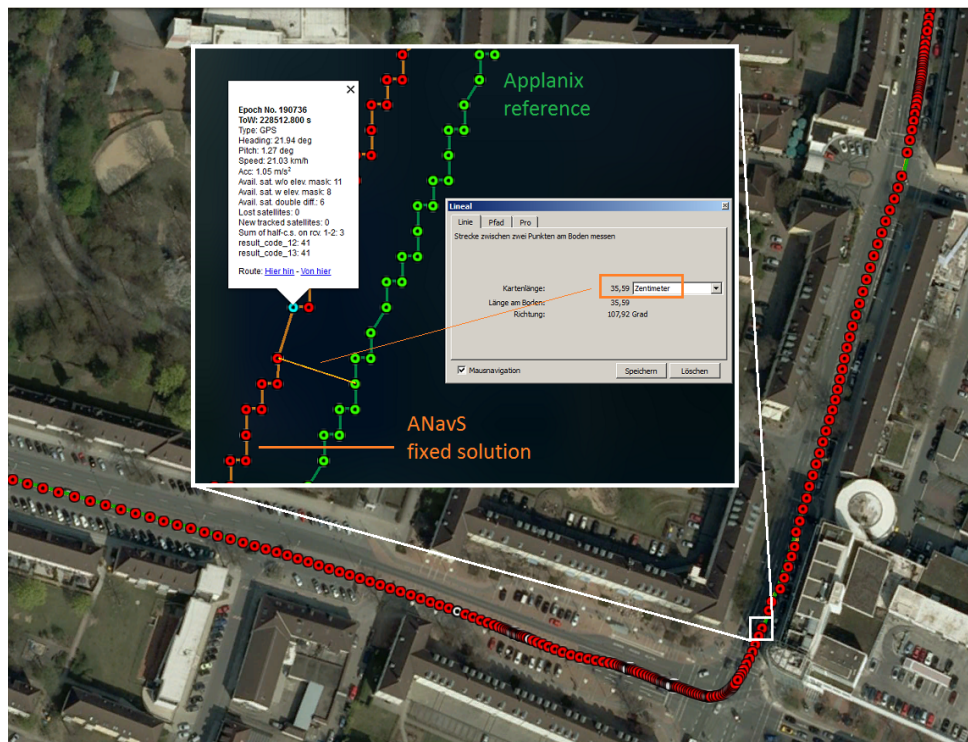


Figure 7.4: Map-section in an urban environment with high buildings and high rotation dynamic. Plotted are the fixed tight-coupled solution (orange) and the reference-solution (green)

the position-error happens after the exit of the tunnel, as soon as enough and reliable satellites are visible again. One can also see the re-initialization of the position and double-difference (DD) ambiguities based on the dynamic float filter, what performs very well in the enlarged plot on the right side.

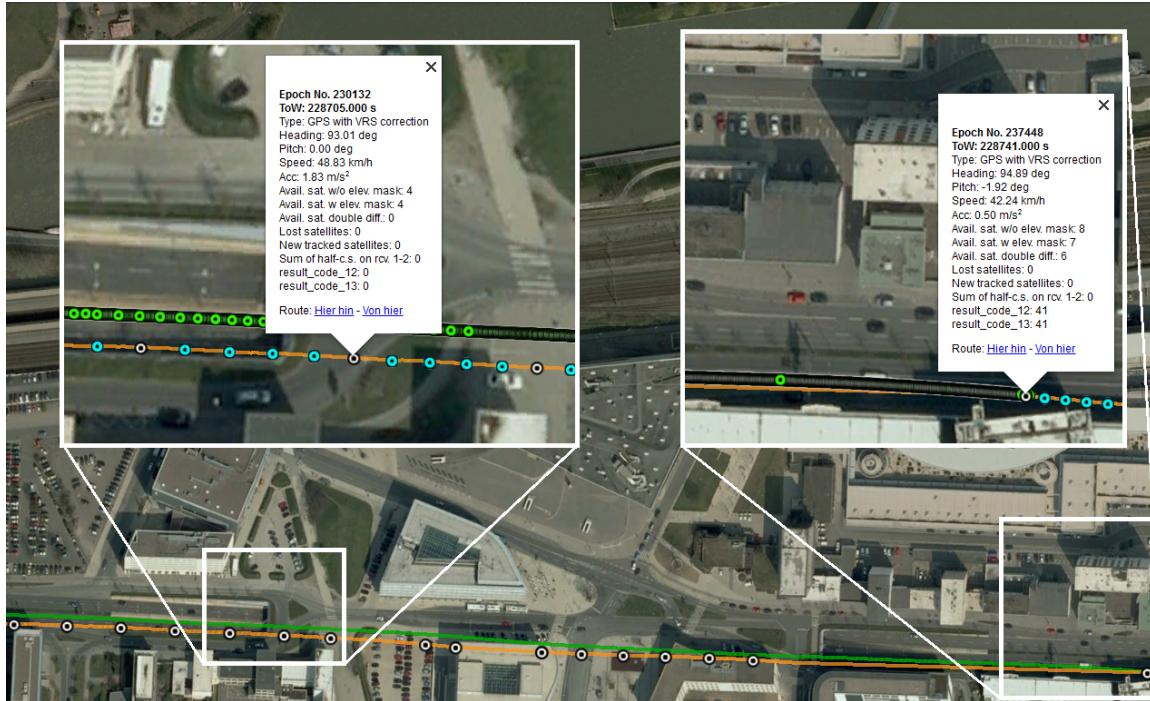


Figure 7.5: Map-section in a tunnel-environment without GPS-signal. Plotted are the fixed tight-coupled solution (orange) and the reference-solution (green). The first enlarged plot (on the left side) shows the beginning of the tunnel, the second the end. In total the section is rough 300 m long.

As next the velocity in north- and east- direction is shown against the reference-solution (see figure 7.6 and 7.7). One can see in both cases a very accurate estimation of this state. The marked signal-outages happens in cases of tunnel-sections, whereby the drift of the accelerometer is also clarified.

In figure 7.8 one compares the estimated heading-solution for the test-drive in the inner-city of Wolfsburg. The tight coupled solution follows clearly the course of the applanix-reference. The enlarged plot shows the small gyroscope-drift over time in a scale of rough 0.5 degree. The reason is given by the in-perfect estimation of the bias for the rotation-rates, which is reduced in conditions with higher dynamic. The noise for the heading-solution is below 0.1 degree and thus negligible.

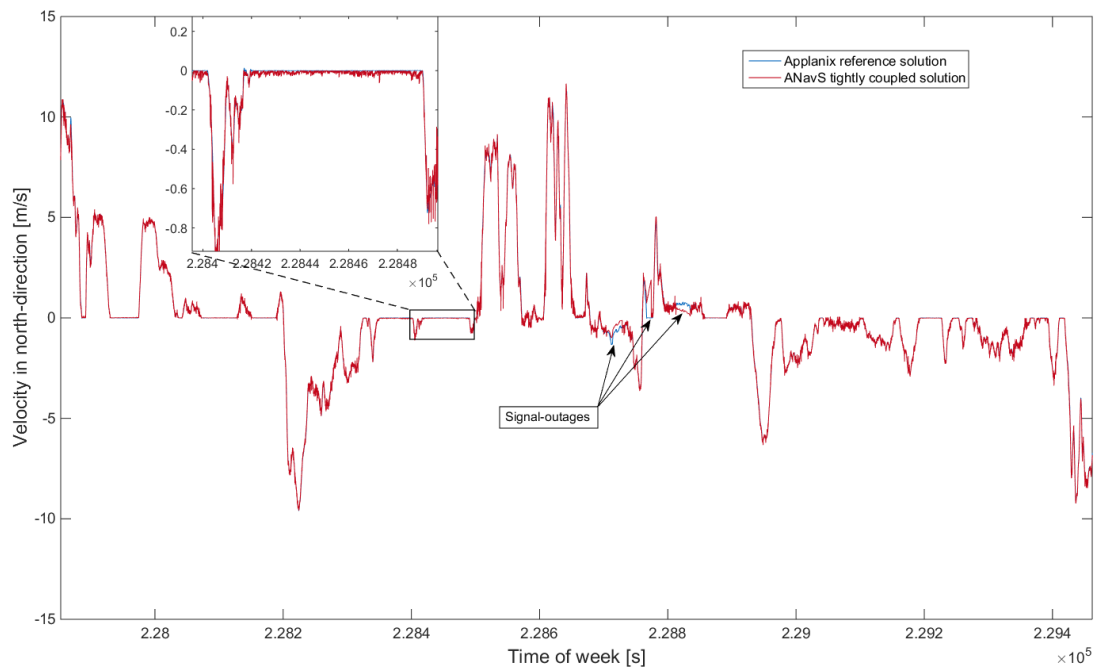


Figure 7.6: Comparison of the estimated tight-coupled velocity-solution in north-direction (red) with the applanix-reference (blue) in an urban environment. Signal-outages are caused by tunnels

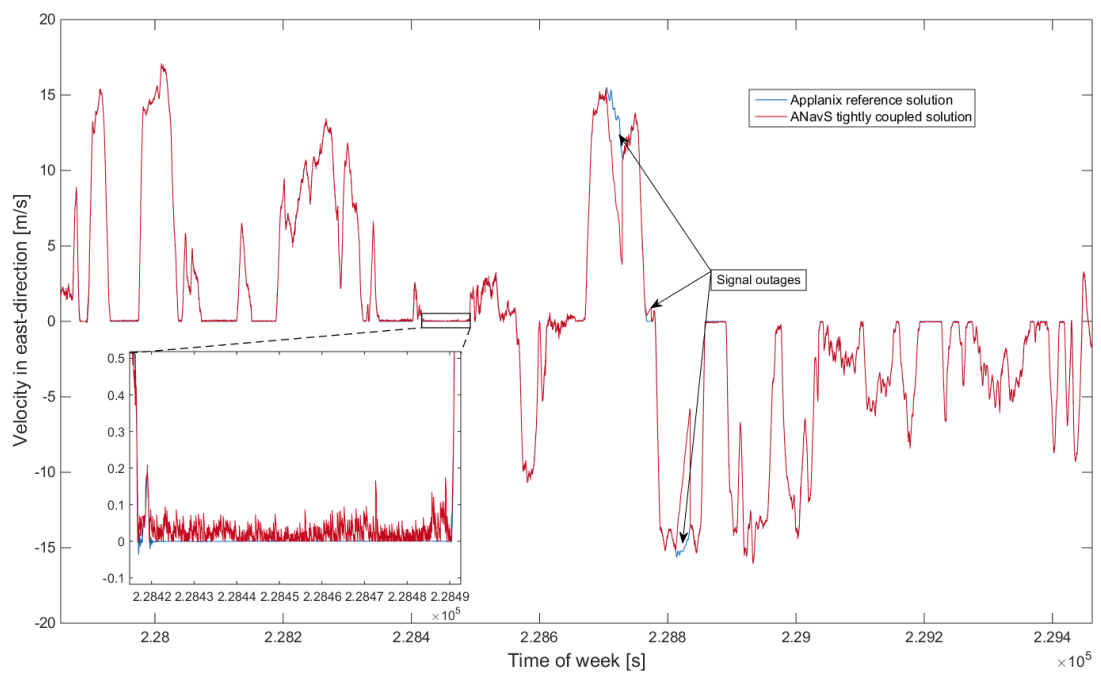


Figure 7.7: Comparison of the estimated tight-coupled velocity-solution in east-direction (red) with the applanix-reference (blue) in an urban environment. Signal-outages are caused by tunnels

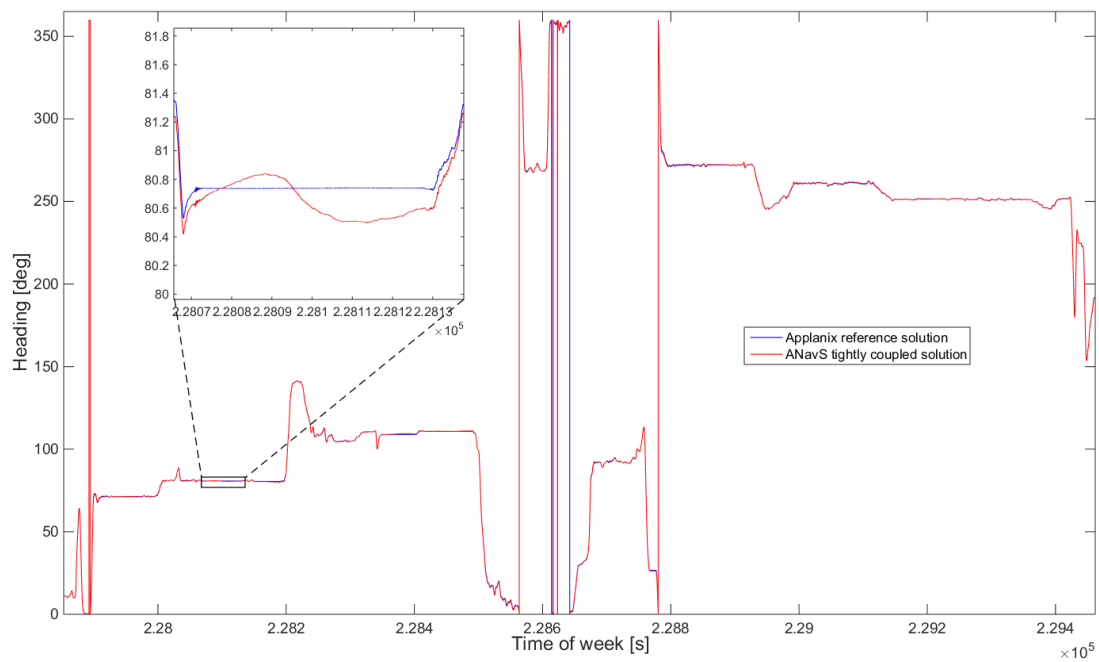


Figure 7.8: Comparison of the estimated tight-coupled heading-solution with the applanix-reference (blue) in an urban environment. The enlarged plot shows the drift of heading for conditions without dynamics.

7.2 The test-drive on a highway

In figure 7.9 a snippet of the course for the test-drive on the highway in the near of Wolfsburg is plotted. The route includes short crossings under bridges, highway-intersections with a high rotation- and driving-dynamics. The developed fixed tightly coupled position- and attitude determination with correction-data shows again in all cases a continuous progress, what is also shown in this chapter in more detail.

Figure 7.10 highlights the absolute position accuracy for the implemented solution of the fixed tightly coupled EKF. It shows a position-accuracy of at least 48 cm in 68 % of time and better than 1 m in more than 98 % of time for the driving-route on the highway.

The next figure 7.11 shows the absolute position-estimation of the fixed tightly coupled solution against the reference-solution for a section below a highway-bridge with losing of almost satellites and state-updates only with IMU-measurements with following high dynamics by crossing the driveway. The deviation is less than 65 cm after the difficulties and thus under the requirements for this thesis.

In figure 7.12 one compares the tight coupled solution under a highway-bridge with the applanix reference-solution. The deviation is here less than 80 cm. One can see, the solution does not drift, nor is the position jumping below or shortly after the bridge.

As next the velocity in north- and east- direction is shown in 7.13 and 7.14 against the reference-solution. One can see in both cases a very accurate estimation of this state. The given drifts in this plot are again in cases with long signal-outages.



Figure 7.9: Map section of the driving route (yellow) on the highway in the near of Wolfsburg at 11.11.2014

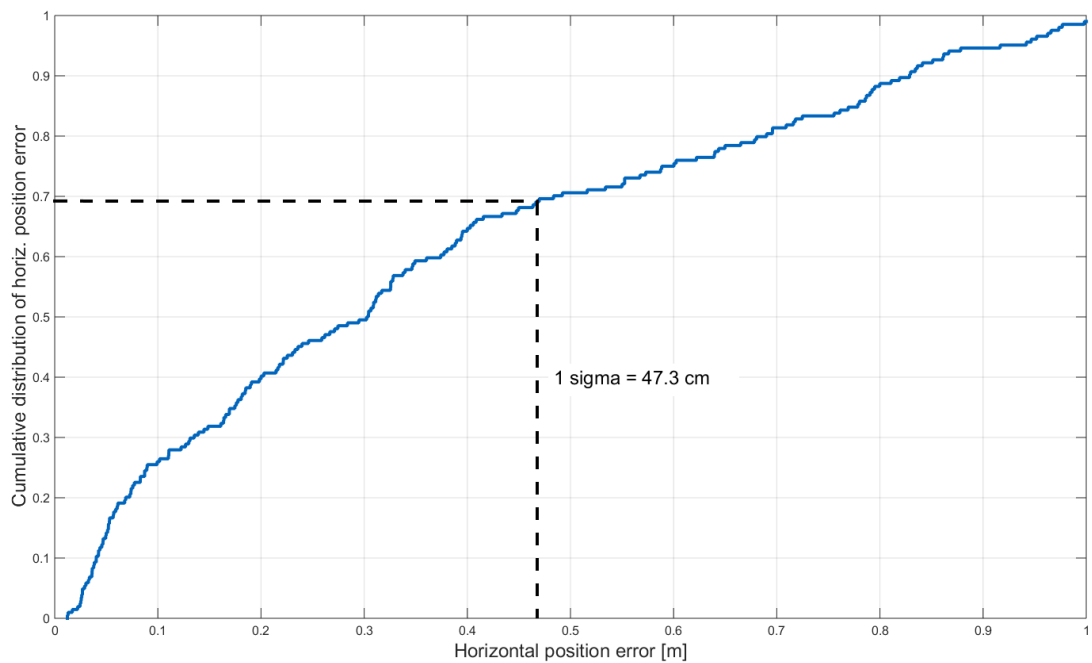


Figure 7.10: Cumulative distribution of the horizontal position-error in the test-driving on a highway. The position-error is maximum 48 cm in 68 % of time.



Figure 7.11: Map-section on a highway. Plotted are the fixed tight-coupled solution (orange) and the reference-solution (green)



Figure 7.12: Map-section on a highway below a bridge. Plotted are the fixed tight-coupled solution (orange) and the reference-solution (green)

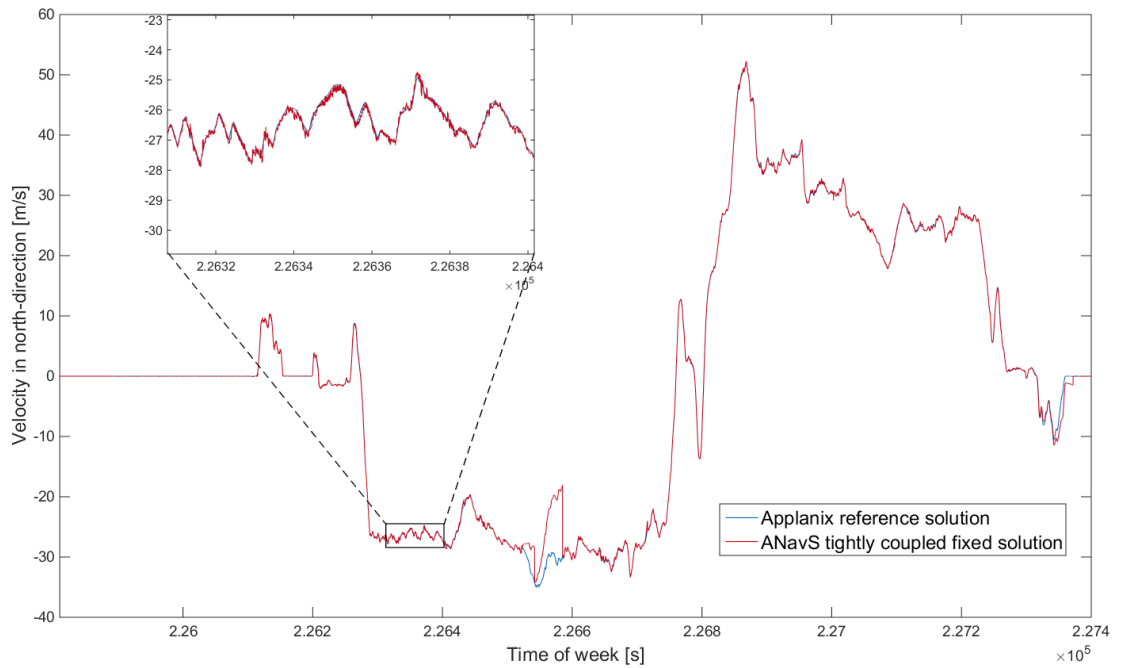


Figure 7.13: Comparison of the estimated tight-coupled velocity-solution in north-direction (red) with the applanix-reference (blue) on a highway. The drifts are given by long signal-outages.

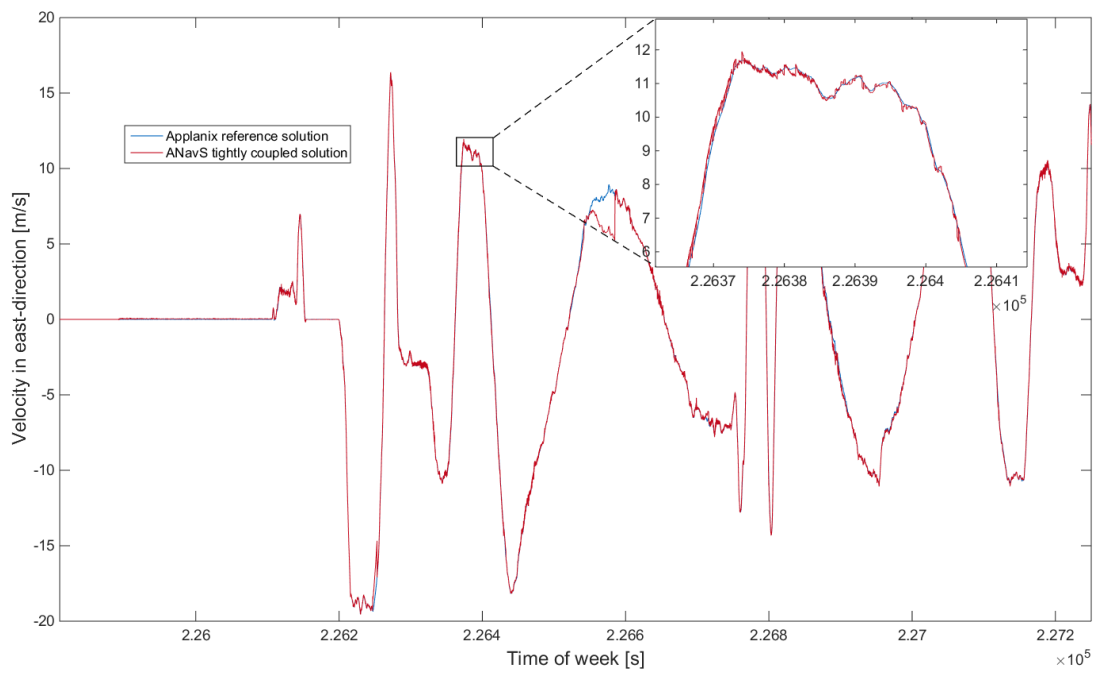


Figure 7.14: Comparison of the estimated tight-coupled velocity-solution in east-direction (red) with the applanix-reference (blue) on a highway. The drifts are given by long signal-outages.

In figure 7.15 one compares the estimated heading-solution with the reference-solution. The tight coupled solution follows clearly the course of the applanix-reference. The enlarged plot shows the small gyroscope-drift over time in a scale of rough 0.5 degree. The reason is given by the in-perfect estimation of the bias for the rotation-rates, which is reduced in conditions with higher dynamic. The noise for the heading-solution is below 0.1 degree and thus negligible.

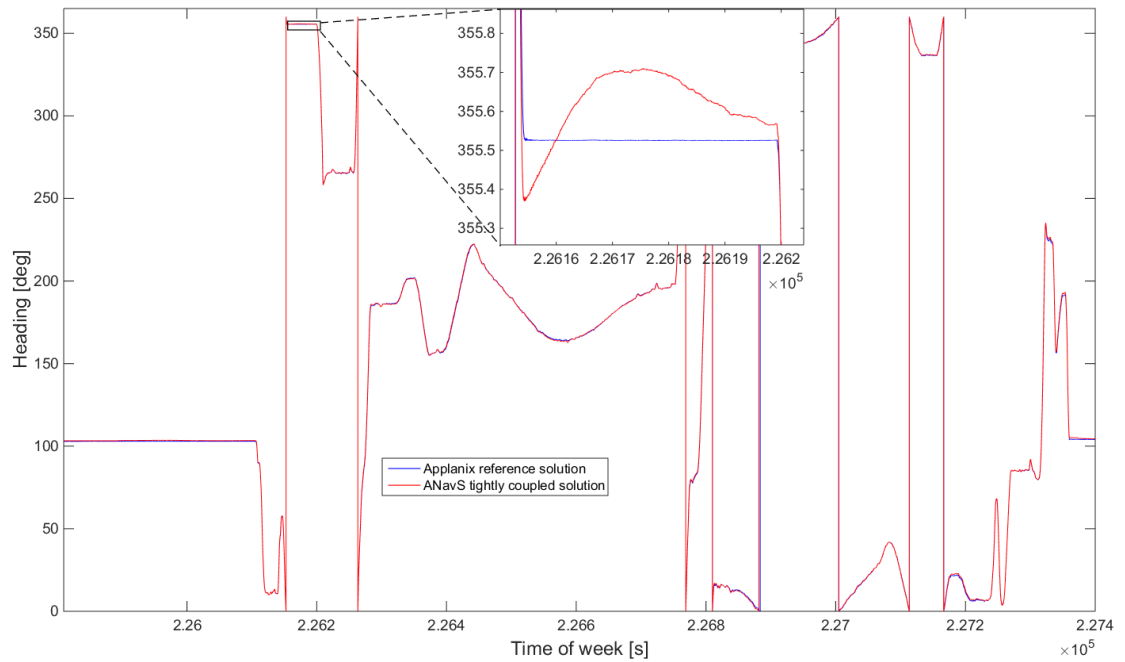


Figure 7.15: Comparison of the estimated tight-coupled heading-solution with the applanix-reference (blue) on a highway. The enlarged plot shows the drift of heading for conditions without dynamics.

Chapter 8

Conclusion

The intention of this work was to implement and to demonstrate a reliable and concurrently accurate solution with the help of low-cost GPS/INS-equipment and correction-data from a VRS for the position and attitude of a car. Especially the possible usage in an autonomous rover should be proven here. As described in a previous chapter, a highly accurate absolute position can be used for lane-detection, car-to-car communication for prediction-models, information-link to infrastructure-systems and more redundancy of state parameters through different sensory. The appealed cost-benefit-problem is also solved with such a tightly coupled GPS/INS-system for a mass-market product.

To enable such a low-cost system to be used for an autonomous car, a precise position solution of at least 1 m must be given in all circumstances. We proved this accuracy in an urban environment and also on a highway. This consideration gives us reliability for nearly all cases on a road what can be driven. Situations with high/low dynamic, high/low multipath, long and short tunnels and bridges with signal-outages and bad/good satellite constellations were considered. The tests showed an accuracy of at least 50 cm in 68 % of time and better than 1 m in more than 95% of time for both test-environments. Jumps in the position-solution are not happening respectively are really smooth. As an absolute position can only be determined with a GNSS-system, the introduced tight coupled RTK-system provides a very interesting option for integrating in the autonomous driving for example.

A next possible step for improving the tight-coupled GPS/INS-system is the integration of more satellite-systems like GLONASS, Galileo and EGNOS for example. The reliability and also the accuracy is well depending on the available count of satellites within the elevation-mask (10 degrees) and with a continuous phase-measurement. Further the integration of odometry-data in the tight-coupling will make the estimation of the position and velocity states more robust. But it's important to mention that odometry-data is not the key for excluding the biased accelerometer-measurements. The resolution of velocity is well depending on the wheel speed of the rover. In cases with low dynamics, the estimation of the velocity and position states is not reliably only with the help of odometry-data respectively the update-rate is to low. The integration of a camera in the tight-coupling is a further possibility for improving the system, especially for the instantaneous (re-) fixing of attitude- and RTK-baseline. Hereby one tries to connect striking features of the environment, like special road markings, with that of a map-service to get an a-priori information about the rough position of the car. This information would lead to a more reliably and faster (re-) fixing of the attitude and RTK ambiguities.

One can see, there are still possibilities to improve the introduced low-cost GNSS/INS-system and maybe also a long road for the integration of such a tightly-coupled system in an autonomous car. But, as mentioned before, it has the best perspective in consideration of costs and benefit

to be used in a mass-market product like a car.

Appendix A

The baseline vector and its linearization

The baseline vector \vec{b}_{12} is defined as the difference of the absolute position between the first and second GPS-antenna:

$$\vec{b}_{12} = \vec{x}_1 - \vec{x}_2 \quad (\text{A.1})$$

As next one expresses the baseline vector in the local navigation- (NED) frame by using the heading (ψ), pitch (θ) and the a-priori baseline length \bar{l} :

$$\vec{b}_{12,NED} = \bar{l} \cdot \begin{pmatrix} \cos(\theta)\cos(\psi) \\ \cos(\theta)\sin(\psi) \\ -\sin(\theta) \end{pmatrix} \quad (\text{A.2})$$

It's derivative w.r.t. time is given by:

$$\frac{\partial}{\partial t} \vec{b}_{12,NED} = \dot{\vec{b}}_{12,NED} = \bar{l} \cdot \begin{pmatrix} -\sin(\theta)\cos(\psi) \\ -\sin(\theta)\sin(\psi) \\ -\cos(\theta) \end{pmatrix} \cdot \dot{\theta} + \bar{l} \cdot \begin{pmatrix} -\cos(\theta)\sin(\psi) \\ \cos(\theta)\cos(\psi) \\ 0 \end{pmatrix} \cdot \dot{\psi} \quad (\text{A.3})$$

Eqn. A.2 and A.3 have now to be linearized so that its linear expression can be used into the measurement model of the tight-coupled Kalman filter given in eqn. 6.22:

$$\begin{aligned} \vec{b}_{12,NED} &= f(\psi, \theta) \\ &\approx \vec{b}_{12,NED} |_{\psi=\hat{\psi}_n, \theta=\hat{\theta}_n} + \dots \\ &\quad \frac{\partial \vec{b}_{12,NED}}{\partial \psi} |_{\psi=\hat{\psi}_n, \theta=\hat{\theta}_n} \cdot (\psi - \hat{\psi}_n) + \frac{\partial \vec{b}_{12,NED}}{\partial \theta} |_{\psi=\hat{\psi}_n, \theta=\hat{\theta}_n} \cdot (\theta - \hat{\theta}_n) \end{aligned} \quad (\text{A.4})$$

$$\begin{aligned}
\dot{\vec{b}}_{12,NED} &= f(\psi, \dot{\psi}, \theta, \dot{\theta}) \\
&\approx \dot{\vec{b}}_{12,NED} \Big|_{\psi=\hat{\psi}_n, \dot{\psi}=\hat{\dot{\psi}}_n, \theta=\hat{\theta}_n, \dot{\theta}=\hat{\dot{\theta}}_n} + \\
&\quad \frac{\partial \dot{\vec{b}}_{12,NED}}{\partial \psi} \Big|_{\psi=\hat{\psi}_n, \dot{\psi}=\hat{\dot{\psi}}_n, \theta=\hat{\theta}_n, \dot{\theta}=\hat{\dot{\theta}}} \cdot (\psi - \hat{\psi}_n) + \frac{\partial \dot{\vec{b}}_{12,NED}}{\partial \dot{\psi}} \Big|_{\psi=\hat{\psi}_n, \dot{\psi}=\hat{\dot{\psi}}_n, \theta=\hat{\theta}_n, \dot{\theta}=\hat{\dot{\theta}}} \cdot (\dot{\psi} - \hat{\dot{\psi}}_n) + \\
&\quad \frac{\partial \dot{\vec{b}}_{12,NED}}{\partial \theta} \Big|_{\psi=\hat{\psi}_n, \dot{\psi}=\hat{\dot{\psi}}_n, \theta=\hat{\theta}_n, \dot{\theta}=\hat{\dot{\theta}}} \cdot (\theta - \hat{\theta}_n) + \frac{\partial \dot{\vec{b}}_{12,NED}}{\partial \dot{\theta}} \Big|_{\psi=\hat{\psi}_n, \dot{\psi}=\hat{\dot{\psi}}_n, \theta=\hat{\theta}_n, \dot{\theta}=\hat{\dot{\theta}}} \cdot (\dot{\theta} - \hat{\dot{\theta}}_n)
\end{aligned} \tag{A.5}$$

with $(\hat{\psi}_n, \hat{\dot{\psi}}_n, \hat{\theta}_n, \hat{\dot{\theta}}_n)$ as the estimated heading, heading rate, pitch and pitch rate values at epoch n . In particular, the above partial derivatives are given by:

$$\frac{\partial \vec{b}_{12,NED}}{\partial \psi} \Big|_{\psi=\hat{\psi}_n, \theta=\hat{\theta}_n} = \bar{l} \cdot \begin{pmatrix} -\cos(\theta)\sin(\psi) \\ \cos(\theta)\cos(\psi) \\ 0 \end{pmatrix} \tag{A.6}$$

$$\frac{\partial \vec{b}_{12,NED}}{\partial \theta} \Big|_{\psi=\hat{\psi}_n, \theta=\hat{\theta}_n} = \bar{l} \cdot \begin{pmatrix} -\sin(\theta)\cos(\psi) \\ -\sin(\theta)\sin(\psi) \\ -\cos(\theta) \end{pmatrix} \tag{A.7}$$

$$\frac{\partial \dot{\vec{b}}_{12,NED}}{\partial \dot{\psi}} \Big|_{\psi=\hat{\psi}_n, \dot{\psi}=\hat{\dot{\psi}}_n, \theta=\hat{\theta}_n, \dot{\theta}=\hat{\dot{\theta}}_n} = \bar{l} \cdot \begin{pmatrix} \sin(\theta)\sin(\psi) \\ -\sin(\theta)\cos(\psi) \\ 0 \end{pmatrix} \cdot \hat{\dot{\psi}}_n + \bar{l} \cdot \begin{pmatrix} -\cos(\theta)\cos(\psi) \\ -\cos(\theta)\sin(\psi) \\ 0 \end{pmatrix} \cdot \hat{\dot{\theta}}_n \tag{A.8}$$

$$\frac{\partial \dot{\vec{b}}_{12,NED}}{\partial \dot{\psi}} \Big|_{\psi=\hat{\psi}_n, \dot{\psi}=\hat{\dot{\psi}}_n, \theta=\hat{\theta}_n, \dot{\theta}=\hat{\dot{\theta}}_n} = \bar{l} \cdot \begin{pmatrix} -\cos(\theta)\sin(\psi) \\ \sin(\theta)\cos(\psi) \\ 0 \end{pmatrix} \tag{A.9}$$

$$\frac{\partial \dot{\vec{b}}_{12,NED}}{\partial \dot{\theta}} \Big|_{\psi=\hat{\psi}_n, \dot{\psi}=\hat{\dot{\psi}}_n, \theta=\hat{\theta}_n, \dot{\theta}=\hat{\dot{\theta}}_n} = \bar{l} \cdot \begin{pmatrix} -\cos(\theta)\cos(\psi) \\ -\cos(\theta)\sin(\psi) \\ -\sin(\theta) \end{pmatrix} \cdot \hat{\dot{\psi}}_n + \bar{l} \cdot \begin{pmatrix} \sin(\theta)\sin(\psi) \\ -\sin(\theta)\cos(\psi) \\ 0 \end{pmatrix} \cdot \hat{\dot{\theta}}_n \tag{A.10}$$

$$\frac{\partial \dot{\vec{b}}_{12,NED}}{\partial \dot{\theta}} \Big|_{\psi=\hat{\psi}_n, \dot{\psi}=\hat{\dot{\psi}}_n, \theta=\hat{\theta}_n, \dot{\theta}=\hat{\dot{\theta}}_n} = \bar{l} \cdot \begin{pmatrix} -\sin(\theta)\cos(\psi) \\ -\sin(\theta)\sin(\psi) \\ -\cos(\theta) \end{pmatrix} \tag{A.11}$$

Appendix B

Covariance-matrix with an elevation-dependent model

This appendix focuses on the method to determine the covariance matrix of the tracked phase and code measurements with an elevation-dependent model. The following model is especially in dynamic conditions used for the tight coupled GPS/INS-system with correction data.

McGraw et al. [29] showed that signals from satellites of lower elevation are typically affected more by multipath than signals from satellites of higher elevation. Also the dependency of the noise standard deviations on the elevation angle can be satisfactorily described by an exponential function.

The exponential multipath delay model for the pseudo-range can be expressed as follows [8]:

$$\sigma_{\rho}^k(E^k) = \sigma_{\rho,0} \cdot e^{-E^k/E_{\rho}} \quad (\text{B.1})$$

with σ_{ρ}^k as the code standard deviation respectively of satellite k with a certain elevation angle (E^k), E_{ρ} as the decay constant and $\sigma_{\rho,0}$ as the upper bounds of the exponential function since both the decay constant and the elevation are strictly positive.

By modeling the noise standard deviations at two constant bounds for the elevation angles $\{E_{\text{low}}, E_{\text{up}}\}$ as $\{\sigma_{\rho,\text{low}}, \sigma_{\rho,\text{up}}\}$, one can derive the decay constant. First the ratio between both standard deviations is taken:

$$\frac{\sigma_{\rho,\text{low}}}{\sigma_{\rho,\text{up}}} = e^{\frac{E_{\text{up}} - E_{\text{low}}}{E_{\rho}}}, \quad (\text{B.2})$$

and then take the logarithm and solve for the decay constant E_{ρ} :

$$E_{\rho} = \frac{E_{\text{up}} - E_{\text{low}}}{\ln(\sigma_{\rho,\text{low}}/\sigma_{\rho,\text{up}})} \quad (\text{B.3})$$

Similarly, one derives the decay constant for the model of the phase noise standard deviation:

$$E_{\varphi} = \frac{E_{\text{up}} - E_{\text{low}}}{\ln(\sigma_{\varphi,\text{low}}/\sigma_{\varphi,\text{up}})} \quad (\text{B.4})$$

Once the decay constants are determined, one can easily derive the upper bounds $\sigma_{\rho,0}$ and $\sigma_{\varphi,0}$:

$$\sigma_{\rho,0} = \frac{\sigma_{\rho,\text{low}}}{e^{(-E_{\text{low}}/E_{\rho})}} \quad \text{and} \quad \sigma_{\varphi,0} = \frac{\sigma_{\varphi,\text{low}}}{e^{(-E_{\text{low}}/E_{\varphi})}} \quad (\text{B.5})$$

Appendix C

Derivations for the decomposition in view of ambiguity fixing

Teunissen showed in [26] and [27] the decomposition of the minimization problem, given in eqn. 5.17. In this appendix, further simplifications are described in more detail.

The relation of $P_H(z - A\check{N}_{12}) = H\check{\check{b}}_{12}(\check{N}_{12})$ is derived as follows:

$$\begin{aligned}
z - A\check{N}_{12} &= H\check{\check{b}}_{12}(\check{N}_{12}) \\
&\Rightarrow \check{\check{b}}_{12}(\check{N}_{12}) = (H^T \Sigma_z^{-1} H)^{-1} H^T \Sigma_z^{-1} (z - A\check{N}_{12}) && / \cdot H \\
&\Rightarrow H\check{\check{b}}_{12}(\check{N}_{12}) = H(H^T \Sigma_z^{-1} H)^{-1} H^T \Sigma_z^{-1} (z - A\check{N}_{12}) \\
&\Rightarrow H\check{\check{b}}_{12}(\check{N}_{12}) = P_H(z - A\check{N}_{12}) && \text{with } P_H = H(H^T \Sigma_z^{-1} H)^{-1} H^T \Sigma_z^{-1}
\end{aligned} \tag{C.1}$$

with \check{N}_{12} as an integer-candidate searched by the LAMBDA-method and $\check{\check{b}}_{12}(\check{N}_{12})$ as the least-squares (LS) solution depending on the integer-candidate.

The relation of $P_{\bar{A}} P_H^\perp z = \bar{A} \hat{N}_{12}$ is derived as follows:

$$\begin{aligned}
z &= H\check{\check{b}}_{12} + AN_{12} + \eta_z && / \cdot P_H^\perp \\
P_H^\perp z &= P_H^\perp AN_{12} + P_H^\perp \eta_z \\
P_H^\perp z &= \bar{A} N_{12} + P_H^\perp \eta_z && \text{with } P_H^\perp A = \bar{A} \\
&\Rightarrow \hat{N}_{12} = (\bar{A}^T \Sigma_z^{-1} \bar{A})^{-1} \bar{A}^T \Sigma_z^{-1} P_H^\perp z && / \cdot \bar{A} \\
&\Rightarrow \bar{A} \hat{N}_{12} = \bar{A} (\bar{A}^T \Sigma_z^{-1} \bar{A})^{-1} \bar{A}^T \Sigma_z^{-1} P_H^\perp z \\
&\Rightarrow \bar{A} \hat{N}_{12} = P_{\bar{A}} P_H^\perp z && \text{with } P_{\bar{A}} = \bar{A} (\bar{A}^T \Sigma_z^{-1} \bar{A})^{-1} \bar{A}^T \Sigma_z^{-1}
\end{aligned} \tag{C.2}$$

with \hat{N}_{12} as the float solution.

Acronyms

GNSS	Global Navigation Satellite System
GPS	Global Positioning System
INS	Inertial Navigation System
RTK	Real Time Kinematic
IMU	Inertial Measurement Unit
MEMS	Micro-electromechanical System
VRS	Virtual Reference Station
KF	Kalman Filter
EKF	Extended Kalman Filter
LOS	Line of Sight
ECEF	Earth-Centered, Earth-Fixed
SD	Single Difference
DD	Double Difference
TD	Triple Difference
SNR	Signal-Noise-Ratio
OSR	Observation-State-Representation
MAC	Master-Auxiliary-Concept
FKP	Flächenkorrekturparameter
RTCM	Radio Technical Commission for Maritime Services
SSR	State Space Representation
LDW	Lane Departure Warning System
MMSE	Minimum Mean Square Error
LS	Least Squares
LAMBDA	Least-Squares Integer Ambiguity Decorrelation Adjustment
SSE	Sum of squared Errors
eqn	Equation

NED	North-East-Down
MAP	Maximum A Posteriori Probability
CSC	Cycle Slip Correction
ILS	Iterative Least Squares
DGPS	Differential Global Positioning System
EGNOS	European Geostationary Navigation Overlay Service

Bibliography

- [1] P. Henkel, *Lecture notes for Precise Point Positioning with GPS and Galileo*. Technische Universität München, 2014.
- [2] P. Henkel and J. Kiam, *Maximum A Posteriori Probability Estimation of Integer Ambiguities and Baseline*, pp. 353–356. Zadar, Croatia: Proc. of 55-th IEEE Symp, 2012.
- [3] J. Coias, J. Sanguino, and P. Oliveira, *Attitude Determination Using the Ambiguity Filter with Single-Frequency L1 GPS Receivers*. International Conference on Localization and GNSS (ICL-GNSS), 2013.
- [4] G. Giorgi and P. Teunissen, *Carrier phase GNSS attitude determination with the Multivariate Constrained LAMBDA method*. Aerospace Conference (IEEE), 2010.
- [5] L. V. Kylen, P. Nemry, F. Boon, A. Simsky, and J. Lorga, *Comparison of Attitude Performance for Multi-Antenna Receivers*, vol. 4, pp. 1–9. European Journal of Navigation, 2006.
- [6] B. Wang, L. Miao, S. Wang, and J. Shen, *A Constrained LAMBDA Method for GPS Attitude Determination*, vol. 13, pp. 97–107. GPS Solutions, 2009.
- [7] P. Henkel, *Tightly coupled precise point positioning and attitude determination*. Accepted for publication in IEEE Transactions on Aerospace and Electronic Systems, 2015.
- [8] J. J. Kiam, “Low-cost GPS-based Compass with Reliable Ambiguity Resolution and Cycle Slip Correction,” Master’s thesis, Technische Universität München, 2013.
- [9] P. Misra and P. Enge, eds., *Global Positioning System: Signals, Measurements and Performance*. Ganga-Jamuna Press, 2 ed., 2006.
- [10] C. Jekeli, ed., *Inertial Navigation Systems with Geodetic Applications*. Bod Third Party Titles, 2001.
- [11] L. Wanninger, *Präzise Positionsbestimmung in Netzen von GNSS-Referenzstationen*. Leibniz Universität Hannover, 2006.
- [12] NovAtel, *Application Note on Network RTK for the OEMV Receivers*. Calgary, Alberta, Canada, apn-041 rev 1a ed., 2006.
- [13] iMAR, “Micro IMS with integrated GPS, Magnetometer, Barometer, Odometrie.” Zugriff am 26. Mai 2015 auf http://www.imar-navigation.de/downloads/IMU_myIMU-01.pdf, 2015.
- [14] Daimler, “Hochautomatisiertes Fahren: Aufgabenteilung zwischen Fahrer und Mensch,” in *Kooperationsforum Fahrassistenzsysteme*, Aschaffenburg, Mai 2015.
- [15] J. Liu, B. Cai, J. Wang, and W. Shangguan, *GNSS/INS-based Vehicle Lane-Change Estimation using IMM and Lane-Level Road Map*. 16th International IEEE Annual Conference on Intelligent Transportation Systems (ITSC), 2013.

-
- [16] R. Schubert, N. Mattern, and G. Wanielik, *An Evaluation of Nonlinear Filtering Algorithms for Integrating GNSS and Inertial Measurements*. IEEE Position, Location and Navigation Symposium, 2008.
- [17] P. Maybeck, ed., *Stochastic models, estimation and control*. Academic Press, 1 ed., 1979.
- [18] P. D. Groves, ed., *Principles of GNSS, Inertial, and Multisensor Integrated Navigation Systems*. Artech House, second ed., 2013.
- [19] J. M. Cardenas, “Precise attitude determination with low-cost GNSS receivers,” Master’s thesis, Technische Universität München, 2013.
- [20] J. K. Ray, M. E. Cannon, and P. Fenton, *GPS Code and Carrier Multipath Mitigation Using a Multiantenna System*, vol. 37, pp. 183–195. IEEE Transactions on Aerospace and Electronic Systems, 2002.
- [21] M. H. Bhuiyan, E. S. Lohan, and M. Renfors, *A Slope-Based Multipath Estimation Technique for Mitigating Short-Delay Multipath in GNSS Receivers*, pp. 3573–3576. Proceedings of the IEEE Circuits and Systems (ISCAS) Symposium, 2010.
- [22] R. D. J. V. Nee, J. Sierveld, P. Fenton, and B. R. Townsend, *The Multipath Estimation Delay Lock Loop: Approaching Theoretical Limits*, pp. 246–251. IEEE Position, Location and Navigation Symposium, 1994.
- [23] M. H. Bhuiyan, X. Hu, E. S. Lohan, and M. Renfors, *Multipath mitigation performance of multi-correlator based code tracking algorithms in closed and open loop model*, pp. 84–89. European Wireless Conference, 2009.
- [24] M. Sahmoudi and R. Landry, *A Nonlinear Filtering Approach for Robust Multi-GNSS RTK Positioning in Presence of Multipath and Ionospheric Delays*, pp. 764 – 776. IEEE Journal of Selected Topics in Signal Processing, 2009.
- [25] A. Bourdeau, M. Sahmoudi, and J.-Y. Tournet, *Constructive Use of GNSS NLOS-Multipath: Augmenting the Navigation Kalman Filter with a 3D Model of the Environment*, pp. 2271 – 2276. 15th International Conference on Information Fusion (FUSION), 2012.
- [26] P. J. G. Teunissen, “The least-squares ambiguity decorrelation adjustment: a method for fast gps integer ambiguity estimation,” *Journal of Geodesy*, vol. 70, pp. 65–82, 1995.
- [27] P. J. G. Teunissen, “Integer least-squares theory for the gnss compass,” *Journal of Geodesy*, vol. 84, pp. 433–447, 2010.
- [28] A. Lipp and X. Gu, *Cycle-slip detection and repair in integrated navigation systems*, pp. 681–688. IEEE Position, Location and Navigation Symposium, 1994.
- [29] G. A. McGraw, T. Murphy, M. Brenner, S. Pullen, and A. J. V. Dierendonck, *Development of the LAAS Accuracy Models*, pp. 764 – 776. Salt Lake City, USA: ION GPS 2000, September 2000.